THE DYNAMICS OF TWO COUPLED VAN DER POL OSCILLATORS WITH DELAY COUPLING

A Dissertation

Presented to the Faculty of the Graduate School

of Cornell University

in Partial Fulfillment of the Requirements for the Degree of

Doctor of Philosophy

by

Stephen Allen Wirkus

August 1999

THE DYNAMICS OF TWO COUPLED VAN DER POL OSCILLATORS WITH DELAY COUPLING

Stephen Allen Wirkus, Ph.D.

Cornell University 1999

In this work, we investigate the dynamics of two weakly coupled van der Pol oscillators in which the coupling terms have time delay τ. Our work is motivated by applications to laser dynamics and the coupling of microwave oscillators. The governing equations are

$$\begin{aligned} \ddot{x}_1 + x_1 - \epsilon\,(1 - x_1^2)\,\dot{x}_1 &= \epsilon\,\alpha\,\dot{x}_2\,(t-\tau), \\ \ddot{x}_2 + x_2 - \epsilon\,(1 - x_2^2)\,\dot{x}_2 &= \epsilon\,\alpha\,\dot{x}_1\,(t-\tau), \end{aligned}$$

where the coupling is chosen to be through the damping terms because this form of coupling occurs in radiatively coupled microwave oscillator arrays. We use the method of averaging to obtain the approximate simplified system of three slow-flow equations

$$\begin{aligned} \dot{R}_1 &= \frac{1}{2}\left[R_1\left(1 - \frac{R_1^2}{4}\right) + \alpha\,R_2\,\cos(\phi+\tau)\right], \\ \dot{R}_2 &= \frac{1}{2}\left[R_2\left(1 - \frac{R_2^2}{4}\right) + \alpha\,R_1\,\cos(\phi-\tau)\right], \\ \dot{\phi} &= \frac{\alpha}{2}\left[-\frac{R_2}{R_1}\,\sin(\phi+\tau) - \frac{R_1}{R_2}\,\sin(\phi-\tau)\right]. \end{aligned}$$

Equilibria of these slow-flow equations correspond to periodic motions in the original equations. In the examination of the stability and bifurcation of the equilibria of these equations, we found that the in-phase and out-of-phase modes coexisted and were both stable in the parameter range for which the delay is about $\frac{1}{4}$ of the unperturbed limit cycle period. We also found that the in-phase mode ceased to exist if the delay was about $\frac{1}{2}$ of the unperturbed period and the coupling was strong enough. Similarly the out-of-phase mode ceased to exist if the delay was approximately the same as that of the unperturbed period. We also found that if the coupling was sufficiently small, various other motions were predicted to exist besides the in-phase and out-of-phase modes. These additional motions were predicted to change their form through a series of elaborate bifurcations. Nevertheless all these motions were predicted to be periodic, and we did not observe chaos for any parameter values.

In order to check the validity of the approximations, we numerically integrated the original differential delay equations for the case $\epsilon << 1$ and $\tau = O(1)$ and compared their predictions regarding the stability of the in-phase and out-of-phase modes with those of the slow-flow analysis. The two sets of results showed excellent agreement.

Biographical Sketch

Stephen Wirkus was born on June 25, 1971 in Kansas City, Missouri, the second child of an eventual seven to Gene and Bebe Wirkus. He spent his early childhood like most children–playing outside and trying to avoid work (both school and house). In the classroom, he always seemed to be one of the better students but was never considered *the* best. Outside of the class, he found a love for running (beginning in fourth grade) and although he was best at his school, he was rarely *the* best when it came to outside competition. Although he never achieved the illusive recognition of being *the* best throughout grade school, high school, college, or graduate school, he continued to strive to be the best. And this perserverance has allowed him to be where he is today.

He ran cross country and track in high school at Bishop Hogan and became a scholarship walk-on in college at the University of Missouri-Kansas City. His high school goal of running at the Division I level was realized as the school made the transition from NAIA to NCAA Division I during his five year tenure there. He also found time to study and obtained B.S. degrees in Mathematics and Physics with Honors while participating in the Honors Program. Although he did not initially

want to go to UMKC, it was the best choice in hindsight.

He chose quaint little Ithaca as his home for the next 5 years because of Cornell's Center for Applied Math and the beautiful countryside which surrounds it. Little did he realize what a tremendous change this would have on his life (even more so than undergrad). He was introduced to nonlinear dynamics his first semester and began working with Richard Rand after his first year while still continuing to run competitively for High Noon A.C. He began helping in a summer research program for undergrads (MTBI) in the summer of 1996 where he met his future wife, Erika Camacho. Spending time with her over the next year changed his life in so many ways (and also let him run his best times ever!). They were married on August 23, 1997 just 4 days before she started grad school. Life over the next year was a big adjustment but the time spent with Erika made it all worthwhile. He was able to finish his Ph.D. in August of 1999. During the summer of 1999 he co-directed the MTBI summer program that he had helped out with the previous 3 years. He will be a Teaching Associate and Visiting Assistant Professor in the Cornell University Math Department for the 1999-2000 academic year and will continue research with Richard Rand on thesis related topics.

To Erika Tatiana—my wife, my best friend, my better half and my soulmate.

Acknowledgements

There are many people I would like to thank for their help/guidance in attaining my Ph.D. I would first like to thank my wonderful wife Erika Tatiana—I couldn't even picture these last three years without her help, support and infinite patience. I would also like to thank Richard Rand for his tireless efforts and seemingly boundless energy with which he approaches all problems. His academic guidance and encouragement is exceptional. A special thanks goes out to my family and Erika's family for supporting me in my endeavors even though few really knew what I was getting myself into.

My other two committee members, John Guckenheimer and Steve Strogatz, also deserve a big thanks for helping shape my thesis—their insights into problems involving non-linear dymnamics are unmatched. They also deserve a special thanks along with Lou Billera, Steve Vavasis and Tom Coleman for looking after the needs of the students in the Center for Applied Mathematics (CAM). Various other people have also influenced my life in a positive way over the last five years. Carlos Castillo-Chavez has helped open my eyes and I thank him for his support, advice, encouragement and unfailing confidence in me and my abilities. Others include James

Curry, Christine O'Brien, Jim Schatz and Ronald Mickens. On the non-academic side, I want to thank Fr. Ed Ondrako for his friendship and spiritual guidance. I also need to thank my undergrad professors at the University of Missouri - Kansas City, especially Joan Dean, Dave Wieliczka, John Urani, Hank Frankel, Paul Liebnitz. Each one has contributed in a substantial way to my progress.

Other people have also helped to make my graduate school experience go a bit smoother. I owe a million thanks to Dolores Pendell, especially for finding me fellowships for my last two years. Others who deserve thanks for their friendship and support include Patty Hough (who has always been a superb friend), Eric van den Berg, Ajay Subramanian, Dave Cimbala, Fang Xue, Aaron Deever, John Dalbec, Don Allers, Hal Schenck, Ivelisse Rubio, Kaila Patel, Katy Simonsen, Ellie Swartwood, Tom Rishel, Herbert Medina, Chuck Benton, Julio Villareal, friends at High Noon A.C. and so many others. Whether it was taking classes, debugging code or drinking at the Chapter House, each definitely helped get me through grad school, especially the first few years. I also need to mention Soundgarden, Sarah McLachlan and so many others whose music also helped keep me sane.

And last but definitely not least, I want to thank those who have given financial support: The Ford Foundation for a three-year fellowship, the NSF through a Graduate Engineering Education Fellowship, the Corning Foundation for a one-year fellowship my fourth year and the Anonymous donor who gave me the fellowship for my fifth and final year. The NSA and NSF also deserve thanks for supporting MTBI since I was paid for the last four summers through those funds.

Table of Contents

List of Figures

Chapter 1

Introduction

1.1 Non-instantaneous Interaction of Oscillators

The instantaneous interaction of a pair of coupled oscillators is something that is often assumed. This is an okay assumption provided the state of one oscillator does not change appreciably in the finite time it takes the signal from the other oscillator to reach it. But consider the case of microwave oscillators which typically have frequencies of around 10 GHz giving them a period of $T = \frac{2\pi}{10^{10}} = 6 \times 10^{-10}$sec. Since signals propagate through space at the speed of light, we see that the signal will move about 18 cm during one full period of the oscillators. If the oscillators are separated by, say, 4 cm, we see that each oscillator will have gone through about $\frac{1}{4}$ period before the signal of the other oscillator reaches it. Thus the time for a signal to travel from one oscillator to the other represents a substantial portion of the period of the uncoupled oscillator. This immediately leads to the inclusion of

delay effects in the coupling terms.

Many examples exist in which the interaction of coupled oscillators must take into account time delay [9],[19],[21],[26],[45]. The work of this thesis is concerned with the mutual interaction of limit cycle oscillators and has application to laser dynamics and, more generally, to the coupling of microwave oscillators [22],[23],[46],[48]. This thesis examines the dynamics of two weakly coupled van der Pol oscillators in which the coupling terms have time delay τ [44]. The coupling has been chosen to be via first derivative terms ("velocity coupling") because this form of coupling occurs in radiatively coupled microwave oscillator arrays [23],[46],[47]. Experimentalists Lynch and York state that the reason for studying periodic motions in the original system is that "in practice, any useful operational mode of a system of coupled oscillators where coherent power combining is desired must exhibit some type of stable periodicity"[23]. We use the method of averaging to obtain an approximate simplified system of three slow-flow equations and then investigate the stability and bifurcation of their equilibria which correspond to periodic motions in the original system. We then compare these results with the numerical integration of the original differential delay equations.

This work has application to high resolution radar systems and satellite communications [22]. Since solid-state devices have trouble handling the desired output power levels at these high frequencies, alternative power devices are being sought. Coupled microwave oscillators have the benefit that they can generate adequate levels of power at such high frequencies, making them a desirable alternative to solid-state devices. This work is related to previous studies of coupled van der Pol

oscillators in which the coupling terms omitted delay effects [5],[32],[37],[38].

1.2 The Literature on Microwave Oscillators

The coupling of microwave oscillators through delayed velocity coupling has been examined in the electrical engineering literature [22],[23],[46],[47],[48]. Two important characteristics of microwave oscillators are negative resistance (which causes the amplitude of the oscillations to grow) and gain saturation (which limits the amplitude of the oscillations) [22],[24]. In the laser physics community, the operation of the ruby laser, for instance, also exhibits such relaxation oscillations [34]. York states that numerous experiments involving microwave oscillators with "significantly different physical mechanisms responsible for the negative resistance and gain saturation" have shown the systems to behave similarly when coupled together [46]. Because of this observation and the presence of relaxation oscillations, the van der Pol oscillator is often considered as a generic microwave oscillator [22],[23],[46],[47],[48].

This work examines two coupled van der Pol oscillators with delayed velocity coupling. It differs from previous work in its treatment of the time delay. Time delay is included explicitly in the differential equations (thus giving rise to differential delay equations), rather than introducing the delay in the averaged equations (cf. [46],[47],[48]); moreover, a mathematical justification is provided and conditions are given under which the approximations of the delay terms will be valid (cf. [22],[23]). Under certain conditions, it is seen that the introduction of delay terms in the averaged equations will be accurate. This is not expected as our origi-

nal differential delay equations must properly be analyzed in an infinite-dimensional space (as an entire delay *interval* is needed to calculate the state of the system), whereas our analysis reduces the system to a finite-dimensional one by making the delay a parameter (thus allowing our system to be analyzed in a three-dimensional space involving two parameters). Previous work has dealt with phase-only oscillators with non-identical frequencies and the stability of these systems was examined in terms of the frequency differences. This work also differs from previous work in that it examines identical oscillators with both phase *and* amplitude and considers the stability of the system in terms of the coupling strength versus the time delay.

1.3 A Brief Overview

We begin Chapter 2 by considering a pair of van der Pol oscillators that have delayed velocity coupling. We average the equations and then approximate the delay terms (under certain restrictions), thereby reducing the system to one that may be analyzed in a finite dimensional space with parameters τ (time delay) and α (coupling strength). We find equations for saddle-node and Hopf bifurcation curves and the intersection of these curves in $\tau - \alpha$ parameter space gives rise to three degenerate equilibria, which we label Q, P and H. Detailed local analyses of the degenerate singularities Q, P and H are performed in Chapters 3, 4 and 5 respectively, and certain global bifurcation curves are able to be observed or deduced from the analyses. At the end of Chapter 5, the fate of all but two of the global bifurcation curves is known. Chapter 6 analyzes the remaining two curves and the end result is that the

complete bifurcation set of the averaged equations is known (where the bifurcation set is defined as the set of points at which the averaged equations are structurally unstable [12]). Chapter 7 describes a modified Runge-Kutta integration scheme by which we are able to numerically integrate the original van der Pol equations. We then compare the predictions from the analysis of the approximate averaged equations with results obtained from the numerical integration of the original equations. Chapter 8 discusses some implications and limitations of our analysis and suggests further research that can be done on similar problems.

Chapter 2

The Slow-Flow Equations

2.1 Derivation of the Slow-Flow Equations

We investigate two van der Pol oscillators with delay coupling [11],[23],[46]:

$$\ddot{x}_1 + x_1 - \epsilon\,(1 - x_1^2)\,\dot{x}_1 \;=\; \epsilon\,\alpha\,\dot{x}_2\,(t-\tau), \tag{2.1}$$

$$\ddot{x}_2 + x_2 - \epsilon\,(1 - x_2^2)\,\dot{x}_2 \;=\; \epsilon\,\alpha\,\dot{x}_1\,(t-\tau), \tag{2.2}$$

where α is a coupling parameter, τ is the delay time, and where $\epsilon << 1$. As mentioned in Chapter 1, we choose van der Pol oscillators with delay coupling in the damping terms because this form of coupling occurs in radiatively coupled microwave oscillator arrays [23],[46]. In terms of the physical problem, x_i represents voltage and the velocity coupling represents the coupling of the oscillators in free-space (where high efficiency is possible [47]). As the voltage is often written in phasor form as $V_k(t) = R_k(t)e^{i\theta(t)}$, it is natural to examine the equations on R_k and

θ_k. When $\epsilon = 0$, the system reduces to $\ddot{x}_i + x_i = 0, i = 1, 2$, with solution:

$$x_1 = R_1 \cos(t + \theta_1), \qquad x_2 = R_2 \cos(t + \theta_2), \tag{2.3}$$

$$\dot{x}_1 = -R_1 \sin(t + \theta_1), \qquad \dot{x}_2 = -R_2 \sin(t + \theta_2). \tag{2.4}$$

For $\epsilon > 0$, we assume (2.3)-(2.4) but treat R_i and θ_i as time dependent. Using variation of parameters, we now differentiate (2.3) and obtain

$$\begin{aligned} \dot{x}_1 &= \dot{R}_1 \cos(t + \theta_1) - R_1 \sin(t + \theta_1) - R_1 \sin(t + \theta_1)\, \dot{\theta}_1, \\ \dot{x}_2 &= \dot{R}_2 \cos(t + \theta_2) - R_2 \sin(t + \theta_2) - R_2 \sin(t + \theta_2)\, \dot{\theta}_2. \end{aligned}$$

Comparison with (2.4) gives

$$\dot{R}_1 \cos(t + \theta_1) - R_1 \sin(t + \theta_1)\, \dot{\theta}_1 = 0 \tag{2.5}$$

$$\dot{R}_2 \cos(t + \theta_2) - R_2 \sin(t + \theta_2)\, \dot{\theta}_2 = 0. \tag{2.6}$$

Calculating the second derivatives, we then obtain

$$\begin{aligned} \ddot{x}_1 &= -\dot{R}_1 \sin(t + \theta_1) - R_1 \cos(t + \theta_1) - R_1 \cos(t + \theta_1)\, \dot{\theta}_1, \\ \ddot{x}_2 &= -\dot{R}_2 \sin(t + \theta_2) - R_2 \cos(t + \theta_2) - R_2 \cos(t + \theta_2)\, \dot{\theta}_2. \end{aligned}$$

Substitution into (2.1)-(2.2) gives

$$\begin{aligned} \ddot{x}_1 + x_1 &= -\dot{R}_1 \sin(t + \theta_1) - R_1 \cos(t + \theta_1)\, \dot{\theta}_1 \\ &= \epsilon\, (1 - x_1^2)\, \dot{x}_1 + \epsilon\, \alpha\, \dot{x}_2(t - \tau) \\ &\equiv \epsilon\, F_1 \end{aligned} \tag{2.7}$$

$$\begin{aligned} \ddot{x}_2 + x_2 &= -\dot{R}_2 \sin(t + \theta_2) - R_2 \cos(t + \theta_2)\, \dot{\theta}_2 \\ &= \epsilon\, (1 - x_2^2)\, \dot{x}_2 + \epsilon\, \alpha\, \dot{x}_1\, (t - \tau) \\ &\equiv \epsilon\, F_2. \end{aligned} \tag{2.8}$$

Using (2.3)-(2.4), the expressions for F_i become

$$\begin{aligned} F_1 &= [1 - R_1^2\ \cos^2(t+\theta_1)]\ [-R_1\ \sin(t+\theta_1)] \\ &\quad + \alpha\ [-\tilde{R}_2\ \sin(t-\tau+\tilde{\theta}_2)], \qquad (2.9) \\ F_2 &= [1 - R_2^2\ \cos^2(t+\theta_2)]\ [-R_2\ \sin(t+\theta_2)] \\ &\quad + \alpha\ [-\tilde{R}_1\ \sin(t-\tau+\tilde{\theta}_1)] \qquad (2.10) \end{aligned}$$

where $\tilde{R}_i = R_i(t-\tau)$ and $\tilde{\theta}_i = \theta_i(t-\tau)$. Solving (2.5)-(2.8) for $\dot{R}_i$ and $\dot{\theta}_i$ and applying the method of averaging, we obtain

$$\begin{aligned} \dot{R}_1 &= -\epsilon\ \sin(t+\theta_1)\ F_1 \approx -\epsilon\ \frac{1}{2\pi}\int_0^{2\pi} \sin(t+\theta_1)\ F_1\ dt, \qquad (2.11) \\ -R_1\ \dot{\theta}_1 &= \epsilon\ \cos(t+\theta_1)\ F_1\ \approx\ \epsilon\ \frac{1}{2\pi}\int_0^{2\pi} \cos(t+\theta_1)\ F_1\ dt, \qquad (2.12) \\ \dot{R}_2 &= -\epsilon\ \sin(t+\theta_2)\ F_2 \approx -\epsilon\ \frac{1}{2\pi}\int_0^{2\pi} \sin(t+\theta_2)\ F_2\ dt, \qquad (2.13) \\ -R_2\ \dot{\theta}_2 &= \epsilon\ \cos(t+\theta_2)\ F_2\ \approx\ \epsilon\ \frac{1}{2\pi}\int_0^{2\pi} \cos(t+\theta_2)\ F_2\ dt, \qquad (2.14) \end{aligned}$$

where the right hand side of (2.11)-(2.14) is the average over one period of the $\epsilon = 0$ system. Calculating $\oint \cos(t+\theta_1)\ F_1\ dt$ using (2.9) and combining with (2.12) gives

$$R_1\ \dot{\theta}_1\ =\ \frac{\epsilon\ \alpha}{2}\ \tilde{R}_2\ \sin(\tilde{\theta}_2 - \theta_1 - \tau) \qquad (2.15)$$

while calculating $\oint \sin(t+\theta_1)\ F_1\ dt$ using (2.9) and combining with (2.11) gives

$$\dot{R}_1\ =\ \frac{\epsilon}{2}\ R_1\ \left(1 - \frac{R_1^2}{4}\right) + \frac{\epsilon\ \alpha}{2}\ \tilde{R}_2\ \cos(\theta_1 - \tilde{\theta}_2 + \tau). \qquad (2.16)$$

Similarly, we calculate

$$\begin{aligned} R_2\ \dot{\theta}_2 &= \frac{\epsilon\ \alpha}{2}\ \tilde{R}_1\ \sin(\tilde{\theta}_1 - \theta_2 - \tau), \qquad (2.17) \\ \dot{R}_2 &= \frac{\epsilon}{2}\ R_2\ \left(1 - \frac{R_2^2}{4}\right) + \frac{\epsilon\ \alpha}{2}\ \tilde{R}_1\ \cos(\tilde{\theta}_1 - \theta_2 - \tau). \qquad (2.18) \end{aligned}$$

Equations (2.15)-(2.18) show that $\dot{R}_i$,$\dot{\theta}_i$ are $O(\epsilon)$. We now Taylor expand $\tilde{R}_i$ and $\tilde{\theta}_i$:

$$\tilde{R}_i = R_i(t-\tau) = R_i(t) - \tau\dot{R}_i(t) + \tau^2\ddot{R}_i(t) + \cdots, \tag{2.19}$$

$$\tilde{\theta}_i = \theta_i(t-\tau) = \theta_i(t) - \tau\dot{\theta}_i(t) + \tau^2\ddot{\theta}_i(t) + \cdots. \tag{2.20}$$

Equations (2.19)-(2.20) indicate that we can replace $\tilde{R}_i$,$\tilde{\theta}_i$ by R_i,θ_i in equations (2.15)-(2.18) since $\dot{R}_i(t)$,$\dot{\theta}_i(t)$ and $\ddot{R}_i(t)$,$\ddot{\theta}_i(t)$ in (2.19)-(2.20) are $O(\epsilon)$ and $O(\epsilon^2)$ respectively, as calculated from equations (2.15)-(2.18). This substitution reduces the delay τ to a parameter. That is, the problem is reduced from an infinite dimensional problem in functional analysis to a finite dimensional problem by assuming the product $\epsilon\tau$ is small. (Note that we do not assume a small delay τ.) This key step enables us to handle the original system of differential delay equations as a system of differential equations [22],[23],[46],[48]. Note that if terms of $O(\epsilon^2)$ were retained in equations (2.19)-(2.20), then the resulting differential equations would be of second order. Thus extending the expansion to higher order in ϵ has the unusual effect of profoundly changing the nature of the approximate system to be solved. Nevertheless the $O(\epsilon)$ truncation studied in this work is valid for small values of $\epsilon\tau$ (see Chapter 7), as demonstrated by comparison of the subsequent slow flow analysis with numerical integration of the original differential delay equations (2.1)-(2.2).

Setting $\phi = \theta_1 - \theta_2$ we then obtain

$$\dot{R}_1 = \frac{\epsilon}{2}\left[R_1\left(1 - \frac{R_1^2}{4}\right) + \alpha\ R_2\ \cos(\phi+\tau)\right], \tag{2.21}$$

$$\dot{R}_2 = \frac{\epsilon}{2}\left[R_2\left(1 - \frac{R_2^2}{4}\right) + \alpha\ R_1\ \cos(\phi-\tau)\right], \tag{2.22}$$

$$\dot{\phi} \;=\; \frac{\epsilon\ \alpha}{2}\ \left[-\frac{R_2}{R_1}\ \sin(\phi+\tau) - \frac{R_1}{R_2}\ \sin(\phi-\tau)\right]. \tag{2.23}$$

In our analytic treatment and subsequent numerical integration of equations (2.21)-(2.23), we avoid having to choose ϵ by making the change of variables $T = \frac{1}{\epsilon}t$. Then $\frac{dT}{dt} = \frac{1}{\epsilon}$ and the ϵ has no explicit appearance. The slow-flow equations are then in the form

$$\dot{R}_1 \;=\; \frac{1}{2}\ \left[R_1\ \left(1 - \frac{R_1^2}{4}\right) + \alpha\ R_2\ \cos(\phi+\tau)\right], \tag{2.24}$$

$$\dot{R}_2 \;=\; \frac{1}{2}\ \left[R_2\ \left(1 - \frac{R_2^2}{4}\right) + \alpha\ R_1\ \cos(\phi-\tau)\right], \tag{2.25}$$

$$\dot{\phi} \;=\; \frac{\alpha}{2}\ \left[-\frac{R_2}{R_1}\ \sin(\phi+\tau) - \frac{R_1}{R_2}\ \sin(\phi-\tau)\right] \tag{2.26}$$

and we will examine equations (2.24)-(2.26) in the ensuing chapters, but now the derivatives are with respect to T, not t. We again note that equilibria in the slow-flow equations correspond to periodic motions in (2.1)-(2.2) and we will define the oscillators to be *1:1 phase locked* if $\phi(t)$ is constant. We also note that periodic motions of (2.24)-(2.26) correspond to quasiperiodic motions of (2.1)-(2.2) and we define the oscillators to be in *1:1 phase entrainment* when $\phi(t)$ varies periodically. The remaining situation occurs when $\phi(t)$ grows unbounded and we define the oscillators in this case to be in *phase drift* [5].

Note that R_1 and R_2 are nonnegative and the vector field associated with equations (2.24)-(2.26) is periodic in ϕ. Thus the phase space is $\mathbf{R}^+ \times \mathbf{R}^+ \times \mathbf{S}^1$. The slow-flow is invariant under the three transformations:

$$(R_1,\ R_2,\ \phi) \mapsto (R_2,\ R_1, -\phi) \tag{2.27}$$

$$\phi \mapsto \phi + \pi, \qquad \alpha \mapsto -\alpha \tag{2.28}$$

$$\phi \mapsto \phi + \pi, \qquad \tau \mapsto \tau + \pi. \tag{2.29}$$

Equations (2.28),(2.29) show an invariance involving only parameters:

$$\alpha \mapsto -\alpha, \qquad \tau \mapsto \tau + \pi. \tag{2.30}$$

It will often be easier to consider $\cos\tau$ (instead of τ) as the delay parameter. This last invariance, equation (2.30), is then written

$$\alpha \mapsto -\alpha, \qquad \cos\tau \mapsto -\cos\tau. \tag{2.31}$$

Equation (2.31) shows that we may assume $\alpha > 0$ without loss of generality since the phase flow for a negative value of α is identical to that of the corresponding positive value of α with the sign of $\cos\tau$ reversed. Since our approximation assumes a small $\epsilon\tau$ term, considering $\cos\tau$ as our delay parameter, we expect the periodic behavior in τ to actually be incorrect (cf. [26],[45]).

2.2 In-phase Mode

Equations (2.24)-(2.26) possess the following equilibrium point which corresponds to the in-phase mode $x_1 \equiv x_2$ in (2.1)-(2.2):

$$R_1 \;=\; R_2 \;=\; 2\sqrt{1+\alpha\ \cos\tau}, \quad \phi \;=\; 0, \qquad 1+\alpha\ \cos\tau > 0. \tag{2.32}$$

The in-phase mode is also referred to as a *mixed mode* since $R_1, R_2 \neq 0,\ \phi = 0$ [2]. Notice that equations (2.32) indicate that the amplitudes R_i approach zero as $1+\alpha\cos\tau$ approaches zero, and that these amplitudes remain zero for $1+\alpha\cos\tau \leq 0$. This result is known as *amplitude death* [33],[42]. Thus the in-phase mode is

predicted to come into existence as we cross the curve $\alpha = -\frac{1}{\cos\tau}$ in the $\cos\tau - \alpha$ parameter plane. This bifurcation is accompanied by a change in stability of the trivial solution $x_1 \equiv x_2 \equiv 0$. In order to show this we must return to the original differential delay equations (2.1)-(2.2), since the slow-flow equations (2.24)-(2.26) are singular for $R_1 = R_2 = 0$. Linearizing equations (2.1)-(2.2) about the trivial solution, we may obtain the condition for a change in stability of $x_1 \equiv x_2 \equiv 0$ by assuming a solution of the form $e^{i\omega t}$. Equating real and imaginary parts of the corresponding characteristic equation, we obtain:

$$\cos\omega\tau = -\frac{1}{\alpha}, \qquad \sin\omega\tau = \frac{1-\omega^2}{\epsilon\alpha\omega}. \tag{2.33}$$

In the small ϵ limit, the second of equations (2.33) gives $\omega = 1$, and then the first of equations (2.33) gives $\alpha = -\frac{1}{\cos\tau}$, in agreement with the birth of the in-phase mode, cf. equation (2.32).

Before proceeding with the analysis of the in-phase mode, we pause to discuss a symmetry associated with it. Recall the invariance given in equation (2.27):

$$(R_1,\ R_2,\ \phi) \mapsto (R_2,\ R_1, -\phi).$$

Because the in-phase mode is given by $R_1 = R_2, \phi = 0$, we see that the in-phase mode is invariant under this transformation. This is particularly important because equilibria which bifurcate from the in-phase mode will always satisfy (2.27). That is, the behavior of one of the newly born equilibria will result in an immediate understanding of its partner, which is given by the mapping (2.27).

2.2.1 Bifurcation Curves

In order to determine the stability of the in-phase mode, we compute the Jacobian matrix of the right-hand side of (2.24)-(2.26) evaluated at the equilibrium given in equation (2.32):

$$\begin{pmatrix} \frac{1}{2} - \frac{3}{2}\,(1+\alpha\ \cos\tau) & \frac{\alpha}{2}\ \cos\tau & -\alpha\ \sin\tau\ \sqrt{1+\alpha\ \cos\tau} \\ \frac{\alpha}{2}\ \cos\tau & \frac{1}{2} - \frac{3}{2}\,(1+\alpha\ \cos\tau) & \alpha\ \sin\tau\ \sqrt{1+\alpha\ \cos\tau} \\ \frac{\alpha\ \sin\tau}{2\ \sqrt{1+\alpha\ \cos\tau}} & -\frac{\alpha\ \sin\tau}{2\ \sqrt{1+\alpha\ \cos\tau}} & -\alpha\ \cos\tau \end{pmatrix}. \quad (2.34)$$

The eigenvalues of (2.34) satisfy the characteristic equation

$$\begin{aligned} &\lambda^3 + \lambda^2\ (2 + 4\ \alpha\ \cos\tau) + \lambda\ (1 + 5\ \alpha\ \cos\tau + \alpha^2 + 4\ \alpha^2\ \cos^2\tau) \\ &\quad +(\alpha\ \cos\tau + 2\ \alpha^2\ \cos^2\tau + \alpha^2 + \alpha^3\ \cos\tau + \alpha^3\ \cos^3\tau) \ = \ 0. \end{aligned} \quad (2.35)$$

When $\lambda = 0$, equation (2.35) gives necessary conditions for generic saddle-node bifurcation curves in the $\cos\tau - \alpha$ parameter plane. The three curves we obtain are

$$\alpha = 0, \quad (2.36)$$

$$\alpha = \frac{-1}{\cos\tau}, \quad (2.37)$$

$$\alpha = \frac{-\cos\tau}{1+\cos^2\tau}. \quad (2.38)$$

In the case of equation (2.36), the original system reduces to the system

$$\ddot{x}_1 + x_1 - \epsilon\ (1 - x_1^2)\ \dot{x}_1 = 0, \quad (2.39)$$

$$\ddot{x}_2 + x_2 - \epsilon\ (1 - x_2^2)\ \dot{x}_2 = 0, \quad (2.40)$$

with $\lambda = -1$ being an eigenvalue of multiplicity two in equation (2.35). This system corresponds to the case of two uncoupled oscillators in the original system and is

not of any importance for our physical system, since we are concerned with coherent coupling.

When equation (2.37) holds, the two non-zero eigenvalues are $\lambda = 1 \pm i \tan\tau$. The R-values of the in-phase mode are given by equation (2.32), which exists only when $1 + \alpha \cos\tau > 0$. As stated above we see that the in-phase mode does not exist for points in the $\cos\tau - \alpha$ parameter plane which lie above equation (2.37). As we cross equation (2.37), the in-phase equilibrium is born.

When equation (2.38) holds, the two other eigenvalues are

$$\lambda = \frac{-1}{1+\cos^2\tau}, \frac{2\cos^2\tau - 1}{1+\cos^2\tau}, \tag{2.41}$$

and we can expect two real, distinct, non-zero eigenvalues for all but one pair of parameter values along this curve. We see that when $\cos^2\tau = \frac{1}{2}$, $\lambda = 0$ will be an eigenvalue of multiplicity two. In the parameter plane, this point is given by

$$\cos\tau = \frac{-1}{\sqrt{2}}, \ \alpha = \frac{\sqrt{2}}{3} \tag{2.42}$$

and we label it "point P." Thus point P has eigenvalues $\lambda_P = -\frac{2}{3}, 0, 0$. (We will see in Chapter 4 that a Takens-Bogdanov bifurcation actually occurs at point P.)

As we will discuss in greater detail later in this thesis, center manifold analysis along (2.38) shows the curve is a supercritical pitchfork bifurcation for

$$-1 > \cos\tau > \frac{-1}{\sqrt{3}} \tag{2.43}$$

and it is a subcritical pitchfork bifurcation for

$$\frac{-1}{\sqrt{3}} > \cos\tau > 0. \tag{2.44}$$

Another point of interest occurs where the bifurcation curve switches from a supercritical to a subcritical pitchfork. We will call this point in the parameter plane "point Q" and note that it has values

$$\cos\tau = \frac{-1}{\sqrt{3}},\ \alpha = \frac{\sqrt{3}}{4}. \tag{2.45}$$

We note that point Q has eigenvalues $\lambda_Q = -\frac{3}{4}, -\frac{1}{4}, 0$. Later we will use center manifold theory to examine the flow on the corresponding one-dimensional center manifold.

We can similarly set $\lambda = i\,\omega$ to obtain conditions necessary for a Hopf bifurcation. Omitting extraneous roots, the characteristic equation gives

$$\alpha = \frac{-1}{3\ \cos\tau}, \qquad \cos^2\tau < \frac{1}{2}. \tag{2.46}$$

Note that this curve "ends" at point P (see Figure 2.1).

Examining the τ values, we see that this Hopf bifurcation curve from the in-phase mode, equation (2.46), joins to the pitchfork bifurcation curve of the in-phase mode, equation (2.38), at point P. Point P will be examined in more detail in Chapter 4.

Equations (2.37),(2.38) and (2.46) represent stability boundaries for the in-phase mode $x_1 \equiv x_2$ in the $\cos\tau - \alpha$ parameter plane (see Figure 2.2).

These results are in agreement with numerical integration of equations (2.24)-(2.26). DsTool shows an unstable limit cycle is created as the in-phase mode goes from unstable to stable [13]. Thus the Hopf bifurcation, given by (2.46), is subcritical. The slow-flow limit cycles born in the Hopf bifurcation correspond to quasiperiodic motions in the original equations; however, since the limit cycle created in the Hopf bifurcation is unstable, it is of no practical importance in the coherent coupling

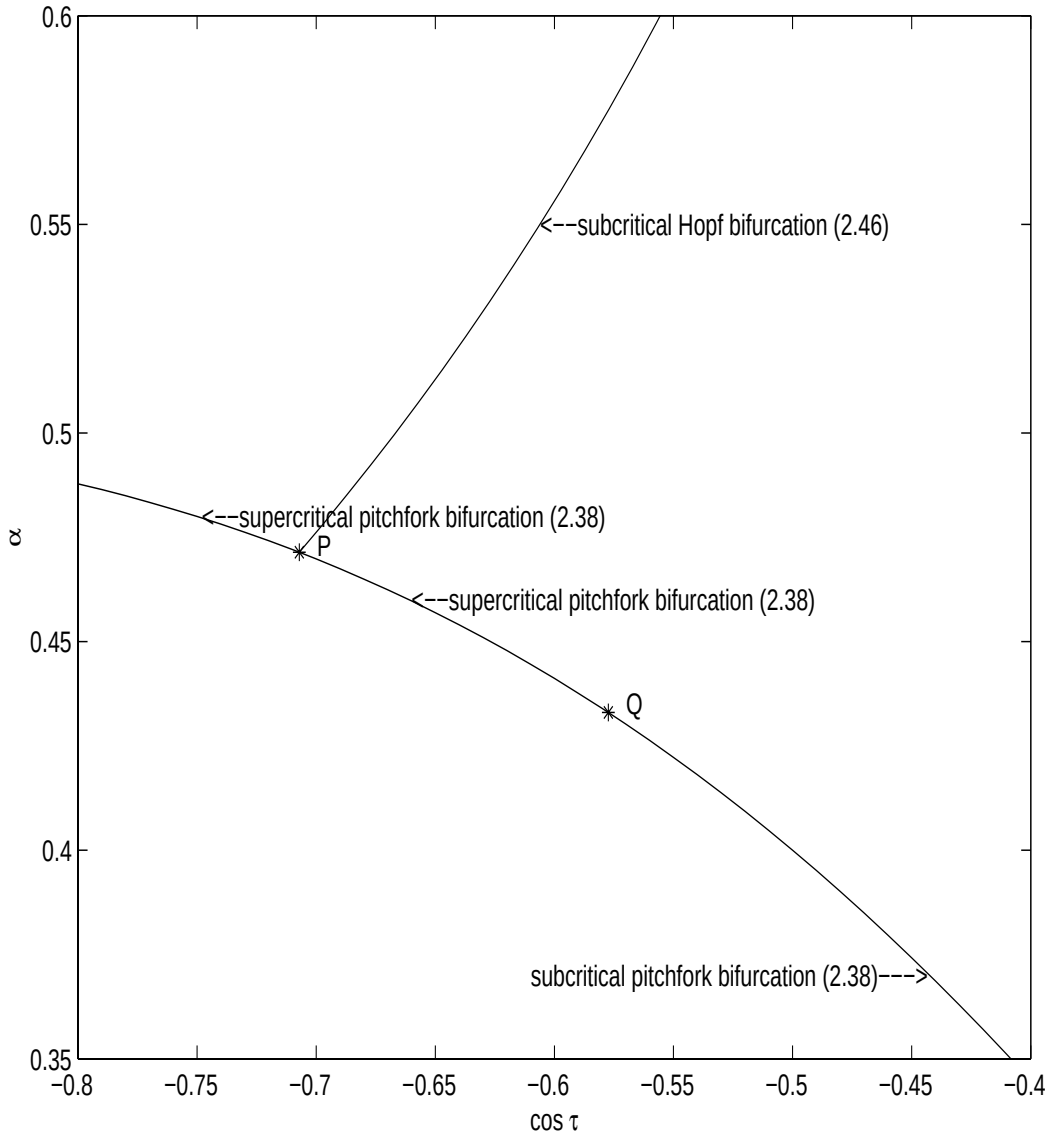

Figure 2.1: Partial bifurcation set of the in-phase mode.

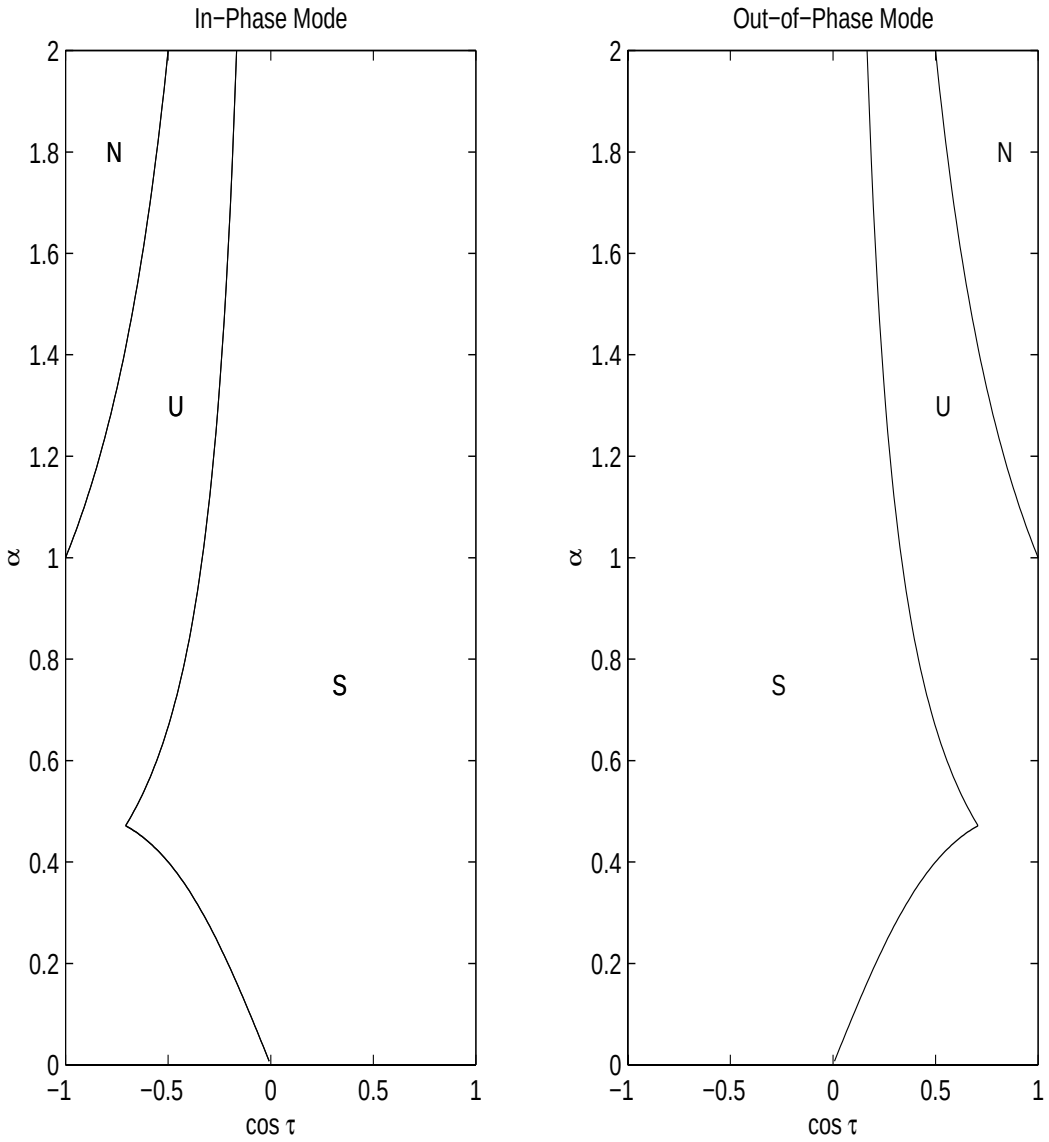

Figure 2.2: Stability of the in-phase and out-of phase modes: S=Stable, U=Unstable, N=does not exist.

of the oscillators except for the fact that its stable manifold will separate the basins of attractions of the stable fixed points. Note that quasiperiodic motion corresponds to the two oscillators varying about a periodic motion and so they are frequency locked when averaged over one cycle.

2.3 Out-of-phase Mode

In addition to the in-phase mode, equations (2.24)-(2.26) also possess an equilibrium which corresponds to the out-of-phase mode $x_1 \equiv -x_2$:

$$R_1 \;=\; R_2 \;=\; 2\,\sqrt{1-\alpha\;\cos\tau}, \quad \phi \;=\; \pi, \qquad 1-\alpha\;\cos\tau > 0. \tag{2.47}$$

The out-of-phase mode is also referred to as a *mixed mode* since $R_1, R_2 \neq 0,\ \phi = \pi$ [2]. In order to determine the stability of this mode we could proceed in an analogous fashion to that used for the in-phase mode; however, a more direct approach is available to us due to the symmetry discussed in equations (2.28)-(2.30). The out-of-phase mode (2.47) maps to the in-phase mode (2.32) under the transformation (2.29), $\phi \mapsto \phi + \pi, \tau \mapsto \tau + \pi$. But since the entire phase flow is invariant under this transformation, the stability of (2.47) is seen to be identical to that of (2.32) with the parameter change $\tau \mapsto \tau + \pi$, i.e., $\cos\tau \mapsto -\cos\tau$. That is, the out-of-phase mode has the same stability chart as the in-phase mode, reflected about the α-axis (see Figure 2.2). Thus, in the remainder of the thesis, when we examine bifurcation curves near the in-phase mode we can immediately deduce the existence of an identical curve under the parameter change $\cos\tau \mapsto -\cos\tau$. Also, in our original equations (2.1)-(2.2), the stability of the out-of-phase mode has the same

stability as the in-phase mode under the mapping $\alpha \mapsto -\alpha$ but we can conclude nothing about the stability of the two modes through the mapping $\tau \mapsto \tau + \pi$. This again indicates that the periodic behavior we detect will only be valid for the regime $\epsilon\tau << 1$.

2.4 Unsymmetrical Equilibria

2.4.1 Saddle-node Bifurcations

Having investigated the stability of the symmetrical slow-flow equilibria corresponding to the in-phase and out-of-phase modes, we now look for any other slow-flow equilibria, each of which corresponds to a periodic motion in the original equations (2.1)-(2.2). In contrast to the in-phase and out-of-phase modes, these unsymmetrical equilibria correspond to motions which are phase and frequency locked but where the phase is neither 0 nor π. These unsymmetrical equilibria are also referred to as *travelling waves* [2]. Our task is to solve equations (2.24)-(2.26) for equilibrium values of R_1, R_2 and ϕ. We solve (2.25) for R_1, substitute the result into (2.26) and solve for R_2^2. Call the result "equation A". Then we solve (2.25) for R_1 and substitute the result into (2.24), giving a polynomial on R_2^2. We substitute "equation A" into this polynomial, giving an equation with no R_1 or R_2 in it. Algebraic and trigonometric simplification of the resulting equation gives:

$$\alpha^2 \sin^2\tau \cos^4\phi + (2\ \alpha^2 \sin^2\tau - 1)\cos^2\tau \cos^2\phi + \cos^4\tau(1 + \alpha^2 \sin^2\tau) = 0. \quad (2.48)$$

Equation (2.48) is a quadratic on $\cos^2\phi$. We may obtain up to 4 real values for $\cos\phi$, corresponding to 8 equilibria in our slow-flow since each value of $\cos\phi$ has two corresponding values of ϕ; however, we only see 4 of these equilibria because 4 of them have negative R_i values. The 4 that we do see come in pairs and satisfy the symmetry given in equation (2.27).

Bifurcations of these equilibria result from setting $\cos\phi = 1$ in equation (2.48) since $\cos^2\phi \leq 1$. This gives equation (2.38) and its reflection in the symmetry (2.29). Along this curve we now have the unsymmetrical equilibria being born in addition to the in-phase mode becoming stable. Bifurcations also occur in equation (2.48) if the discriminant vanishes. This results in the condition

$$\alpha^2 = \frac{1}{8(1-\cos^2\tau)}, \qquad \cos^2\tau < \frac{1}{3}. \tag{2.49}$$

When we cross this curve in the $\cos\tau - \alpha$ plane coming from above, *two pair* of fixed points are born in a double saddle-node bifurcation. This bifurcation curve joins to the in-phase bifurcation curve equation (2.38) at point Q. That is, a saddle-node bifurcation curve for the unsymmetrical equilibria joins to the in-phase mode bifurcation curve at exactly the point where the curve switches from a supercritical pitchfork to a subcritical pitchfork bifurcation. The subcritical pitchfork bifurcation given by equation (2.38) destroys the two unstable fixed points at the same time the in-phase mode switches from stable to unstable. Trajectories which leave the neighborhood of the unstable in-phase mode are attracted to the two unsymmetrical equilibria which are present and stable.

Equation (2.49) is displayed in Figure 2.3 along with the previously obtained

bifurcation curves (2.37),(2.38),(2.46).

The total number of slow-flow equilibria in equations (2.24)-(2.26) depends on the parameters α and τ, see Figure 2.3. The maximum number is six, consisting of the in-phase mode, the out-of-phase mode, and the four additional equilibria associated with equation (2.48). Note that none of these additional equilibria can occur if the coupling α is sufficiently large.

2.4.2 Hopf Bifurcations

Numerical simulation suggests the equilibria discussed in this section undergo Hopf bifurcations in the regions marked '4' and '6' in Figure 2.3. To find this Hopf bifurcation curve analytically, we calculate the general characteristic equation from the matrix of partial derivatives obtained from the slow flow equations (2.24)-(2.26):

$$p(R_1, R_2, \phi, \tau, \alpha) = 0.$$

Using the Hopf condition $\lambda = i\,\omega$ we obtain an equation of the form

$$C_1\ \omega^3\ i + C_2\ \omega^2 + C_3\ \omega\ i + C_4 = 0 \tag{2.50}$$

where $C_i = C_i(R_1, R_2, \phi, \tau, \alpha)$. This gives two equations in ω^2 (where $\omega^2 \geq 0$). Subtract them from each other and call this equation $F(R_1, R_2, \phi, \tau, \alpha) = 0$.

We now need estimates for the values of R_1, R_2, and ϕ near the Hopf bifurcation. We solve (2.25) for R_1, substitute the result into (2.26) and solve for R_2 to obtain

$$\begin{aligned} R_1 &= \frac{\frac{1}{4}R_2^3 - R_2}{\alpha\cos(\phi-\tau)} \\ R_2 &= 2\sqrt{1+\alpha\cot(\phi-\tau)\sqrt{-\sin(\phi-\tau)\sin(\phi+\tau)}}. \end{aligned} \tag{2.51}$$

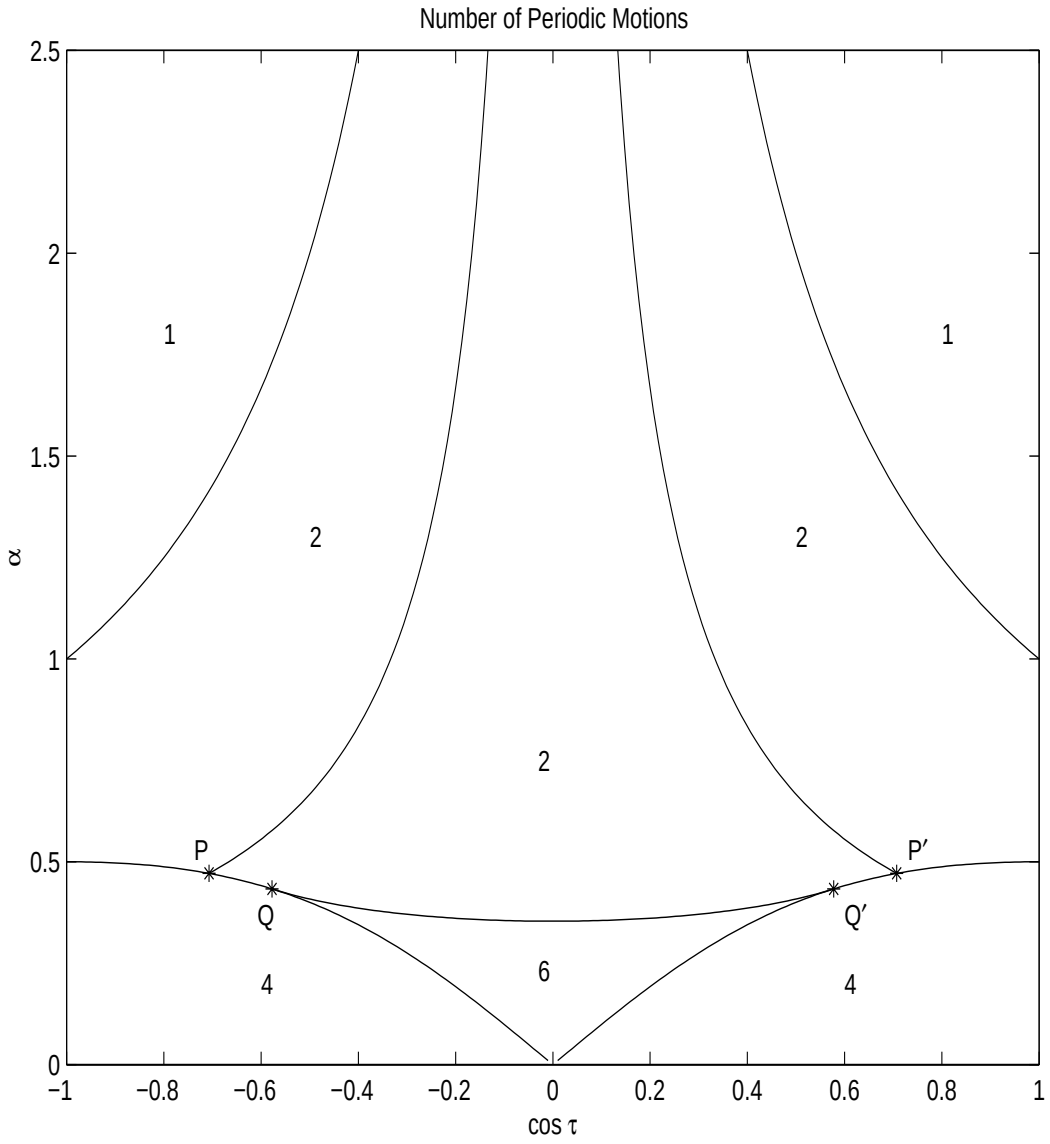

Figure 2.3: Number of periodic motions exhibited by the slow-flow (2.24)-(2.26). The displayed curves are the bifurcation equations (2.37), (2.38), (2.46), (2.48).

We can solve equation (2.48) for ϕ to obtain $\phi = H(\tau, \alpha)$.

We then substitute this solution into $F(R_1, R_2, \phi, \tau, \alpha)$ to find an expression for the Hopf bifurcation; however, due to the extreme complexity of the resulting expressions, we were not able to find a closed form condition for these Hopf bifurcations (even using the computer algebra programs MAPLE and MACSYMA [6],[25], [29]). We look for a numerical approximation for the curve as follows:

1. Fix a value for τ and find an approximate (lower) value of α.

2. Find numerical estimates for $\phi = H(\tau, \alpha)$, $R_2 = G_2(\phi, \tau, \alpha)$, and $R_1 = G_1(R_2, \phi, \tau, \alpha)$, using equations (2.48),(2.51).

3. Plug these values into the Hopf condition $F(R_1, R_2, \phi, \tau, \alpha)$ along with the current values of τ and α.

4. Evaluate. A point on the Hopf curve satisfies $F = 0$. If the value is not zero, continue to step 5.

5. Advance α a small step size. Re-evaluate $\phi = H(\tau, \alpha), R_2 = G_2(\phi, \tau, \alpha)$, and $R_1 = G_1(R_2, \phi, \tau, \alpha)$ using the new values of τ, α.

6. Repeat steps 3-5 until a switch in the sign of $F(R_1, R_2, \phi, \tau, \alpha)$ is seen.

(Alternatively, we could use Newton's method instead of steps 5 and 6 above to find the α which satisfies the equation $F = 0$.) As we cross the Hopf bifurcation curve coming from above in the $\cos\tau - \alpha$ parameter plane, two of the unsymmetrical fixed points become unstable and DsTool shows that a small stable limit cycle is born. The Hopf bifurcation is thus supercritical.

This Hopf bifurcation curve joins the previously known bifurcation curves at point P in the parameter plane. It also joins to the saddle-node bifurcation curve

of the unsymmetrical equilibria at

$$\cos\tau \approx -0.487950,\ \alpha \approx 0.405046 \tag{2.52}$$

and we will call this "point H," see Figure 2.4.

To be precise, we define H to be the one point along the double saddle-node bifurcation curve (with $-1 \leq \cos\tau \leq 0$) which has two eigenvalues satisfying $\lambda = 0$, since at all other points along the double saddle-node curve we had only one eigenvalue satisfying $\lambda = 0$. The equilibria which undergo the Hopf bifurcation have a pair of eigenvalues satisfying $\lambda_1 + \lambda_2 = 0$ where λ_1, λ_2 are pure imaginary, while the remaining eigenvalue satisfies $\lambda_3 < 0$. To the right of point H in $\cos\tau - \alpha$ space, the conditions $\lambda_1 + \lambda_2 = 0$ and $\lambda_3 < 0$ still hold (for reasons that will be explained in Chapters 5, 6); however, $\lambda_1, \lambda_2 \in \mathbf{R}$. The curve satisfying $\lambda_1 + \lambda_2 = 0$ extends from point P to its reflection about the $\alpha-$ axis, point P', and passes through point H and its reflection point H'.

This curve is approximately given by the empirical equation

$$\alpha = -0.045\cos^4\tau + 0.29\cos^2\tau + 0.33932 \tag{2.53}$$

which gives a maximum relative error of 0.35% while the equation

$$\alpha = -0.045266\cos^4\tau + 0.286920\cos^2\tau + 0.3393455 \tag{2.54}$$

gives a maximum relative error of only 0.025% where

$$0.238095 \leq \cos^2\tau \leq 0.5. \tag{2.55}$$

As mentioned above, numerical simulation has shown the resulting limit cycles to be stable. Recall these periodic slow-flow motions correspond to quasiperiodic

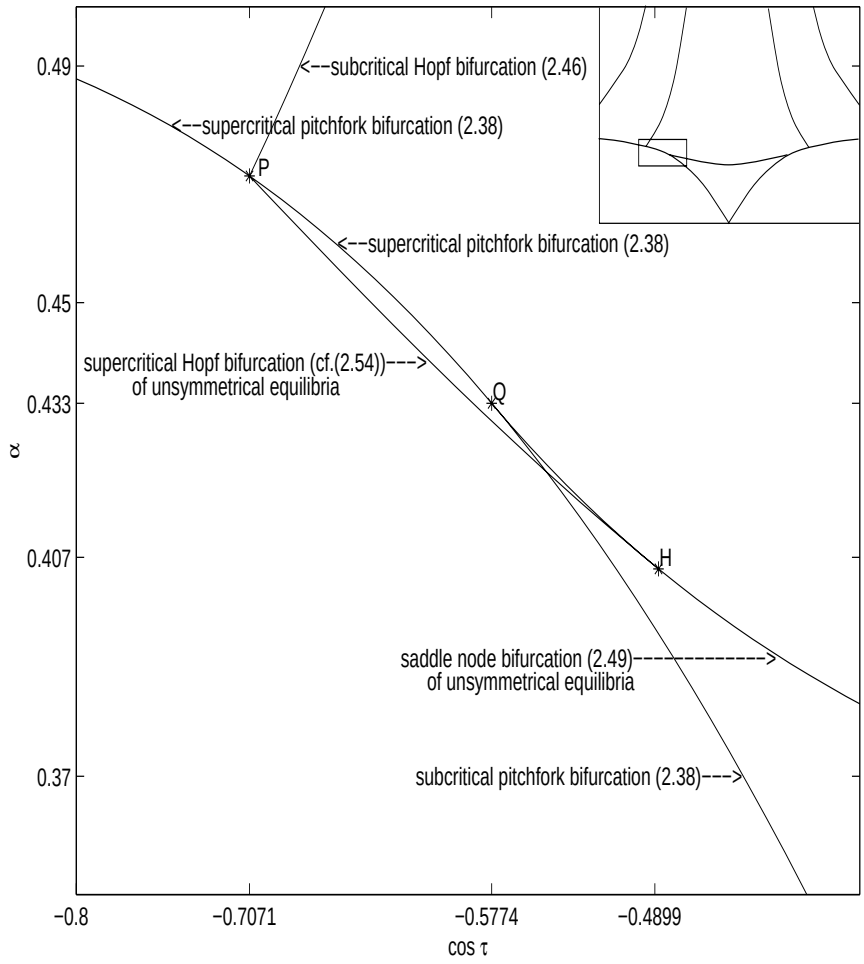

Figure 2.4: Partial bifurcation set of the in-phase and unsymmetrical modes.

motions in the original equations (2.1)-(2.2). Thus the stable limit cycles may be of some practical importance; however, these stable limit cycles only exist in a very narrow strip in parameter space. It should also be noted that although the unsymmetrical Hopf bifurcation curve (cf. equation (2.54)) crosses the in-phase mode pitchfork bifurcation curve (2.38) in the parameter plane, the intersection does not correspond to the same point in phase space; however, when the bifurcation curves of the unsymmetrical equilibria join at points P, Q, and H, the R_1, R_2, ϕ values are identical. In any case, we define the parameter plane intersection of the unsymmetrical Hopf and the in-phase mode pitchfork bifurcation curves as "point T."

2.4.3 A Brief Overview

Let us now pause to examine what we have so far. We are looking for periodic stable motions of the original system of equations (2.1)-(2.2) which are seen as stable equilibria in our slow-flow equations (2.24)-(2.26). We have found a number of bifurcation curves in the parameter plane which separate the various regions of stability for particular equilibria. There are two questions we now ask:

1. Are these the only bifurcation curves which occur?

2. What happens to the stable limit cycles born from the unsymmetrical Hopf bifurcation?

A possible approach to the first question would be to numerically check the parameter plane in order to look for any other equilibria not already found. A second possibility is to examine the degenerate points— Q, P and H—to see if any

other bifurcation curves might actually join at those points. The latter approach will also allow us to answer the second question about the fate of the limit cycles which were created. Both are done through a combination of center manifold theory and an unfolding of the points in question.

One might ask at this point for an explanation on physical grounds for examining such a narrow region (cf. Figure 2.4), especially given that the method of averaging, combined with our reduction of the infinite-dimensional problem to a finite-dimensional one already leaves us two steps removed from the original problem. Recall that we hope to find all stable periodic solutions of the original equations. In our case, stable quasiperiodicity might be equally valid and it would not do justice to the analysis to just ignore or avoid this region in parameter space because it is too small. Also our goal is to be able to describe the behavior of the system given *any* set of parameter values. Although it may or may not be desirable to be restricted to such a small range of parameter values, it may indeed be the case that our system will be affected in some way and we will be thrust either into or out of this region of space. Knowing each and every bifurcation curve is thus very important to understanding the global picture.

Chapter 3

Point Q

3.1 Introduction

Recall that point Q is defined as the point where the double saddle-node bifurcation curve (2.49) joins with the in-phase mode pitchfork bifurcation curve (2.38), which occurs at

$$\cos\tau = \frac{-1}{\sqrt{3}},\ \alpha = \frac{\sqrt{3}}{4}. \tag{3.1}$$

Since $\cos^{-1}$ is multivalued, there are actually two τ values which satisfy this condition. We will pick $0 < \tau < \pi$. Thus as τ increases, $\cos\tau$ will decrease. When comparing our $\tau - \alpha$ parameter plane picture with the $\cos\tau - \alpha$ parameter plane picture, we must remember that the bifurcation curves will be reflections of each other about the line $\tau = \pi$.

We expect a pitchfork bifurcation to switch from supercritical to subcritical at point Q. In particular, we know that we must have one eigenvalue satisfying $\lambda = 0$.

We state the following theorem which tells us that our analysis can be carried out at point Q on a one-dimensional manifold, the center manifold:

Theorem 3.1.1 (Center Manifold Theorem [12],[27]) *Let f be a C^r vector field on $\mathbf{R^n}$ which satisfies $f(0) = 0$ and suppose that $A = Df(0)$ has k eigenvalues satisfying $Re(\lambda) < 0$, j eigenvalues satisfying $Re(\lambda) > 0$, and the remaining $m = n - k - j$ eigenvalues satisfying $Re(\lambda) = 0$. Let E^s, E^c, E^u denote the generalized stable, center, and unstable eigenspaces, respectively. Then there exists an m-dimensional C^{r-1} center manifold W^c tangent to E^c at 0 and C^r stable and unstable invariant manifolds W^s and W^u tangent to E^s and E^u. The manifolds W^s, W^c, W^u are all invariant for the flow f.*

We note that we cannot simply project our original system onto the linear subspace spanned by E^c if we want to capture the correct qualitative behavior [12]. To show how the above theorem comes into play, consider the following system already in eigencoordinates

$$\begin{aligned} \dot{x} &= Ax + g_1(x, y, z) \\ \dot{y} &= By + g_2(x, y, z) \end{aligned} \tag{3.2}$$

where $x \in \mathbf{R^k}$, $y \in \mathbf{R^m}$, A is a k-by-k matrix whose eigenvalues have negative real part, B is an m-by-m matrix whose eigenvalues have zero real part, and $g_1(0) = g_2(0) = Dg_1(0) = Dg_2(0) = 0$. From Theorem 3.1.1, we know the center manifold is tangent to the center eigenspace, E^c and so we can represent it locally as a graph [4],[12]:

$$W^c = \{(x, y) |\ x = h(y)\},\ h(0) = Dh(0) = 0, \tag{3.3}$$

where $h : \mathbf{R^m} \mapsto \mathbf{R^k}$ is defined on some neighborhood of the origin. If we now consider the projection of the vector field on $x = h(y)$ onto E^c, we obtain

$$\dot{y} = By + g_2(h(y), y). \tag{3.4}$$

The remarkable conclusion is that all the essential behavior of the system (3.2) in the neighborhood of the origin, will be captured by (3.4). In particular, we have the following theorem:

Theorem 3.1.2 ([4],[12]) *If the origin of (3.4) is stable (unstable), then the origin of (3.2) is also stable (unstable).*

These theorems will be used in our analysis of point Q, but we take one more detour and examine exactly what behavior we expect at point Q, where our pitchfork bifurcation switches from supercritical to subcritical. The normal form for a supercritical pitchfork bifurcation is

$$\dot{z} = r\ z - z^3 \tag{3.5}$$

and the normal form for a subcritical pitchfork bifurcation is

$$\dot{z} = r\ z + z^3. \tag{3.6}$$

Since these equations model a physical system and because the symmetry associated with (2.27) will take the form $z \mapsto -z$ on the one-dimensional center manifold, we expect the instability of the subcritical pitchfork to be countered by some stabilizing force of $O(z^5)$ or higher [41]. That is, we expect the normal form for the subcritical pitchfork to actually be

$$\dot{z} = r\ z + z^3 - z^5. \tag{3.7}$$

We expect very degenerate behavior at this point since the cubic term in the normal form switches from negative to positive as the bifurcation switches from supercritical to subcritical. We can see this better by inserting another parameter p into the system. Thus in order for the bifurcation to go from a supercritical pitchfork to a subcritical pitchfork, the parameter p in the normal form

$$\dot{z} = r\ z + p\ z^3 \tag{3.8}$$

must switch from negative to positive. And in order for us to see this switch, we will need to keep terms of $O(z^5)$ and thus we will expect the normal form

$$\dot{z} = r\ z + p\ z^3 - z^5. \tag{3.9}$$

This will be useful to remember as we examine point Q in more detail.

3.2 Linearization

From the previous discussion of the in-phase mode, we can calculate the eigenvalues at point Q. It is important to note that one of the eigenvalues is zero while the other two are negative. As stated in Section 3.1, the Center Manifold Theorem tells us that we can expect a one-dimensional center manifold to capture the essential behavior of the system. We begin with the three slow-flow equations (2.24)-(2.26) and linearize about the in-phase mode equilibrium at point Q

$$R_1 = R_2 = 2\ \sqrt{1 + \alpha\ \cos\tau} = \sqrt{3}, \qquad \phi = 0. \tag{3.10}$$

To make this explicit, we let

$$R_1 \ = \ \sqrt{3} + x, \tag{3.11}$$

$$R_2 = \sqrt{3} + y, \tag{3.12}$$

$$\phi = z. \tag{3.13}$$

We can do the center manifold analysis in any coordinates but the calculations are easier if we switch to eigencoordinates. We can easily obtain the eigenvalues from (2.41) but since we also need the eigenvectors, we proceed with the linearization. The coordinates x, y, z are physical coordinates which are local about point Q. Substituting equations (3.11)-(3.13) into the slow-flow equations (2.24)-(2.26), setting $\mu = \nu = 0$ and ignoring higher order terms, we find that

$$\frac{d}{dt}\begin{pmatrix} x \\ y \\ z \end{pmatrix} = A\begin{pmatrix} x \\ y \\ z \end{pmatrix} \tag{3.14}$$

where

$$A = \begin{pmatrix} \frac{-5}{8} & \frac{-1}{8} & \frac{-\sqrt{6}}{8} \\ \frac{-1}{8} & \frac{-5}{8} & \frac{\sqrt{6}}{8} \\ \frac{\sqrt{6}}{12} & \frac{-\sqrt{6}}{12} & \frac{1}{4} \end{pmatrix}. \tag{3.15}$$

We then calculate the eigenvalues of A as

$$\lambda_1 = \frac{-3}{4}, \quad \lambda_2 = \frac{-1}{4}, \quad \lambda_3 = 0$$

with corresponding eigenvectors v_1, v_2, v_3. Let $\Lambda = (v_1 \quad v_2 \quad v_3)$ be the matrix with the eigenvectors as its columns.

We could proceed with the analysis of point Q in the physical x, y, z coordinates but since we have one zero eigenvalue, it will be useful to rotate to eigencoordinates before using center manifold theory to examine the behavior of the system.

Thus we seek expressions for the eigencoordinates, (x_1, y_1, z_1), which are defined by the equation

$$\begin{pmatrix} x \\ y \\ z \end{pmatrix} = \Lambda \begin{pmatrix} x_1 \\ y_1 \\ z_1 \end{pmatrix} \tag{3.16}$$

where

$$\Lambda = \begin{pmatrix} 1 & -\frac{\sqrt{6}}{2} & -1 \\ 1 & \frac{\sqrt{6}}{2} & 1 \\ 0 & 1 & \frac{2\sqrt{6}}{3} \end{pmatrix}. \tag{3.17}$$

We substitute these values of x, y, z into (3.14). We solve for $\dot{x}_1, \dot{y}_1, \dot{z}_1$ and Taylor expand the expressions, keeping quadratic terms in μ, ν and quintic terms in x_1, y_1, z_1 (cf.(3.7)). This will allow us to obtain the flow in terms of the eigencoordinates.

Since we want to unfold point Q, we will also make the substitution

$$\begin{aligned} \tau &= \cos^{-1}\left(\frac{-1}{\sqrt{3}}\right) + \nu \\ \alpha &= \frac{\sqrt{3}}{4} + \mu \end{aligned} \tag{3.18}$$

into the previous result. As mentioned above, we take $0 < \tau < \pi$ so that an increase in τ implies a decrease in $\cos\tau$. This will allow for a local analysis about point Q in the parameter plane.

Before continuing, we note that the expressions of the two curves coming into point Q are

$$\begin{aligned} \alpha &= \frac{-\cos\tau}{1+\cos^2\tau}, \\ \alpha^2 &= \frac{1}{8(1-\cos^2\tau)}, \qquad \cos^2\tau < \frac{1}{3} \end{aligned}$$

where the first of these equations is the in-phase mode bifurcation curve (2.38) and the second is from the double saddle-node bifurcation curve (2.49). Thus we can examine the corresponding expressions in terms of the local parameter coordinates, μ and ν. Since the slope of each curve is the same at point Q, when we substitute (3.18), we need to keep quadratic terms in μ, ν in our Taylor expansion. We obtain

$$\mu = \frac{\sqrt{6}}{8}\nu - \frac{5\sqrt{3}}{16}\nu^2 + O(\nu^3) \tag{3.19}$$

$$\mu = \frac{\sqrt{6}}{8}\nu + \frac{\sqrt{3}}{4}\nu^2 + O(\nu^3) \tag{3.20}$$

for the in-phase and double saddle-node local bifurcation curves, respectively. Knowing these expressions will provide a check on our unfolding calculation, which will in addition permit us to see if there are any other bifurcations at point Q.

3.3 Unfolding Q

To begin the unfolding, we start with the three differential equations in terms of the eigencoordinates x_1, y_1, z_1. We substitute in equations (3.18) and obtain three equations:

$$\dot{x}_1 = G_1(x_1, y_1, z_1, \mu, \nu) \tag{3.21}$$

$$\dot{y}_1 = G_2(x_1, y_1, z_1, \mu, \nu) \tag{3.22}$$

$$\dot{z}_1 = G_3(x_1, y_1, z_1, \mu, \nu), \tag{3.23}$$

where $x_1, y_1 \in W^s, z_1 \in W^c$ at the bifurcation point (cf. Theorem 3.1.1). We know the center manifold, W^c, is tangent to E^c and thus can locally be represented as a

graph. Recall that the flow on the center manifold is going to be given by a one-dimensional equation. In our case, this equation involves only z_1 and will be given by equation (3.23) once we have expressions for the center manifold, i.e., once we have x_1, y_1 in terms of z_1. We need to assume an appropriate form for the center manifold in order to express x_1 and y_1 in terms of z_1. The fact that we want to keep quintic terms in the eigencoordinates and quadratic terms in μ, ν leads us to assume a center manifold of the form

$$\begin{aligned} x_{1,cm} &= a_1\ z_1^4 + (a_2 + a_3\ \mu + a_4\ \nu + a_5\ \mu\ \nu + a_6\ \mu^2 + a_7\ \nu^2) z_1^3 \\ &+ (a_8 + a_9\ \mu + a_{10}\ \nu + a_{11}\ \mu\ \nu + a_{12}\ \mu^2 + a_{13}\ \nu^2) z_1^2 \\ &+ (a_{15}\ \mu + a_{16}\ \nu + a_{17}\ \mu\ \nu + a_{18}\ \mu^2 + a_{19}\ \nu^2) z_1 \\ &+ (a_{21}\ \mu + a_{22}\ \nu + a_{23}\ \mu\ \nu + a_{24}\ \mu^2 + a_{25}\ \nu^2) \end{aligned} \tag{3.24}$$

for x_1 and a similar form for $y_{1,cm}$. Comparing with (3.3), we see that the center manifold will be given by

$$W^c = \{x_1, y_1, z_1) |\ x_1 = h_1(z_1), y_1 = h_2(z_1)\} \tag{3.25}$$

where $h_i : \mathbf{R} \mapsto \mathbf{R}$ with $h_1(0) = h_2(0) = Dh_1(0) = Dh_2(0)$. (Here $h_1(z_1) = x_{1,cm}, h_2(z_1) = y_{1,cm}$ and $a_{14} = a_{20} = 0$ in (3.24) to avoid any $O(1)$ translation in the linear or constant terms.) We substitute these equations into the differential equations (3.21)-(3.22). This will introduce $\dot{z}_1$ terms after the differentiation is carried out. We then substitute in equation (3.23) which reintroduces x_1, y_1 into the equations but rids the equations of any $\dot{x}_1, \dot{y}_1, \dot{z}_1$ terms. One more substitution of equation (3.24) and the corresponding $y_{1,cm}$ equation into the new versions of (3.21)-(3.22) gives two equations which only have z_1 terms. For each equation, we move

all terms to one side and Taylor expand the expressions, keeping quadratic terms in μ, ν and quintic terms in z_1. We then have two equations, $\tilde{G}_1(z_1, \mu, \nu) = 0$ and $\tilde{G}_2(z_1, \mu, \nu) = 0$, and we compare $\tilde{G}_1$ with the assumed form of the center manifold, equation (3.24), since we want an expression for $x_{1,cm}, y_{1,cm}$ which is valid at the equilibrium point. We then do a similar comparison for $\tilde{G}_2$. This allows us to obtain the coefficients of $x_{1,cm}, y_{1,cm}$. We find that

$$\begin{aligned}
x_{1,cm} &= -\frac{43\sqrt{3}}{24}\, z_1^4 - \frac{\sqrt{3}}{2} z_1^2 \\
&+ \left(\frac{-311}{9}\mu + \frac{61\sqrt{6}}{36}\,\nu + \frac{1195\sqrt{2}}{18}\,\mu\nu - \frac{13639\sqrt{3}}{27}\,\mu^2 + \frac{41\sqrt{3}}{9}\,\nu^2\right) z_1^2 \\
y_{1,cm} &= \frac{13}{9} z_1^3 \\
&+ \left(\frac{11294\sqrt{3}}{81}\,\mu - \frac{547\sqrt{2}}{27}\,\nu - \frac{178954\sqrt{6}}{243}\,\mu\nu + \frac{3252502}{243}\,\mu^2 - \frac{2083}{81}\,\nu^2\right) z_1^3 \\
&+ \left(\frac{92\sqrt{3}}{9}\,\mu - \frac{4\sqrt{2}}{3}\,\nu - \frac{112\sqrt{6}}{27}\,\mu\nu + \frac{7684}{27}\,\mu^2 - \frac{55}{9}\,\nu^2\right) z_1. \qquad (3.26)
\end{aligned}$$

Now that we have expressions for the center manifold, we substitute (3.26) into (3.23). The resulting equation describes the flow on the center manifold. We obtain the following expression:

$$\begin{aligned}
\dot{z}_1 &= -\,2z_1^5 \\
&+ \left(\frac{2788123\sqrt{3}}{19440}\mu - \frac{94267\sqrt{2}}{5184}\nu - \frac{35604121\sqrt{6}}{38880}\mu\nu + \frac{360207083}{19440}\mu^2 - \frac{47251}{1080}\nu^2\right) z_1^5 \\
&+ \left(\frac{-400\sqrt{3}}{27}\,\mu + \frac{23\sqrt{2}}{9}\,\nu + \frac{1154\sqrt{6}}{9}\,\mu\nu - \frac{45520}{27}\,\mu^2 - \frac{15}{2}\,\nu^2\right) z_1^3 \\
&+ \left(\frac{-4\sqrt{3}}{3}\,\mu + \frac{\sqrt{2}}{2}\,\nu + \frac{10\sqrt{6}}{3}\,\mu\nu - \frac{128}{3}\,\mu^2 + \frac{1}{4}\,\nu^2\right) z_1. \qquad (3.27)
\end{aligned}$$

We now want to examine the bifurcations of equation (3.27). We note that the first $O(1)$ term in μ, ν appears in the z_1^5 term (cf. equation (3.9)). We can factor

out the root $z_1 = 0$ (which corresponds to the in-phase mode) and we are left with a fourth order polynomial on z_1. We will have bifurcations associated with this. If we consider equation (3.27) as a quadratic on z_1^2, the first bifurcation will correspond to the condition for the existence of four real roots of this equation and so we need both roots of z_1^2 to be nonnegative. Thus this bifurcation will occur when $z_1^2 = 0$. From this we recover (3.19) and no new equations. We note that the saddle-node bifurcation will not occur when $z_1^2 < 0$. To leading order, we find that $z_1^2 = -\frac{3\sqrt{2}}{4}\nu$ and thus we need $\nu < 0$. That is, our saddle-node bifurcation curve is a one-sided curve (which checks with what we expected from equation (2.49)). The second bifurcation occurs when the discriminant of z_1^2 vanishes. This results in (3.20), see Figure 3.1.

Since we only want to consider real roots, these are the only bifurcation curves which result. Thus the unfolding at Q confirms what we expected from the larger picture in the parameter plane, see Figure 3.2.

If we rewrite (3.27) as $\dot{z}_1 = r\ z_1 + p\ z_1^3 - 2z_1^5$, we see that p switches sign as we go through the point Q along the in-phase pitchfork bifurcation curve, given by (3.19). We thus see that we do indeed switch from a supercritical to a subcritical pitchfork at point Q.

3.4 Bifurcation Sequence Near Point Q

Note that our unfolding was done locally about point Q. A little below and to the left of point Q (in the $\cos\tau - \alpha$ parameter plane), DsTool reveals that we have

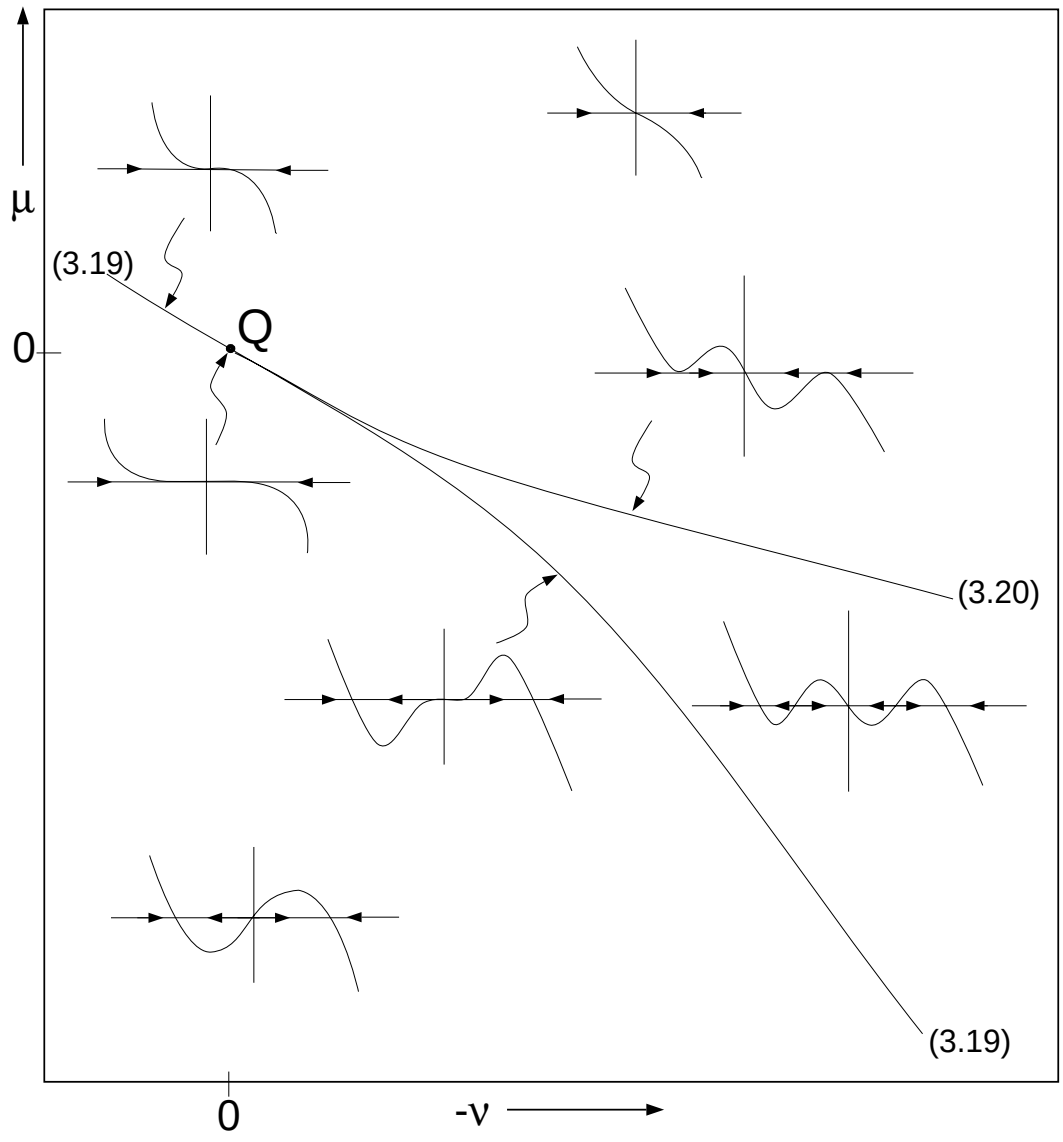

Figure 3.1: Bifurcation set in the neighborhood of point Q. Flows are on the line since we have a one-dimensional center manifold. Note that the bifurcation curves near point Q are drawn slightly distorted for better viewing.

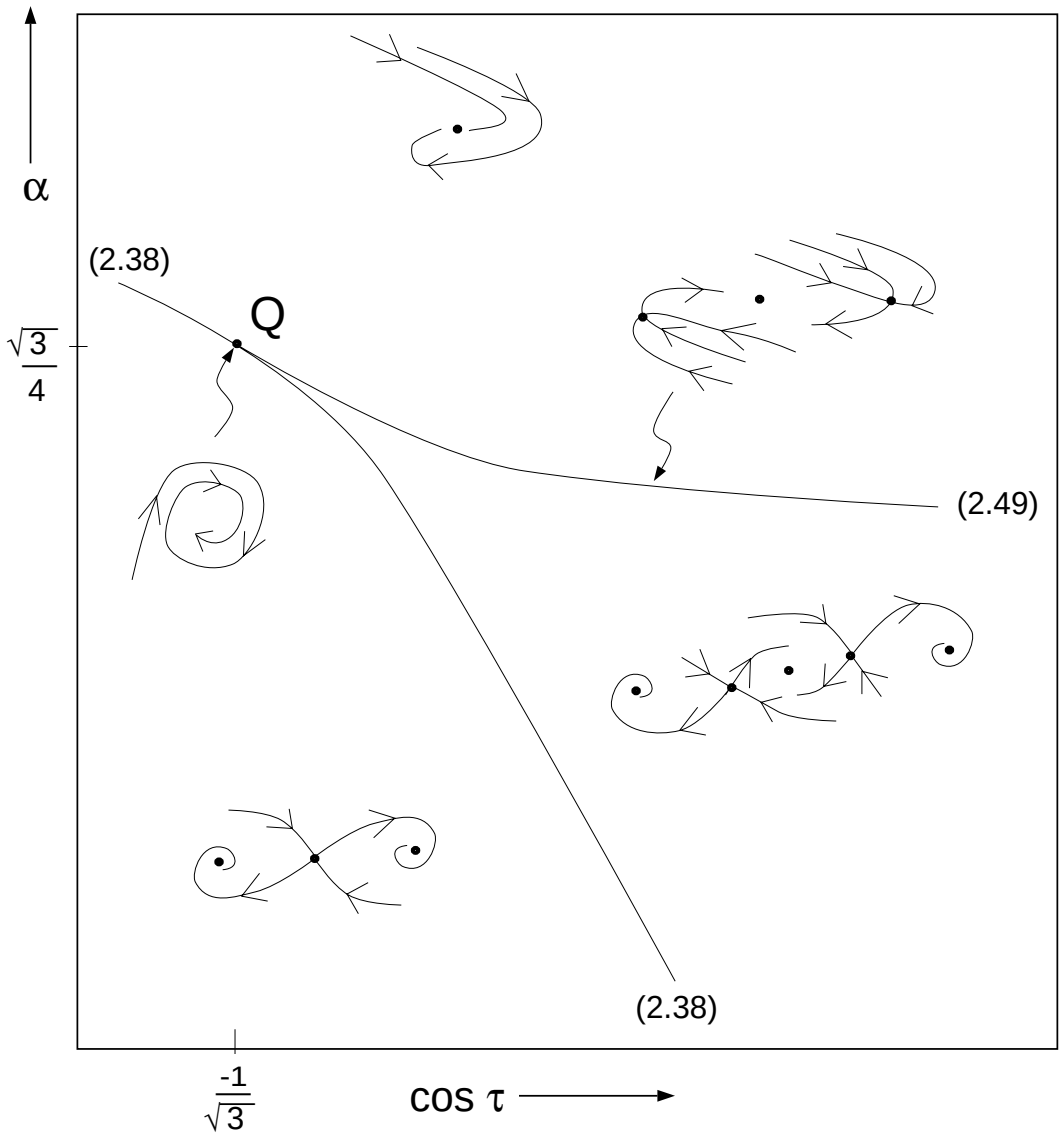

Figure 3.2: Phase portraits corresponding to Figure 3.1. Note that the third eigendirection is contracting and comes into the plane of this page (nearly normal). Also, the bifurcation curves near point Q are drawn slightly distorted for better viewing.

a supercritical Hopf bifurcation and below this curve stable limit cycles surround the two unsymmetrical equilibria. Examining the phase portraits for fixed τ while lowering α shows the existence of a symmetry breaking homoclinic bifuration during which the two stable limit cycles both join at the in-phase mode in a double homoclinic loop and then form a large stable limit cycle, see Figure 3.3.

But throughout this entire bifurcation sequence, the unstable limit cycle created in the in-phase mode Hopf bifurcation surrounds the in-phase mode and all the unsymmetrical equilibria, while the out-of-phase mode exists far away from all these bifurcations. This observation is crucial because for slightly lower values of α, no limit cycles exist and we deduce the existence of a limit cycle fold along which the stable and unstable limit cycles coalesce. This bifurcation sequence is given in Figure 3.3. We note that the pictures in Figure 3.3 are drawn as if they are two-dimensional even though they are in fact three-dimensional. This is because numerical simulation of the slow-flow equations (2.24)-(2.26) indicates that all trajectories are quickly drawn onto a somewhat curved two-dimensional surface on which the dynamics shown in the figure occur. The same situation occurs near points P and H and thus all of our drawings near those points will also be shown as two-dimensional. We can also examine a bifurcation diagram by encircling point Q, see Figure 3.4.

The bifurcation sequence occurring to the right of point Q is more intricate and will be discussed in Chapter 5 during the discussion of point H.

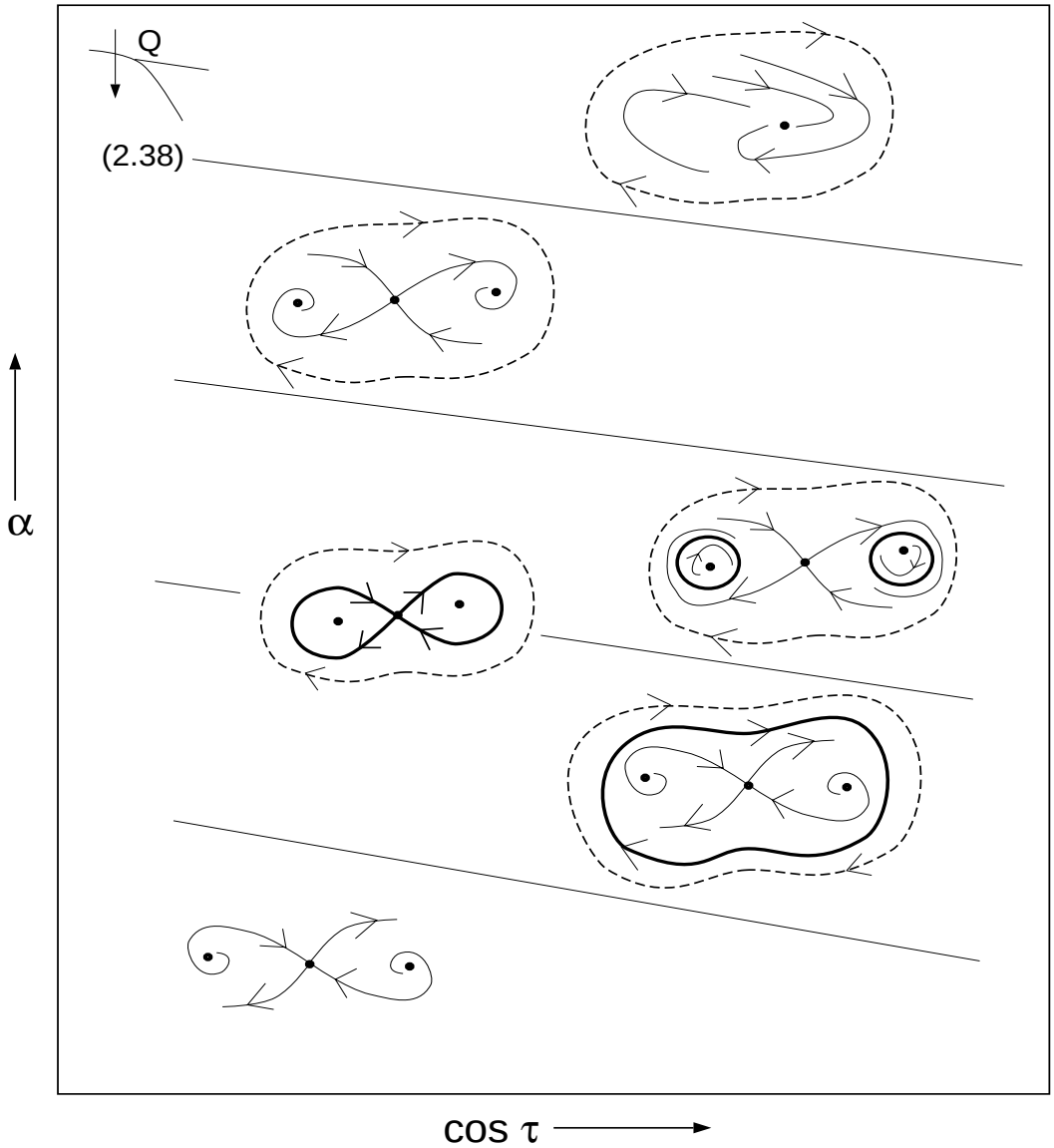

Figure 3.3: Bifurcation sequence observed numerically to the left of point Q in the $\cos\tau - \alpha$ parameter plane. Note that the out-of-phase mode exists throughout, but far away from, this sequence. Also, the third eigendirection is contracting and comes into the plane of this page (nearly normal).

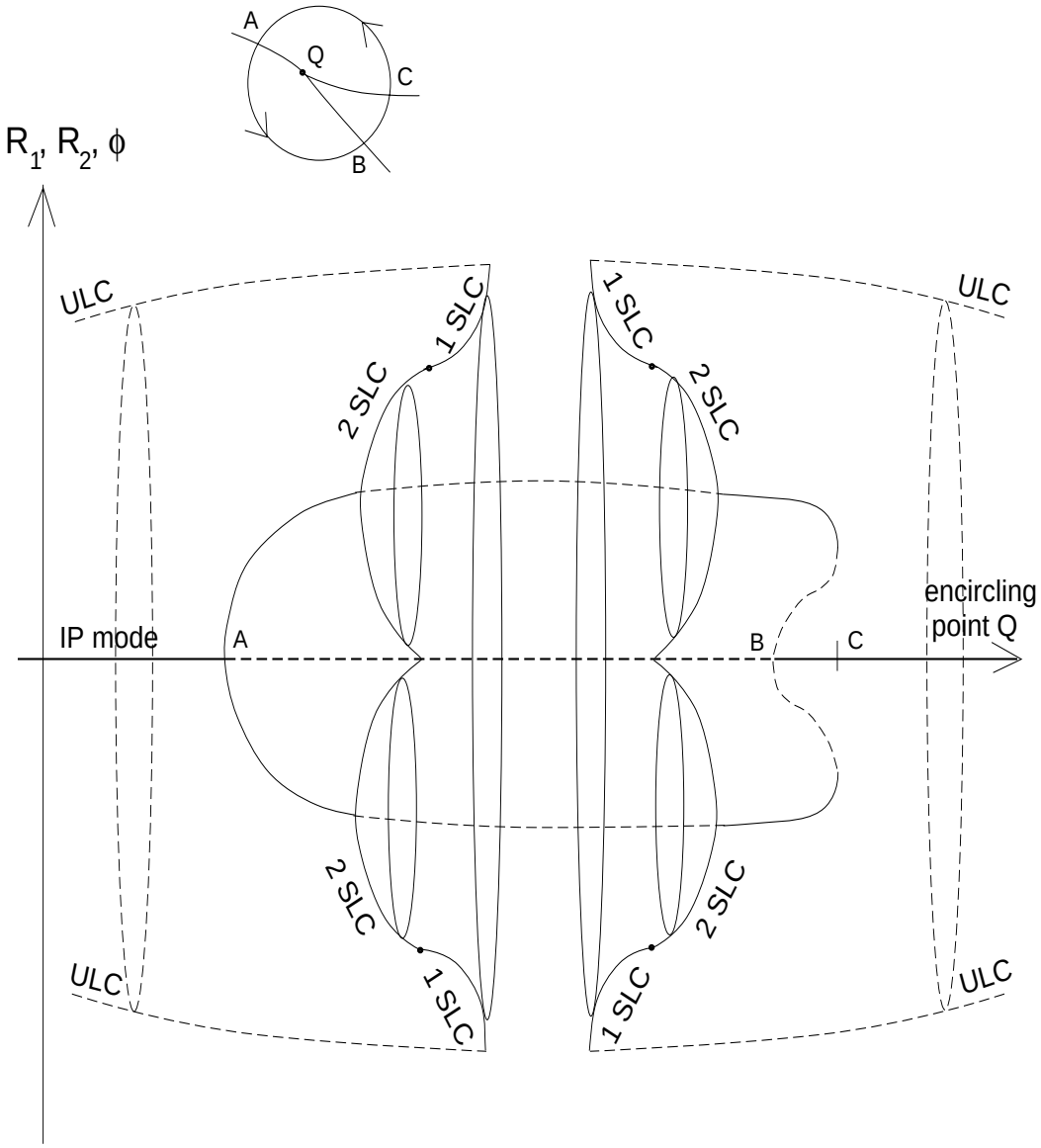

Figure 3.4: Bifurcation diagram encircling point Q. Note that stable and unstable limit cycles (SLC and ULC, respectively) are shown. The solid lines represent stability and the dashed lines instability.

Chapter 4

Point P

4.1 Introduction

Recall point P is defined as the point where the in-phase Hopf bifurcation curve (2.46) and the in-phase pitchfork bifurcation curve (2.38) join together:

$$\cos\tau = \frac{-1}{\sqrt{2}},\ \alpha = \frac{\sqrt{2}}{3}. \tag{4.1}$$

In examining point P, we will again pick the root which satisfies $0 < \tau < \pi$.

Because two of the eigenvalues are zero, the Center Manifold Theorem (Theorem 3.1.1) tells us that we will have a two-dimensional center manifold which will capture the behavior of the full three-dimensional system. The corresponding linear system at point P has two possibilities

$$\frac{d}{dt}\begin{pmatrix} y \\ z \end{pmatrix} = \begin{pmatrix} 0 & 0 \\ 0 & 0 \end{pmatrix}\begin{pmatrix} y \\ z \end{pmatrix} \quad \text{or} \quad \frac{d}{dt}\begin{pmatrix} y \\ z \end{pmatrix} = \begin{pmatrix} 0 & 1 \\ 0 & 0 \end{pmatrix}\begin{pmatrix} y \\ z \end{pmatrix}.$$

The first of these is the trivial case where there exist two linear independent eigenvectors. We will see in the next section that the second case actually occurs at point P. This case corresponds to the case of only one linearly independent eigenvector. Thus our linear system is not diagonalizable. We seek the next best thing—the Jordan canonical form [17],[27]. (We give a brief review of Jordan form in the remainder of this section.) For any n-by-n matrix A, there exists an invertible matrix R such that $R^{-1}AR = J$ where J is in block diagonal form. The number of blocks in J correspond to the number of eigenvectors possessed by A. Thus

$$J = \begin{pmatrix} J_1 & 0 & \cdots & 0 \\ 0 & J_2 & \cdots & 0 \\ \vdots & \vdots & \ddots & \vdots \\ 0 & 0 & \cdots & J_m \end{pmatrix} \tag{4.2}$$

where A has m linearly independent eigenvectors. The diagonal of each block J_i has the eigenvalue corresponding to that eigenvector and the superdiagonal has the entry 1. That is,

$$J_i = \begin{pmatrix} \lambda & 1 & \cdots & 0 \\ 0 & \lambda & \ddots & \vdots \\ \vdots & & \ddots & 1 \\ 0 & 0 & \cdots & \lambda \end{pmatrix}.$$

In the case when A is diagonalizable, we see that each block is of size 1-by-1 and the matrix J is just the matrix A in eigencoordinates; however, when A does not possess a full set of eigenvectors, we must construct a set of *generalized* eigenvectors from the known ones. In doing so we will construct our matrix R.

We let v be an eigenvector corresponding to the eigenvalue λ. We seek *chain vectors* u_i that satisfy $(A - \lambda I)u_{i+1} = u_i$ for $i \geq 1$, where $u_1 \equiv v$. When we reach an integer n such that $(A - \lambda I)u_{n+1} = u_n$ cannot be solved, we stop. The set of vectors

$$S = \{v, u_2, u_3, \ldots, u_n\} \tag{4.3}$$

are the generalized eigenvectors corresponding to λ. The number of generalized eigenvectors in S indicate the size of the Jordan block corresponding to λ. This process is repeated with the remaining eigenvalues until a full set of generalized eigenvectors are found. The vectors in this set S then form the columns of R.

4.2 Linearization

We again begin with the three slow-flow equations (2.24)-(2.26) and linearize about the in-phase equilibrium point

$$R_1 = R_2 = 2\sqrt{1 + \alpha\ \cos\tau} = \frac{2}{3}\sqrt{6}, \qquad \phi = 0. \tag{4.4}$$

Thus, we let

$$R_1 = \frac{2}{3}\sqrt{6} + x, \tag{4.5}$$

$$R_2 = \frac{2}{3}\sqrt{6} + y, \tag{4.6}$$

$$\phi = 0 + z. \tag{4.7}$$

The coordinates x, y, z are now local about point P. Substituting (4.5)-(4.7) into the slow-flow equations (2.24)-(2.26), setting $\mu = \nu = 0$ and ignoring higher order

terms, we obtain

$$\frac{d}{dt}\begin{pmatrix} x \\ y \\ z \end{pmatrix} = A\begin{pmatrix} x \\ y \\ z \end{pmatrix} \tag{4.8}$$

where we now have

$$A = \begin{pmatrix} \frac{-1}{2} & \frac{-1}{6} & \frac{-\sqrt{6}}{9} \\ \frac{-1}{6} & \frac{-1}{2} & \frac{\sqrt{6}}{9} \\ \frac{\sqrt{6}}{12} & \frac{-\sqrt{6}}{12} & \frac{1}{3} \end{pmatrix}.$$

We find the eigenvalues of A are

$$\lambda_1 = \frac{-2}{3}, \quad \lambda_2 = 0, \quad \lambda_3 = 0.$$

Recall that the Center Manifold Theorem (Theorem 3.1.1) tells us that studying the flow of equations (2.24)-(2.26) at point P can be reduced to studying the flow on a two-dimensional center manifold which is tangent to E^c, while still capturing the essential behavior of the system. We thus need to again rotate to the appropriate coordinates. A simple calculation shows that A does not have a full set of eigenvectors and thus is not diagonalizable; however, we know there exists two distinct eigenvalues and the eigenvalue $\lambda = 0$ posseses only one eigenvector. Thus we find the generalized eigenvector by the above process. One possible choice is $u_2 = (3, \ -3, \ 0)$. Then R is of the form

$$R = \begin{pmatrix} 1 & -1 & 3 \\ 1 & 1 & -3 \\ 0 & \frac{\sqrt{6}}{2} & 0 \end{pmatrix} \tag{4.9}$$

and thus

$$R^{-1}AR = J = \begin{pmatrix} -\frac{2}{3} & 0 & 0 \\ 0 & 0 & 1 \\ 0 & 0 & 0 \end{pmatrix}. \tag{4.10}$$

Comparing with the previously discussed theory, we see that there are two Jordan blocks —the 1-by-1 block with eigenvalue $\lambda = -\frac{2}{3}$ corresponding to the stable eigenvalue and the 2-by-2 block $\begin{pmatrix} 0 & 1 \\ 0 & 0 \end{pmatrix}$ corresponding to the double zero eigenvalue.

Now possessing a full set of generalized eigenvectors, we can proceed. We let the generalized eigenvectors be denoted v_1, v_2, v_3 and we obtain our R (the same as that in (4.9)) by defining $R = (v_1 \quad v_2 \quad v_3)$. The coordinates corresponding to Jordan canonical form, (x_1, y_1, z_1), are then defined by the equation

$$\begin{pmatrix} x \\ y \\ z \end{pmatrix} = R \begin{pmatrix} x_1 \\ y_1 \\ z_1 \end{pmatrix}.$$

We substitute these values of x, y, z into (4.8). We solve for $\dot{x}_1, \dot{y}_1, \dot{z}_1$ and Taylor expand the expressions, keeping quadratic terms in μ, ν and cubic terms in x_1, y_1, z_1. This will allow us to obtain the flow on the center manifold in terms of the eigencoordinates.

Since we want to unfold point P, we will also make the substitution

$$\begin{aligned} \tau &= \cos^{-1}\left(\frac{-1}{\sqrt{2}}\right) + \nu \\ \alpha &= \frac{\sqrt{2}}{3} + \mu \end{aligned} \tag{4.11}$$

into the previous result. We again take $0 < \tau < \pi$ so that an increase in τ implies a decrease in $\cos\tau$. Unlike with the unfolding of Q, however, we do not have analytic expressions for all the bifurcation curves emanating from point P. We are able to calculate two of the expected curves as

$$\begin{aligned} \alpha &= \frac{-\cos\tau}{1+\cos^2\tau}, \\ \alpha &= -\frac{1}{3\ \cos\tau}, \qquad \cos^2\tau < \frac{1}{2} \end{aligned}$$

where the first corresponds to the in-phase pitchfork bifurcation curve (2.38) and the second to the in-phase Hopf bifurcation curve (2.46). From here we can examine the corresponding expressions in terms of the local parameter coordinates, μ and ν. After substituting in equation (4.11) into (2.38), (2.46) and keeping quadratic terms in μ, ν in the Taylor expansion, we obtain

$$\mu = \frac{\sqrt{2}}{9}\nu - \frac{13\sqrt{2}}{54}\nu^2 + O(\nu^3) \tag{4.12}$$

$$\mu = -\frac{\sqrt{2}}{3}\nu + \frac{\sqrt{2}}{2}\nu^2 + O(\nu^3) \tag{4.13}$$

for the local bifurcation curves of the in-phase mode pitchfork and in-phase mode Hopf, respectively. But since we were not able to calculate the unsymmetrical Hopf bifurcation curve analytically, we do not know what local expression to expect. The best expression we have is the polynomial approximation given by equation (2.54). As we will soon see, this approximation is valid locally only up to linear terms.

Since we have both a subcritical Hopf bifurcation (from the in-phase mode) and a supercritical Hopf bifurcation (from the unsymmetrical mode) joining at point P, we might also expect some types of global bifurcation curves to also join at P. This is indeed the case as the subsequent analysis will reveal.

4.3 Unfolding P

For the unfolding of P, we begin with the three differential equations in terms of the eigencoordinates x_1, y_1, z_1. We substitute in equation (4.11) and obtain three equations:

$$\dot{x}_1 = G_1(x_1, y_1, z_1, \mu, \nu) \tag{4.14}$$

$$\dot{y}_1 = G_2(x_1, y_1, z_1, \mu, \nu) \tag{4.15}$$

$$\dot{z}_1 = G_3(x_1, y_1, z_1, \mu, \nu). \tag{4.16}$$

We note that although the notation is the same as that used in the analysis of point Q, the values of the variables G_i (and $\tilde{G}_i$ mentioned later) are not the same at the two degenerate points; however, we use the same letters for convenience. Recall that the flow on the center manifold is going to be given by a two-dimensional system of equations. In terms of the eigencoordinates, only the x_1 direction has a nonzero eigenvalue, $\lambda = \frac{-2}{3}$, and so our center manifold will involve both y_1 and z_1 terms. We thus want to express x_1 in terms of y_1, z_1. To do this, we need to assume an appropriate form for the center manifold. Trying to stay as general as possible, we assume the form

$$\begin{aligned} x_{1,cm} &= z_1^2(a_1 + a_2\ \mu + a_3\ \nu + a_4\ \mu^2 + a_5\ \mu\ \nu + a_6\ \nu^2) \\ &+ z_1\ y_1(a_7 + a_8\ \mu + a_9\ \nu + a_{10}\ \mu^2 + a_{11}\ \mu\ \nu + a_{12}\ \nu^2) \\ &+ y_1^2(a_{13} + a_{14}\ \mu + a_{15}\ \nu + a_{16}\ \mu^2 + a_{17}\ \mu\ \nu + a_{18}\ \nu^2) \\ &+ z_1(a_{20}\ \mu + a_{21}\ \nu + a_{22}\ \mu^2 + a_{23}\ \mu\ \nu + a_{24}\ \nu^2) \\ &+ y_1(a_{26}\ \mu + a_{27}\ \nu + a_{28}\ \mu^2 + a_{29}\ \mu\ \nu + a_{30}\ \nu^2) \end{aligned}$$

$$+ \quad (a_{32}\ \mu + a_{33}\ \nu + a_{34}\ \mu^2 + a_{35}\ \mu\ \nu + a_{36}\ \nu^2) \tag{4.17}$$

where we set $a_{19} = a_{25} = a_{31} = 0$ since we do not want any $O(1)$ translation in the linear or constant terms. Comparing with (3.3), we see that the center manifold at point P will be given by

$$W^c = \{(x_1, y_1, z_1)|\ x_1 = h(y_1, z_1)\} \tag{4.18}$$

with $h(0) = Dh(0) = 0$ and $h(y_1, z_1) = x_{1,cm}$. We substitute equation (4.17) into (4.14). This will introduce $\dot{y_1}, \dot{z_1}$ terms after the differentiation is carried out. We then substitute equations (4.15)-(4.16) which reintroduces x_1 into the equations but rids them of any $\dot{x_1}, \dot{y_1}, \dot{z_1}$ terms. One more substitution of equation (4.17) into the new version of equation (4.14) gives an equation which only has y_1, z_1 terms. We move all the terms to one side and Taylor expand the expressions, keeping quadratic terms in μ, ν and cubic terms in y_1, z_1. Our resulting equation $\tilde{G}_1(y_1, z_1, \mu, \nu) = 0$ can then be compared to equation (4.17) since we want an expression for $x_{1,cm}$ which is valid at the equilibrium point. We thus obtain the center manifold

$$\begin{aligned}
x_{1,cm} &= \frac{-3\sqrt{6}}{8}y_1^2 + \frac{15\sqrt{6}}{4}z_1y_1 - 9\sqrt{6}z_1^2 \\
&+ y_1^2\left(\frac{159\sqrt{3}}{32}\mu + \frac{5\sqrt{6}}{32}\nu - \frac{16407\sqrt{6}}{512}\mu^2 - \frac{115\sqrt{6}}{256}\nu^2\right) \\
&+ z_1y_1\left(\frac{-99\sqrt{3}}{2}\mu - 3\sqrt{6}\nu + \frac{21627\sqrt{6}}{64}\mu^2 + \frac{1125\sqrt{3}}{16}\mu\nu + \frac{147\sqrt{6}}{32}\nu^2\right) \\
&+ z_1^2\left(\frac{2079\sqrt{3}}{16}\mu + \frac{261\sqrt{6}}{16}\nu - \frac{114939\sqrt{6}}{128}\mu^2 - \frac{10827\sqrt{3}}{32}\mu\nu - \frac{2061\sqrt{6}}{64}\nu^2\right) \\
&- \frac{\sqrt{3}}{2}\mu - \frac{\sqrt{6}}{6}\nu - \frac{3\sqrt{6}}{32}\mu^2 - \frac{5\sqrt{3}}{8}\mu\nu + \frac{\sqrt{6}}{16}\nu^2.
\end{aligned} \tag{4.19}$$

Now that we have an expression for the center manifold, we substitute equation

(4.19) into equations (4.15)-(4.16) and obtain

$$\begin{aligned}
\dot{y_1} &= y_1^3\left(\frac{5}{48}+\frac{161\sqrt{2}}{128}\mu+\frac{41}{192}\nu-\frac{11169}{1024}\mu^2-\frac{367\sqrt{2}}{512}\mu\nu-\frac{287}{1536}\nu^2\right)\\
&+ z_1y_1^2\left(\frac{21}{16}-\frac{1575\sqrt{2}}{128}\mu-\frac{309}{64}\nu+\frac{154359}{1024}\mu^2+\frac{9657\sqrt{2}}{512}\mu\nu+\frac{771}{512}\nu^2\right)\\
&+ z_1^2y_1\left(-\frac{45}{4}+\frac{2889\sqrt{2}}{64}\mu+\frac{747}{32}\nu-\frac{2673}{4}\mu^2-\frac{8289\sqrt{2}}{64}\mu\nu-\frac{1071}{64}\nu^2\right)\\
&+ y_1\left(-\frac{\sqrt{2}}{8}\mu+\frac{7}{12}\nu-\frac{33}{64}\mu^2+\frac{25\sqrt{2}}{32}\mu\nu+\frac{3}{32}\nu^2\right)\\
&+ z_1^3\left(\frac{135}{8}-\frac{3969\sqrt{2}}{64}\mu-\frac{1107}{32}\nu+\frac{241299}{256}\mu^2+\frac{30051\sqrt{2}}{128}\mu\nu+\frac{5481}{128}\nu^2\right)\\
&+ z_1\left(1+\frac{15\sqrt{2}}{8}\mu-\frac{3}{4}\nu+\frac{99}{64}\mu^2-\frac{27\sqrt{2}}{32}\mu\nu-\frac{25}{32}\nu^2\right) \qquad (4.20)\\
\dot{z_1} &= y_1^3\left(-\frac{1}{6}+\frac{181\sqrt{2}}{64}\mu+\frac{71}{288}\nu-\frac{901\sqrt{2}}{768}\nu\mu-\frac{17097}{512}\mu^2-\frac{141}{256}\nu^2\right)\\
&+ z_1y_1^2\left(\frac{67}{16}-\frac{4497\sqrt{2}}{128}\mu-\frac{339}{64}\nu+\frac{474957}{1024}\mu^2+\frac{21843\sqrt{2}}{512}\nu\mu+\frac{3521}{512}\nu^2\right)\\
&+ z_1^2y_1\left(-\frac{171}{8}+\frac{4905\sqrt{2}}{32}\mu+\frac{543}{16}\nu-\frac{271215}{128}\mu^2-\frac{20475\sqrt{2}}{64}\nu\mu-\frac{3357}{64}\nu^2\right)\\
&+ y_1\left(-\frac{\sqrt{2}}{2}\mu+\frac{1}{9}\nu+\frac{7\sqrt{2}}{48}\nu\mu-\frac{1}{32}\mu^2+\frac{23}{144}\nu^2\right)\\
&+ z_1^3\left(\frac{63}{2}-\frac{14445\sqrt{2}}{64}\mu-\frac{2151}{32}\nu+\frac{806517}{256}\mu^2+\frac{81945\sqrt{2}}{128}\nu\mu+\frac{16083}{128}\nu^2\right)\\
&+ z_1\left(\frac{13\sqrt{2}}{8}\mu+\frac{5}{12}\nu-\frac{19}{32}\nu^2+\frac{33}{64}\mu^2+\frac{23\sqrt{2}}{32}\nu\mu\right) \qquad (4.21)
\end{aligned}$$

as the equations describing the flow on the center manifold. We would like to examine the bifurcations associated with the above equations. When $\mu=\nu=0$ in the linear case, we see that these equations reduce to

$$\frac{d}{dt}\begin{pmatrix} y \\ z \end{pmatrix} = \begin{pmatrix} 0 & 1 \\ 0 & 0 \end{pmatrix}\begin{pmatrix} y \\ z \end{pmatrix}.$$

As expected, this is the case of the double zero eigenvalue, whose universal unfolding is discussed in Guckenheimer and Holmes [12].

4.3.1 Normal Form at Point P

Although the in-phase mode pitchfork and Hopf bifurcations are straightforward, albeit tedious, calculations, the above expressions are too algebraically complicated to find the unsymmetrical Hopf bifurcation; however, the behavior of this system can be found more readily when they are in normal form. Our goal is to convert (4.20)-(4.21) to the form

$$\begin{aligned} \dot{y} &= z \\ \dot{z} &= a_1 y + a_2 y^2 + a_3 y^3 + b_1 yz + b_2 y^2 z \\ &\quad b_3 y z^2 + c_1 z + c_2 z^2 + c_3 z^3 \end{aligned} \tag{4.22}$$

where $a_i = a_i(\mu, \nu), b_i = b_i(\mu, \nu)$. Due to the symmetry in our system, we do expect $a_2 = b_1 = c_2 = 0$, i.e., we do not expect any quadratic terms but we will assume this general form for now. By having the flow on the center manifold in the form of equation (4.22), we are immediately able to identify $z = 0$ as a condition for equilibria. Finding y-values that satisfy $\dot{z}|_{z=0} = 0$ then give the location of the other equilibria and the subsequent analysis is greatly reduced in difficulty.

A brief explanation of the normal form calculation will be given using equations (4.20)-(4.21) with $\mu = \nu = 0$. The other five transformations are then performed in a similar manner. Setting $\mu = 0, \nu = 0$, equations (4.20)-(4.21) reduce to

$$\dot{y_1} = \frac{135}{8} z_1^3 - \frac{45}{4} y_1 z_1^2 + \frac{21}{16} y_1^2 z_1 + z_1 + \frac{5}{48} y_1^3$$

$$\dot{z_1} = \frac{63}{2}z_1^3 - \frac{171}{8}y_1z_1^2 + \frac{67}{16}y_1^2z_1 - \frac{y_1^3}{6}. \tag{4.23}$$

The key to converting the equations to normal form is the use of the near-identity transformation [30]. In our case, we posit a near-identity transformation of the form:

$$\begin{aligned} y_1 &= y_2 + a_1z_2^3 + a_2y_2z_2^2 + a_3y_2^2z_2 + a_4y_2^3 \\ z_1 &= z_2 + b_1z_2^3 + b_2y_2z_2^2 + b_3y_2^2z_2 + b_4y_2^3. \end{aligned} \tag{4.24}$$

The a_i, b_i coefficients (not the same variables as in equation (4.22)) are to be chosen such that the $\dot{y}$ equation of (4.23) is of a simpler form, even at the expense of making the $\dot{z}$ equation of (4.23) more complicated. We plug equation (4.24) into equation (4.23) and obtain new equations on y_2 and z_2:

$$\begin{aligned} \dot{y_2} = \; & z_2 + \left(b_4 + \frac{5}{48}\right)y_2^3 + \left(b_3 - 3a_4 + \frac{21}{16}\right)z_2y_2^2 \\ & + \left(b_2 - 2a_3 - \frac{45}{4}\right)z_2^2y_2 + \left(b_1 - a_2 + \frac{135}{8}\right)z_2^3 \\ \dot{z_2} = \; & -\frac{1}{6}y_2^3 + \left(\frac{67}{16} - 3b_4\right)y_2^2z_2 + \left(-\frac{171}{8} - 2b_3\right)y_2z_2^2 \\ & + \left(\frac{63}{2} - b_2\right)z_2^3. \end{aligned} \tag{4.25}$$

Then we choose the a_i's and b_i's to clean up these equations on y_2 and z_2. The beauty of the near identity transformation is that we are free to choose any values we want for the coefficients a_i, b_i, and so we naturally assign them values which will zero out as many terms as possible in the $\dot{y}_2$ equation of (4.25). Appropriate choices for the a_i, b_i coefficients leads us to choose the near-identity transformation as

$$\begin{aligned} y_1 &= y_2 + \frac{135}{8}y_2z_2^2 + \frac{81}{8}y_2^2z_2 - \frac{25}{8}y_2^3 \\ z_1 &= z_2 + \frac{63}{2}y_2z_2^2 - \frac{171}{16}y_2^2z_2 - \frac{5}{48}y_2^3. \end{aligned} \tag{4.26}$$

Substitution of equation (4.26) into equation (4.23) yields

$$\begin{aligned} \dot{y_2} &= z_2 \\ \dot{z_2} &= \frac{9}{2}y_2^2 z_2 - \frac{1}{6}y_2^3. \end{aligned} \tag{4.27}$$

Since our goal is to obtain equations of the form given in equation (4.22) with μ, ν *not* zero, we must perform successive transformations to convert equations (4.20)-(4.21) to the correct form. The above example took care of the terms when $\mu = \nu = 0$. Now we posit a transformation of the form

$$\begin{aligned} y_2 &= y_3 + \mu(a_1 z_3^3 + a_2 y_3 z_3^2 + a_3 y_3^2 z_3 + a_4 y_3^3) \\ z_2 &= z_3 + \mu(b_1 z_3^3 + b_2 y_3 z_3^2 + b_3 y_3^2 z_3 + b_4 y_3^3) \end{aligned} \tag{4.28}$$

which will allow us to clean up the $O(\mu)$ terms when $\nu = 0$. We then do similar transformations to clean up the $O(\mu^2)$ terms when $\nu = 0$, the $O(\nu)$ terms when $\mu = 0$, the $O(\nu^2)$ terms when $\mu = 0$, and finally the $O(\mu\nu)$ terms. After renaming the variables, the result is that equations (4.20)-(4.21) are now in normal form:

$$\begin{aligned} \dot{y} &= z \\ \dot{z} &= y^3\left(-\frac{1}{6} - \frac{175\sqrt{2}}{192}\mu - \frac{367}{288}\nu - \frac{1523}{256}\mu^2 - \frac{317}{128}\nu^2 - \frac{1945\sqrt{2}}{384}\mu\nu\right) \\ &+ y^2 z\left(\frac{9}{2} + \frac{21\sqrt{2}}{4}\mu + \frac{19}{2}\nu - \frac{11763}{32}\mu^2 + \frac{729}{16}\nu^2 - \frac{1029\sqrt{2}}{16}\mu\nu\right) \\ &+ y\left(-\frac{\sqrt{2}}{2}\mu + \frac{1}{9}\nu - \frac{3}{2}\mu^2 - \frac{1}{6}\nu^2 - \frac{\sqrt{2}}{6}\mu\nu\right) \\ &+ z\left(\frac{3\sqrt{2}}{2}\mu + \nu - \frac{1}{2}\nu^2 + \frac{3\sqrt{2}}{2}\mu\nu\right). \end{aligned} \tag{4.29}$$

These are the equations that we will examine for the remainder of our analysis at point P, since they too describe the flow on the center manifold at point P.

4.3.2 Bifurcation Curves

We immediately observe that $z = 0$ is a condition for equilibria in equation (4.29) and the other condition, $\dot{z} = 0$, gives

$$\begin{aligned} 0 &= y^3\left(-\frac{1}{6} - \frac{175\sqrt{2}}{192}\mu - \frac{367}{288}\nu - \frac{1523}{256}\mu^2 - \frac{317}{128}\nu^2 - \frac{1945\sqrt{2}}{384}\mu\nu\right) \\ &+ y\left(-\frac{\sqrt{2}}{2}\mu + \frac{1}{9}\nu - \frac{3}{2}\mu^2 - \frac{1}{6}\nu^2 - \frac{\sqrt{2}}{6}\mu\nu\right) \end{aligned} \tag{4.30}$$

which is an expression with only y, y^3 terms. Thus $y = 0$ is an equilibrium and we know this corresponds to the in-phase mode.

To see the bifurcation curves associated with the equilibrium $y = 0, z = 0$, we first perform the linearization by calculating the Jacobian of equation (4.29) evaluated at the equilibrium point and then finding the characteristic equation. For a pitchfork bifurcation, we set $\lambda = 0$ in the characteristic equation. Requiring our solution to be of the form $\mu = a_1\nu + a_2\nu^2$, we find

$$\mu = \frac{\sqrt{2}}{9}\nu - \frac{13\sqrt{2}}{54}\nu^2 + O(\nu^3)$$

which is the in-phase mode pitchfork bifurcation curve (4.12) that we expected. If instead we substitute $\lambda = i\omega$ into the characteristic equation, we find the conditions describing the in-phase mode Hopf bifurcation. Equating real and imaginary parts to zero gives us two equations. Since we need $\omega \in \mathbf{R}$ i.e., $\omega^2 > 0$, one equation gives the condition for existence while the other gives the actual equation for the curve. Again, requiring our solution to be of the form $\mu = a_1\nu + a_2\nu^2$, we find

$$\mu = -\frac{\sqrt{2}}{3}\nu + \frac{\sqrt{2}}{2}\nu^2 + O(\nu^3)$$

to be the equation of the Hopf bifurcation curve and it exists as long as

$$\mu > \frac{\sqrt{2}}{9}\nu - \frac{13\sqrt{2}}{54}\nu^2 + O(\nu^3)$$

which corresponds to the condition $\omega^2 > 0$. We see that the equation of the Hopf bifurcation is equation (4.13), as expected, while the condition for its existence states that equation (4.13) must lie above the in-phase pitchfork bifurcation curve in the $\cos\tau - \alpha$ plane.

Calculating the unsymmetrical Hopf bifurcation curve is more algebraically involved. We first find the roots of equation (4.30). We then evaluate the Jacobian of equation (4.29) at one of these roots and calculate the characteristic equation. Setting $\lambda = 0$ gives equation (4.13). Thus we see there are no new saddle-node or pitchfork bifurcation curves coming into point P; however, setting $\lambda = i\omega$ and equating real and imaginary parts to zero, we obtain conditions on the unsymmetrical Hopf bifurcation curve. Taylor expanding and again requiring our solution to be of the form $\mu = a_1\nu + a_2\nu^2$, we find

$$\mu = \frac{\sqrt{2}}{6}\nu + \frac{47\sqrt{2}}{512}\nu^2 + O(\nu^3) \tag{4.31}$$

as the equation of the unsymmetrical Hopf bifurcation. It will exist as long as

$$\mu < \frac{\sqrt{2}}{9}\nu - \frac{13\sqrt{2}}{54}\nu^2 + O(\nu^3) \tag{4.32}$$

which says that it must lie below the in-phase pitchfork bifurcation curve in the $(-\nu) - \mu$ plane, see Figure 4.1. Thus our analysis has allowed us to obtain an analytic expression which locally describes the unsymmetrical Hopf bifurcation curve for which we previously only had numerical confirmation of its existence.

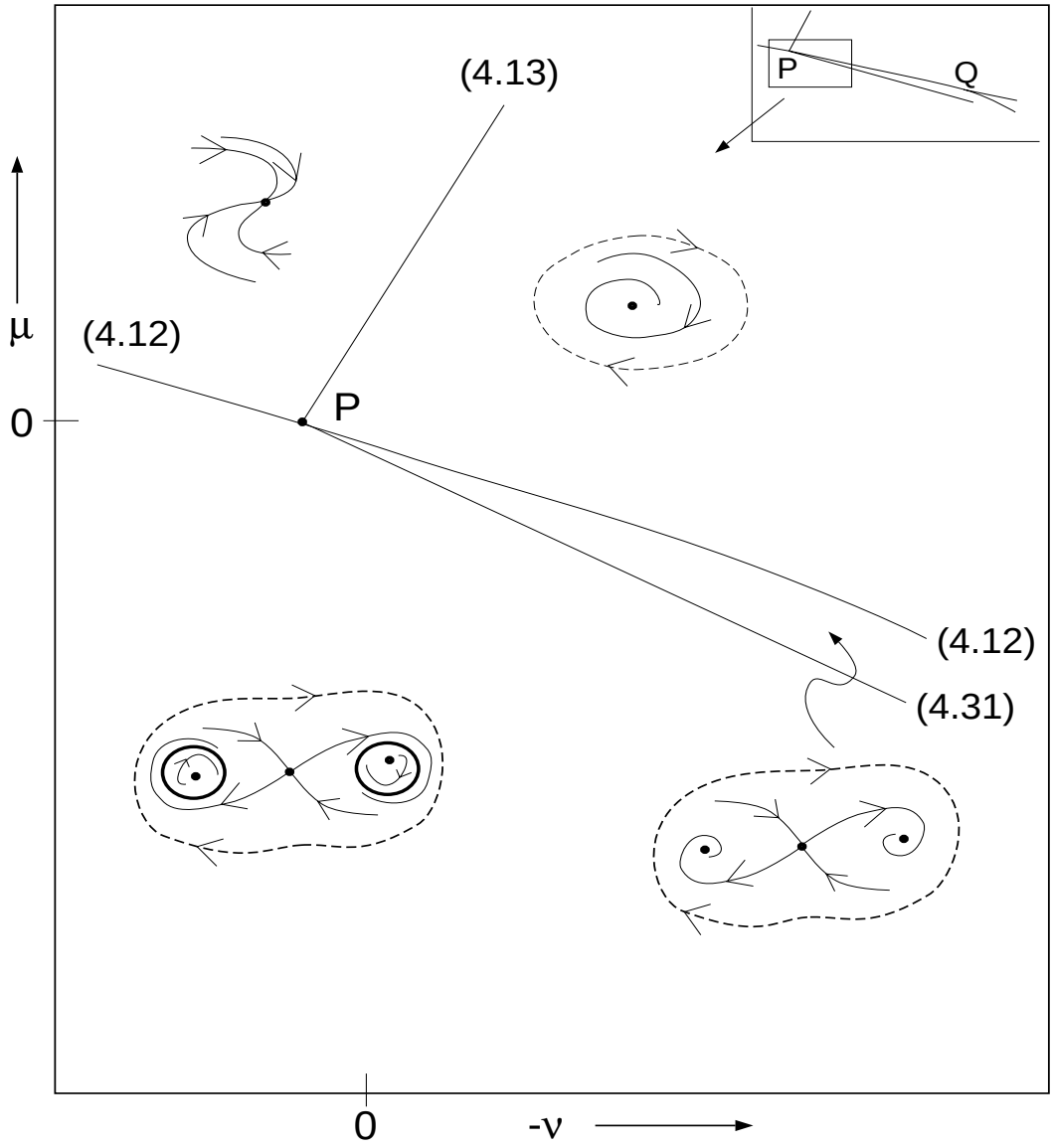

Figure 4.1: Partial bifurcation set and phase portraits near point P via center manifold theory.

We should note at this point that the polynomial approximation for the unsymmetrical Hopf bifurcation curve (2.54) yields the local curve

$$\mu = 0.00008 + 0.24165\nu - 0.045266\nu^2 + O(\nu^3) \tag{4.33}$$

which we see is only a "good" approximation for the linear term to the actual curve (4.31), given numerically as $\mu = 0.23570\nu + 0.12982\nu^2 + O(\nu^3)$.

4.4 Global Results

When we examine Figure 4.1, we see that the phase portraits to the left of point P in the $(-\nu) - \mu$ plane above and below equation (4.12) are not homeomorphic since there exists a limit cycle below but not above the curve. We thus expect some type of global bifurcations to occur. From the phase portraits obtained from our analysis of the flow on the center manifold at point P, we see that we have two stable limit cycles born as the supercritical unsymmetrical Hopf bifurcation curve is crossed from above in the $\cos\tau - \alpha$ plane (oriented as the $(-\nu) - \mu$ plane in the above analysis, cf. Figure 4.1). Just above and just below the curve, the unstable limit cycle from the in-phase Hopf bifurcation encircles (i) the in-phase mode equilibrium, (ii) the two points born in the supercritical pitchfork bifurcation off of it, and (iii) the two stable limit cycles born off these two new equilibria. In the unfolding of P, we are able to see these results locally—even though they are global results. Our local analysis was performed on a two-dimensional center manifold, which is guaranteed to capture the full behavior of the system. Thus, when we say "encircle" in the full system, we can picture it as a limit cycle lying on some two-dimensional surface (the

center manifold) which also contains the other points in question.

Numerical integration of the equations describing the flow on the center manifold, (4.29), indicates that shortly after the unsymmetrical Hopf bifurcation curve is crossed, a symmetry-breaking *double* homoclinic bifurcation occurs where both stable limit cycles join to the in-phase saddle point separating them and then both join together to form a single stable limit cycle. For slightly lower α values, a coalescence of the newly created stable limit cycle and the unstable limit cycle (from the in-phase mode) is observed. Due to the narrow strip of parameter values for which these events occur, it is important that we try and obtain analytical expressions for these global bifurcation curves in the neighborhood of P, if possible.

4.4.1 Symmetry-breaking Homoclinic Bifurcation

In order to obtain a closed form expression for the homoclinic bifurcation in (4.29), we perturb off the homoclinic orbit. This works in systems of the form

$$\begin{aligned} \dot{y} &= z \\ \dot{z} &= ay - N(y) + \epsilon g(y, z, t) \end{aligned} \tag{4.34}$$

where a is a non-zero constant, $N(y)$ is a nonlinear function of y with $N(0) = 0$, and the $\epsilon = 0$ system possesses a homoclinic loop through the origin [30]. This last condition gives motivation to the idea that for small ϵ, the homoclinic orbit might still persist. For $\epsilon \neq 0$, we want the contour integral around the closed saddle loop to vanish. That is, we want $M \equiv \oint g dy$ to vanish. This condition will result in the desired homoclinic curve. Our goal is thus to transform (4.29) to the form (4.34)

and then examine parameter values μ, ν to see when the saddle connection remains for $\epsilon > 0$.

The flow on the center manifold at point P is given by equation (4.29) which we now write as

$$\dot{y} = z \tag{4.35}$$

$$\dot{z} = -A_1 y - A_2 y^3 - A_3 z - A_4 y^2 z \tag{4.36}$$

where we have merely renamed coefficients. We follow a calculation similar to that of Guckenheimer and Holmes, who studied the unfolding of systems which preserve symmetry under rotation through π [12]. We first recall that the derivatives in (4.35)-(4.36) are given with respect to T where $T = \frac{1}{\epsilon}t$ was used to eliminate ϵ from (2.21)-(2.23). As mentioned before, we need to convert equations (4.35)-(4.36) to the form of equation (4.34). To do so we let

$$y = \epsilon u, \quad z = \epsilon^2 v, \quad \tilde{T} = \epsilon T. \tag{4.37}$$

Then (4.35) becomes $u' = v$ and (4.36) becomes

$$\epsilon^3 v' = -A_1 \epsilon u - A_2 \epsilon^3 u^3 - A_3 \epsilon^2 v - A_4 \epsilon^4 u^2 v, \tag{4.38}$$

where $'$ denotes differentiation with respect to $\tilde{T}$. If we then set

$$A_1 = \epsilon^2 B_1, \quad A_2 = B_2, \quad A_3 = \epsilon^2 B_3, \quad A_4 = B_4, \tag{4.39}$$

we obtain

$$u' = v$$

$$v' = -B_1 u - B_2 u^3 - \epsilon B_3 v - \epsilon B_4 u^2 v. \tag{4.40}$$

We see that equation (4.40) for $\epsilon = 0$ is of Hamiltonian form with Hamiltonian

$$H(u,v) = \frac{v^2}{2} + B_1\frac{u^2}{2} + B_2\frac{u^4}{4}. \tag{4.41}$$

Thus equation (4.41) can be rewritten as

$$\begin{aligned} u' &= H_v \\ v' &= -H_u + \epsilon(-B_3 v - B_4 u^2 v). \end{aligned} \tag{4.42}$$

where the subscript denotes partial differentiation.

We know from the discussion at the beginning of this section that the condition for a homoclinic bifurcation in our case is

$$\oint (B_3 v + B_4 u^2 v)du = 0, \tag{4.43}$$

since this is the condition for the saddle loop becoming the separatrix when $\epsilon = 0$. Back substitution shows this to be

$$\oint (A_3 z + A_4 y^2 z)dy = 0, \tag{4.44}$$

or equivalently

$$M(\mu,\nu) \equiv \int_{-\infty}^{\infty} (A_3\dot{y} + A_4 y^2\dot{y})\dot{y}dt = 0, \tag{4.45}$$

where we have used $\dot{y} = \frac{dy}{dt}$ to convert the contour integral over the closed orbit to a time integral. For the homoclinic solution, equations (4.35)-(4.36) become

$$\ddot{y} + A_1 y + A_2 y^3 = 0, \tag{4.46}$$

where

$$\begin{aligned} A_1 &= \frac{\sqrt{2}}{2}\mu - \frac{1}{9}\nu + O(\mu^2, \nu^2, \mu\nu) < 0, \\ A_2 &= \frac{1}{6} + O(\mu,\nu). \end{aligned} \tag{4.47}$$

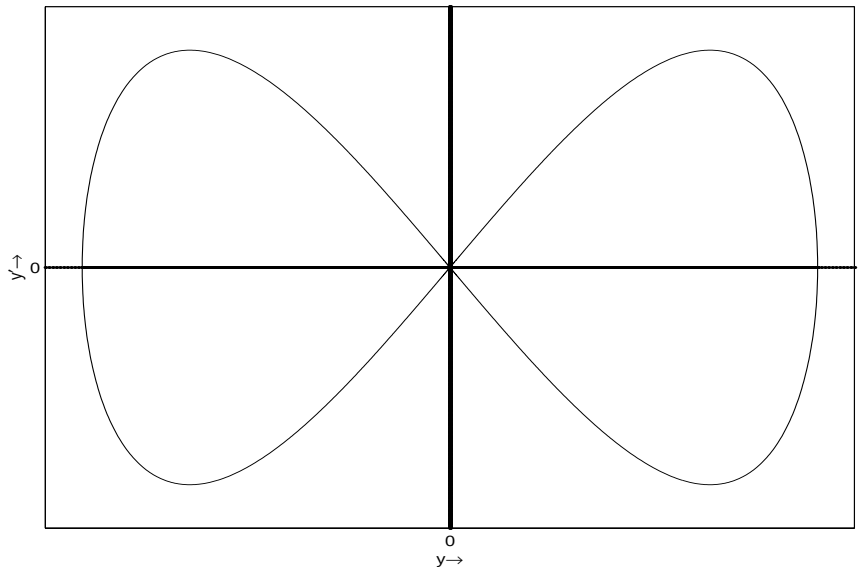

Figure 4.2: Homoclinic solution, $y = \frac{\alpha}{\cosh \beta t}$, plotted in the $y - \dot{y}$ plane.

Equation (4.46) has a solution of the form $y = \frac{\alpha}{\cosh \beta t}$, where $\beta = \sqrt{-A_1}$ and $\alpha = \sqrt{\frac{-2A_1}{A_2}}$, representing the flow along the separatrix (see Figure 4.2). Calculating the parts in equation (4.45), we find

$$\int_{-\infty}^{\infty} \dot{y}^2 dt = \frac{2}{3}\alpha^2\beta, \qquad \int_{-\infty}^{\infty} y^2\dot{y}^2 dt = \frac{4}{15}\alpha^4\beta, \tag{4.48}$$

and thus we have

$$\frac{2}{3}A_3\alpha^2\beta + \frac{4}{15}A_4\alpha^4\beta = 0$$

i.e.,

$$\frac{2}{3}A_3\left(\frac{-2A_1}{A_2}\right)\sqrt{-A_1} + \frac{4}{15}A_4\left(\frac{-2A_1}{A_2}\right)^2\sqrt{-A_1} = 0. \tag{4.49}$$

Solutions of equation (4.49) are $A_1 = 0$ and $4A_1A_4 = 5A_2A_3$. Since we required $A_1 < 0$ for the homoclinic solution, only the second solution is of concern. Substituting

the known expressions for A_1, A_2, (4.47), noting that

$$\begin{aligned} A_3 &= -\nu - \frac{3\sqrt{2}}{2}\mu, \\ A_4 &= -\frac{9}{2} - \frac{19}{2}\nu - \frac{21\sqrt{2}}{4}\mu, \end{aligned} \tag{4.50}$$

and assuming a solution of the form $\mu = a_1\nu + a_2\nu^2$, we obtain the homoclinic bifurcation curve

$$\mu = \frac{17\sqrt{2}}{93}\nu + \frac{38173\sqrt{2}}{178746}\nu^2 + O(\nu^3). \tag{4.51}$$

Numerically, this is given as $\mu \approx 0.2585\nu + 0.3020\nu^2 + O(\nu^3)$, see Figure 4.3.

4.4.2 Coalescence of Limit Cycles

In order to find the bifurcation curve along which the limit cycles coalesce, we will need to perturb using Jacobian elliptic functions. These functions can be thought of as generalizations of the well-known trigonometric functions. Unlike trig functions that are functions of only one variable (the argument), elliptic functions depend on two variables—the argument u and the modulus k [3],[30]. There are three main elliptic functions:

$$sn(u,k), \qquad cn(u,k), \qquad dn(u,k). \tag{4.52}$$

When $k = 0$, we have

$$sn(u,0) = \sin(u), \qquad cn(u,0) = \cos(u), \qquad dn(u,0) = 1, \tag{4.53}$$

which illustrates why these can be thought of as generalizations of the trig functions. (Note, however, that there is no trigonometric function which is analagous

to $dn(u,k)$.) In addition, for $k = 1$, we have $sn(u,1) = \tanh(u)$, $cn(u,1) = \operatorname{sech}(u)$, $dn(u,1) = \operatorname{sech}(u)$. The modulus k, which normally ranges between 0 and 1, is thus seen to affect the period of the function. For notational purposes, we write $cn(u,k) = cn$ and similarly $sn(u,k) = sn$, $dn(u,k) = dn$. Each of these elliptic functions is periodic—the first two having period $4K(k)$ while the last has period $2K(k)$ where $K(k)$ is the complete elliptic integral of the first kind. Defining

$$\frac{\partial cn(u,k)}{\partial u} \equiv cn' \tag{4.54}$$

and similarly for sn and dn, we note the identities

$$\begin{aligned} cn' = -sn\ dn, \quad sn' &= cn\ dn, \quad dn' = -k^2 sn\ cn, \\ sn^2 + cn^2 = 1, &\qquad dn^2 = 1 - k^2 sn^2. \end{aligned} \tag{4.55}$$

One final note: we adopt the notation used by Byrd and Friedman, as opposed to Abramowitz and Stegun. The latter use $m = k^2$ instead of k [1], [3], [30].

As discussed in the previous sections, numerical integration suggests that the symmetry-breaking homoclinic bifurcation creates one stable limit cycle which eventually coalesces with the unstable limit cycles created from the in-phase mode Hopf bifurcation. Alternatively, we recall

Bendixon's Criterion ([12]) *Consider the system* $\dot{y} = f_1(y,z)$, $\dot{z} = f_2(y,z)$ *on a simply connected region* $D \subseteq \mathbf{R}^2$ *and denote it's Jacobian matrix* $A = \begin{pmatrix} \frac{\partial f_1}{\partial y} & \frac{\partial f_1}{\partial z} \\ \frac{\partial f_2}{\partial y} & \frac{\partial f_2}{\partial z} \end{pmatrix}$. *If* $\mathbf{tr}\ A$ *is not identically zero and does not change sign, then the system has no closed orbits lying entirely in* D.

The coalescence of limit cycles is suggested by observing that for our system the

trace of the Jacobian matrix of equation (4.29)

$$\mathbf{tr}(\mathbf{D}f) = y^2\left(\frac{9}{2} + \frac{21\sqrt{2}}{4}\mu + \frac{19}{2}\nu\right) + \left(\frac{3\sqrt{2}}{2}\mu + \nu\right) + O(\mu^2, \nu^2, \mu\nu) \tag{4.56}$$

together with Bendixon's criterion imply that no closed orbits exist for $\mu > -\frac{\sqrt{2}}{3}\nu$. This condition corresponds to the in-phase mode Hopf bifurcation curve which only exists above the in-phase pitchfork bifurcation curve (in the parameter plane) but now gives a bound on the existence of this limit cycle *and* the one created in the symmetry-breaking homoclinic bifurcation when both are below the in-phase mode pitchfork bifurcation curve. We therefore expect a bifurcation curve corresponding to the coalescence of limit cycles to occur somewhere between $\mu = \frac{17\sqrt{2}}{93}\nu$ in the third quadrant and $\mu = -\frac{\sqrt{2}}{3}\nu$ in the fourth quadrant of the $\nu - \mu$ plane. We will see it is far closer to the first of these curves and we will show this analytically by perturbation using Jacobian elliptic funtions (cf. [3],[8],[12]).

As with the homoclinic bifurcation, we consider the integrable system

$$\ddot{y} + A_1 y + A_2 y^3 = 0, \tag{4.57}$$

where A_1, A_2 are defined by equation (4.47). Whereas we previously considered perturbations of the homoclinic orbit, we now must consider perturbations of the closed level curves of the Hamiltonian lying inside and outside of this homoclinic orbit. We again consider the Melnikov function

$$M(\mu, \nu) = A_3 \int_{-\infty}^{\infty} \dot{y}^2 dt + A_4 \int_{-\infty}^{\infty} y^2 \dot{y}^2 dt \tag{4.58}$$

and note that the condition $M(\mu, \nu) = 0$ must be satisfied in order for a given closed

orbit to remain after perturbation. We assume a solution of the form

$$y = Ccn(u,k), \qquad u = At + B \tag{4.59}$$

for $M(\mu,\nu) = 0$, where $cn(u,k)$ is a Jacobian elliptic function, A and C are positive constants and B is the phase angle.

Substituting equation (4.59) into equation (4.57), we find

$$[CA^2(2k^2-1) + A_1C]cn + [C^3A_2 - 2k^2A^2C]cn^3 = 0. \tag{4.60}$$

We seek nontrivial solutions, i.e., $C \neq 0$ and thus obtain

$$A^2(1-2k^2) = A_1, \tag{4.61}$$

$$C^2A_2 = 2k^2A^2. \tag{4.62}$$

Solving equations (4.61)-(4.62), we find

$$A^2 = A_1 + A_2C^2, \tag{4.63}$$

$$k^2 = \frac{A_2C^2}{2(A_1 + A_2C^2)}. \tag{4.64}$$

Recall our purpose for performing these calculations is to evaluate the Melnikov function $M(\mu,\nu)$ given by (4.58). The first term can be written

$$\begin{aligned} A_3\int_{-\infty}^{\infty} \dot{y}^2 dt &= A_3 \oint C^2A^2(cn')^2 du \frac{dt}{du} \\ &= A_3C^2A \oint sn^2 dn^2 du \\ &= A_3C^2A\left\{\oint sn^2 du - k^2 \oint sn^4 du\right\}. \end{aligned} \tag{4.65}$$

Because both integrals are evaluated over a closed path, equation (4.65) becomes

$$A_3C^2A\left\{\frac{1}{k^2}\left[K - E\right] - k^2\left[\frac{1}{3k^4}\left((2+k^2)K - 2(1+k^2)E\right)\right]\right\} \tag{4.66}$$

where E is the complete elliptic integral of the second kind and the dependence of E and K on k has been supressed. Equation (4.66) further simplifies to

$$A_3C^2A\left\{K\left[\frac{1}{3k^2}\left(1-k^2\right)\right]+E\left[\frac{1}{3k^2}\left(-1+2k^2\right)\right]\right\}. \tag{4.67}$$

The second term of the Melnikov function can also be evaluated. We have

$$\begin{aligned} A_4\int_{-\infty}^{\infty} y^2\dot{y}^2dt &= A_4C^4A\oint cn^2(cn')^2du \\ &= A_4C^4A\oint cn^2(sn^2(1-k^2sn^2))du \\ &= A_4C^4A\oint[(1-k^2)cn^2+(2k^2-1)cn^4-k^2cn^6]du. \end{aligned} \tag{4.68}$$

Evaluating each term of the contour integral and simplifying, we find equation (4.68) becomes

$$A_4C^4A\left\{-\frac{1}{15k^4}\left(K[k^4-3k^2+2]+E[-2k^4+2k^2-2]\right)\right\}. \tag{4.69}$$

Our Melnikov function $M(\mu,\nu)$ now has a dependence on C and so we write

$$\begin{aligned} M(C,\mu,\nu) &= A_3C^2A\left\{\frac{1}{k^2}\left[K-E\right]-k^2\left[\frac{1}{3k^4}\left((2+k^2)K-2(1+k^2)E\right)\right]\right\} \\ &+ A_4C^4A\left\{-\frac{1}{15k^4}\left(K[k^4-3k^2+2]+E[-2k^4+2k^2-2]\right)\right\} \end{aligned} \tag{4.70}$$

where $k^2=\frac{A_2C^2}{2(A_1+A_2C^2)}$.

We know that the existence of a limit cycle corresponds to $M(C,\mu,\nu)=0$. Just after the symmetry-breaking homoclinic bifurcation, $M(C,\mu,\nu)=0$ has two roots, corresponding to the unstable limit cycle and the stable limit cycle created from the in-phase mode Hopf and symmetry-breaking homoclinic bifurcations, respectively. The coalescence of these two limit cycles implies a second condition, namely

$\frac{\partial}{\partial C}M(C,\mu,\nu)=0$. Thus our task is to simultaneously solve

$$M(C,\mu,\nu)=0, \quad \frac{\partial M}{\partial C}=0, \tag{4.71}$$

by eliminating C and examining the remaining equation in μ,ν.

Using equation (4.64) and the identities

$$\frac{dK}{dk}=\frac{E-(1-k^2)K}{k(1-k^2)}, \quad \frac{dE}{dk}=\frac{E-k}{k} \tag{4.72}$$

we can calculate $\frac{\partial M}{\partial C}=\frac{\partial M}{\partial k}\frac{\partial k}{\partial C}$. Equation (4.64) can then be used to eliminate C from (4.71), leaving equations involving k and not C; however, only even powers of k appear. Thus we make the substitution $m=k^2$ and proceed to solve $f\equiv M(m,\mu,\nu)$, $g\equiv\frac{\partial M(m,\mu,\nu)}{\partial C}$ for the value of m that satisfies both equations. Since μ,ν are assumed to be small, we make the substitutions

$$\begin{aligned} m &= m_0+m_1\mu+m_2\nu, && (4.73)\\ K(m) &= K(m_0)+\left(\frac{E(m_0)-(1-m)K(m_0)}{2m(1-m)}\right)(m_1\mu+m_2\nu), && (4.74)\\ E(m) &= E(m_0)+\left(\frac{E(m_0)-K(m_0)}{2m}\right)(m_1\mu+m_2\nu) && (4.75) \end{aligned}$$

into f and g and Taylor expand, keeping only up to linear terms in μ,ν. We now have two homogeneous linear algebraic equations in μ,ν. For a nontrivial solution, we must have

$$\begin{vmatrix} \frac{\partial f}{\partial \mu} & \frac{\partial f}{\partial \nu} \\ \frac{\partial g}{\partial \mu} & \frac{\partial g}{\partial \nu} \end{vmatrix}=0. \tag{4.76}$$

Equation (4.76) is given by

$$\begin{aligned} &(-4K^2m^2+7K^2m-3K^2+8Km^2E-18KmE+8KE\\ &\quad +10mE^2-5E^2)(m-1)(2m-1)m^6=0. \end{aligned} \tag{4.77}$$

At this point we pause to consider the roots of this equation. The root $m = 0$ can immediately be discarded as it corresponds to the trivial solution $y = 0$, since $m = 0 \Rightarrow C = 0$. Likewise, the root $m = 1$ can be discarded because it corresponds to the condition $A_1 = 0$, i.e., $\mu = \frac{\sqrt{2}}{9}\nu$ which is the equation for the in-phase mode pitchfork bifurcation and we know limit cycles exist on both sides of this curve in the parameter plane. The root $m = \frac{1}{2}$ might be considered valid but if we consider the case $\mu = \nu = 0$ (which implies $A_3 = A_1 = 0$), we find the limit cycle has zero size. Thus the value of m corresponding to the condition for coalescence of the two limit cycles is given by

$$(-4K^2m^2+7K^2m-3K^2+8Km^2E-18KmE+8KE+10mE^2-5E^2) = 0. \quad (4.78)$$

We denote the root of this equation by m_0 and note $m_0 \approx 0.92939$. (Note that $m_0 = \frac{1}{2}$ is also a root of equation (4.78) but we ignore it for the reasons mentioned above.) Solving $M(m_0, \mu, \nu) = 0$ for μ then gives

$$\mu = \frac{\sqrt{2}}{3}\left[\frac{32m_0^2E - 17K + 33Km_0 - 16m_0^2K + 17E - 32Em_0}{-31K - 8m_0^2K + 31E + 39Km_0 + 16m_0^2E - 16Em_0}\right]\ \nu \quad (4.79)$$

where $E = E(k) = E(\sqrt{m_0}), K = K(k) = K(\sqrt{m_0})$ are known quantities. Thus, numerically, the curve along which the limit cycles coalesce is

$$\mu \approx 0.26606\nu + O(\nu^2). \quad (4.80)$$

Figure 4.3 shows the completed bifurcation set and phase portraits at point P. We can also examine the bifurcation diagram by encircling point P, as seen in Figure 4.4.

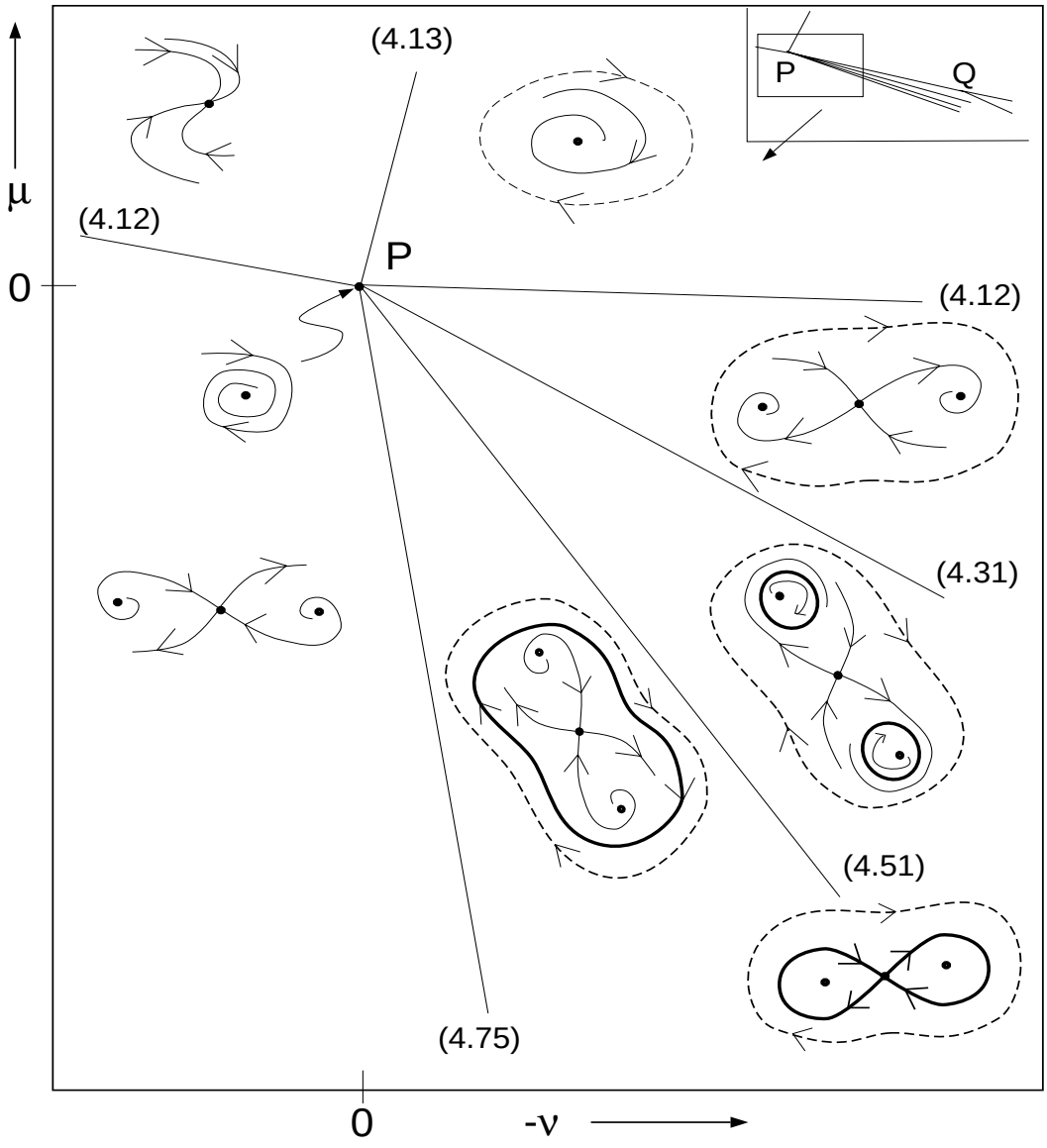

Figure 4.3: Bifurcation set at point P, with curves drawn distorted for better viewing. Note that the out-of-phase mode exists throughout, but far away from, this sequence. Also, the third eigendirection comes into the plane of this page (nearly normal).

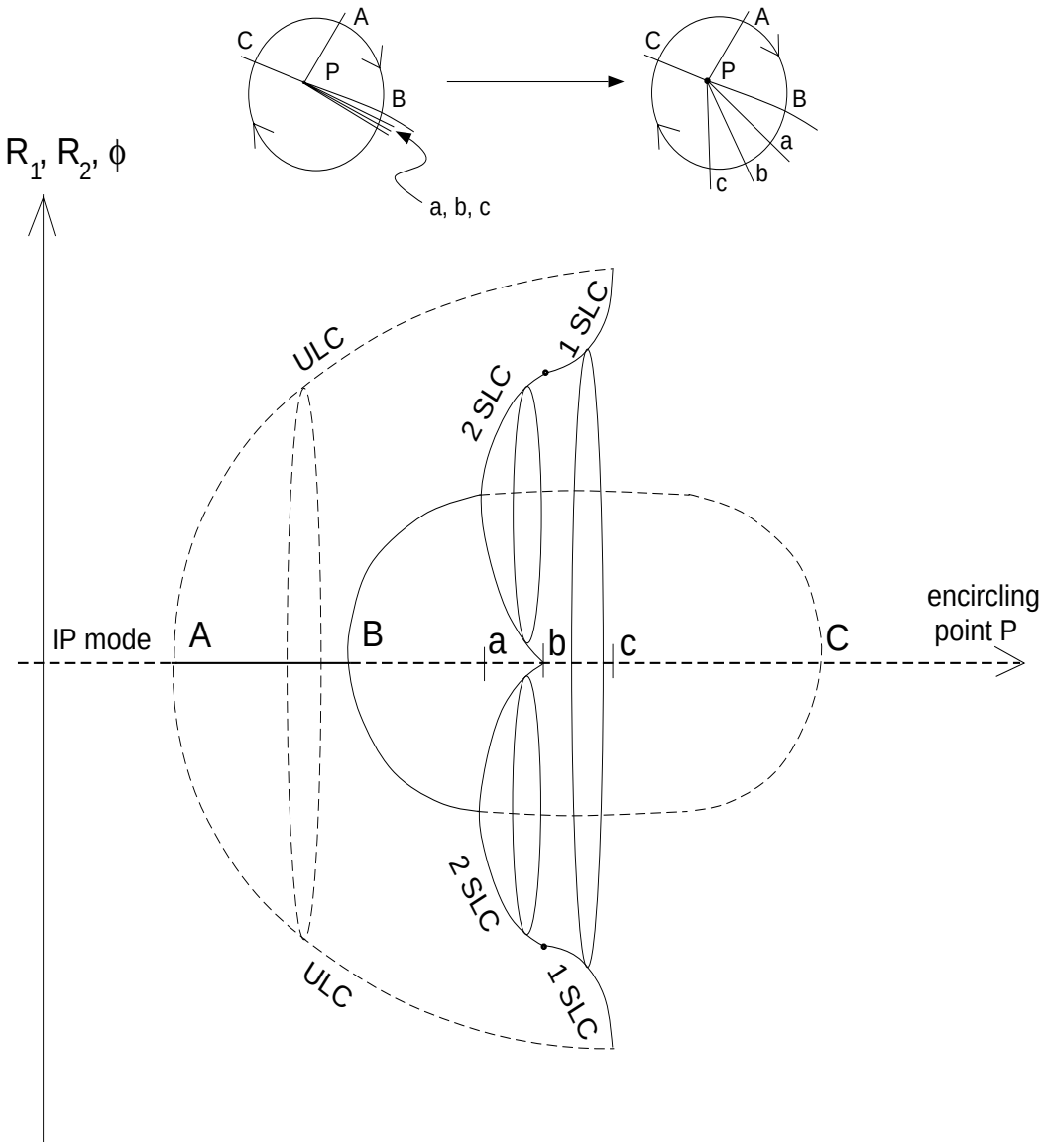

Figure 4.4: Bifurcation diagram encircling point P. Note that stable and unstable limit cycles are shown.

Chapter 5

Point H

5.1 Introduction

We have finished the analysis of point Q which had a one-dimensional center manifold and of point P which had a two-dimensional center manifold. Recall that we defined point H as the one point along the double saddle-node bifurcation curve in $\cos\tau - \alpha$ parameter space which has two eigenvalues satisfying $\lambda = 0$ (where we pick $\cos\tau \leq 0$ as we did with points Q and P since all have a mirror image for $\cos\tau \mapsto -\cos\tau$). But unlike points Q and P, we have no analytic expression for the parameter values corresponding to point H. We can only hope to proceed in the same manner as with our analysis of point P, since both have two-dimensional center manifolds; however, we must be extra careful in interpreting our (numerical) results. We will also see that some of the straightfoward calculations used in the analysis of points Q and P will be altered because of problems caused by not

having the values of $R_1, R_2, \phi, \tau, \alpha$ in closed form. Before proceeding, we note that point H—although defined uniquely in the parameter plane—has two different sets of (R_1, R_2, ϕ) values in the phase plane, since it is the unsymmetrical equilibria which undergo bifurcations. These values are related by (2.27):

$$(R_1, R_2, \phi) \mapsto (R_2, R_1, -\phi).$$

Without loss of generality, we pick the equilibrium point

$$R_1 = 2.0151, \quad R_2 = 1.3926, \quad \phi = 0.56394 \tag{5.1}$$

for the values about which we linearize. For points Q and P, we chose $0 < \tau < \pi$. Our unfolding resulted in a picture that needed to be reflected about $\cos\tau = 0$ to compare with the expected incoming curves. Since we expect many other difficulties here, we avoid this situation by taking $\pi < \tau < 2\pi$. Thus point H is given approximately by

$$\tau = 4.2026, \alpha = 0.40506, \tag{5.2}$$

where we are able to find these values to as many significant figures as desired, even though we cannot obtain a closed form answer. That is, we can obtain values for $R_1, R_2, \phi, \tau, \alpha$ which are as accurate as we want but they are no more accurate than specified. Thus, we cannot require arbitrarily small errors but we can require them to be less than, say, 10^{-50}.

We note that point H can be written in an exact, *implicit* representation. We solve the three equations which give the condition for the existence of slow-flow equilibria, $f(R_1, R_2, \phi, \tau, \alpha) = 0$, together with the equations $c_1 = c_0 = 0$ where c_1

and c_0 are the coefficients of the linear and the constant terms in the characteristic polynomial of the Jacobian of the system given by f. Explicity, we have the characteristic equation for f as $\lambda^3 + c_2\lambda + c_1\lambda + c_0$ where c_0 and c_1 are

$$\begin{aligned}
c_0 &= \frac{R_1^2\alpha}{128R_2^2}\Big(16\alpha R_1^4\cos^2(\phi-\tau) - 12R_1^6\alpha\cos^2(\phi-\tau) + 16\alpha R_2^4\cos^2(\phi+\tau) \\
&+ 12\alpha R_2^6 - 12\alpha R_2^6\cos^2(\phi+\tau) - 16\alpha^2 R_2R_1^3\cos(\phi+\tau) - 16\alpha R_1^4 + 12R_1^6\alpha \\
&- 16\alpha R_2^4 - 16R_1R_2^3\alpha^2\cos(\phi-\tau) - 12R_2^3R_1^3\cos(\phi-\tau) + 16R_2R_1^3\cos(\phi-\tau) \\
&+ 32\alpha R_1^2R_2^2\sin(\phi-\tau)\sin(\phi+\tau) - 12R_1^3R_2^3\cos(\phi+\tau) - 12R_1^5R_2\cos(\phi-\tau) \\
&+ 9R_1^3R_2^5\cos(\phi+\tau) + 9R_1^5R_2^3\cos(\phi-\tau) - 12R_1^4R_2^2\alpha\sin(\phi-\tau)\sin(\phi+\tau) \\
&- 12R_1R_2^5\cos(\phi+\tau) + 16\alpha^2R_1R_2^3\sin(\phi+\tau)\cos(\phi+\tau)\sin(\phi-\tau) \\
&+ 16R_1R_2^3\cos(\phi+\tau) - 12\alpha R_2^4R_1^2\sin(\phi-\tau)\sin(\phi+\tau) \\
&+ 16R_1^3R_2\alpha^2\cos(\phi-\tau)\sin(\phi+\tau)\sin(\phi-\tau)\Big), \qquad (5.3)\\
c_1 &= \frac{-R_1^2}{64R_2^2}\Big(-16R_1^2R_2^2 + 32\alpha^2R_1^4\cos^2\phi\cos^2\tau - 16\alpha^2R_1^4\cos^2\tau - 16\alpha^2R_2^4\cos^2\tau \\
&- 24R_2^3\alpha R_1^3\cos\phi\cos\tau + 32R_2\alpha R_1^3\cos\phi\cos\tau + 32R_2\alpha R_1^3\sin\phi\sin\tau \\
&- 16\alpha^2R_2^4\cos^2\phi - 16\alpha^2R_1^2R_2^2 + 32\alpha^2R_2^4\cos^2\phi\cos^2\tau \\
&- 32\alpha^2R_2^4\cos\phi\cos\tau\sin\phi\sin\tau + 32R_1\alpha R_2^3\cos\phi\cos\tau - 32R_1\alpha R_2^3\sin\phi\sin\tau \\
&- 12R_1R_2^5\alpha\cos\phi\cos\tau + 12R_1R_2^5\alpha\sin\phi\sin\tau - 12R_1^5R_2\alpha\cos\phi\cos\tau \\
&- 12R_1^5R_2\alpha\sin\phi\sin\tau - 16\alpha^2R_1^4\cos^2\phi + 32\alpha^2R_1^4\cos\phi\cos\tau\sin\phi\sin\tau \\
&- 9R_1^4R_2^4 + 12R_1^4R_2^2 + 12R_2^4R_1^2 - 16\alpha^2R_1^2R_2^2\cos^2\phi + 48\alpha^2R_1^2R_2^2\cos^2\tau\Big). \qquad (5.4)
\end{aligned}$$

The solution of $f(R_1, R_2, \phi, \tau, \alpha) = 0$, together with equations (5.3)-(5.4) both set equal to zero gives us point H; however, trying to manipulate these equations to produce an explicit representation has produced little success. We have tried solving

for the fixed points as a function of the parameters as $R_1(\tau,\alpha), R_2(\tau,\alpha), \phi(\tau,\alpha)$, and have also tried solving for the parameter values as functions of the phase space variables as $\tau = \tau(R_1, R_2, \phi), \alpha = \alpha(R_1, R_2, \phi)$. In both instances, we tried to solve using τ as the delay parameter and then separately using $\cos\tau$ as the delay parameter. We thus resorted to numerically estimating the values $R_1, R_2, \phi, \tau, \alpha$ at point H. Substitution of these values into (2.24)-(2.26) shows the accuracy to be the same order as the last decimal place kept.

To see how our analysis may be affected since we only have estimates of all the values, we will at various times consider simple examples which illustrate the problems we may expect in a given calculation. We will thus bootstrap our way through the analysis of point H. If we follow the analysis of point P, our first step would be to linearize about the equilibrium point (5.1). Our system is then in the form $\dot{\mathbf{x}} = A\mathbf{x}$; however, the entries of A are not exact. It is known that $O(\epsilon)$ changes in our matrix can result in $O(\sqrt{\epsilon})$ changes in the eigenvalue [10]. And although the sensitivity of a numerical estimate is important, the stability of the method chosen for calculating the desired quantities will be very crucial.

5.2 An Example of Expected Problems

We consider the system

$$\begin{aligned} \dot{x} &= x^2 + y^2 \\ \dot{y} &= -y + x^2. \end{aligned} \tag{5.5}$$

We first will analyze this analytically and then contrast what happens when small errors are introduced.

Linearization of (5.5) gives

$$\begin{aligned} \dot{x} &= 0 \\ \dot{y} &= -y. \end{aligned} \tag{5.6}$$

This has one zero eigenvalue and thus we can examine the corresponding one-dimensional center manifold. We assume a center manifold of the form

$$y = ax^2 + \cdots \tag{5.7}$$

so that

$$\dot{y} = 2ax\dot{x} + \cdots. \tag{5.8}$$

As in the previous center manifold calculations, we substitute equations (5.7),(5.8) into the $\dot{y}$ equation of (5.5) and obtain

$$2a\dot{x}x = -(ax^2 + \cdots) + x^2. \tag{5.9}$$

This introduces $\dot{x}$ terms which we clear from the equation by substitution, using equation (5.5):

$$2a(x^2 + y^2)x = -(ax^2 + \cdots) + x^2. \tag{5.10}$$

This introduces y terms and we then substitute in for y using (5.7) to obtain

$$2a(x^2 + (ax^2 + \cdots)^2)x = -ax^2 - bx^3 + x^2. \tag{5.11}$$

Taylor expanding and keeping quadratic terms in x gives $0 = -ax^2 + x^2$. Equating the coefficient of x^2 to zero gives $a = 1$ and the center manifold is thus $y = x^2$.

Substitution into equation (5.5) shows that the flow on our one-dimensional center manifold is then described by

$$\dot{x} = x^2 + x^4. \tag{5.12}$$

If we slightly misidentified our eigenvectors in the above analysis (since inaccurate eigenvalues give inaccurate eigenvectors), our system would be given by

$$\begin{pmatrix} x \\ y \end{pmatrix} = \begin{pmatrix} 1 & \beta \\ \alpha & 1 \end{pmatrix} \begin{pmatrix} x_1 \\ y_1 \end{pmatrix}, \tag{5.13}$$

where α, β are small. Here x, y correspond to our physical coordinates x, y, z at point H, while x_1, y_1 correspond to the approximate eigencoordinates. In our original example, equation (5.5), we thus have

$$\begin{aligned} \dot{x} &= (x_1 + \beta y_1)^2 + (\alpha x_1 + y_1)^2 \\ \dot{y} &= -(\alpha x_1 + y_1) + (x_1 + \beta y_1)^2. \end{aligned} \tag{5.14}$$

Differentiating (5.13) and substituting into (5.14), we are able to solve for x_1, y_1 to obtain expressions of the form

$$\dot{x}_1 = f(x_1, y_1), \qquad \dot{y}_1 = g(x_1, y_1) \tag{5.15}$$

for some functions f, g. Even though these equations have small error terms included, we still hope to be able to perform a one-dimensional center manifold analysis. Proceeding as before, we assume a center manifold of the form $y_1 = Ax_1^2 + \cdots$ so that $\dot{y}_1 = 2Ax_1\dot{x}_1$. Substituting these expressions into the $\dot{y}_1$ equation of (5.15) and Taylor expanding (keeping quadratic terms in x_1) gives

$$0 = -\frac{\alpha}{\alpha\beta - 1} x_1 - \left(\frac{2A\beta\alpha}{\alpha\beta - 1} + \frac{\alpha + \alpha^3 - 1 + A}{\alpha\beta - 1} \right) x_1^2. \tag{5.16}$$

We ignore the x_1 term since we know it is zero and proceed to set the coefficient of the x_1^2 term to zero and obtain

$$A = \frac{1 - \alpha - \alpha^3}{1 + 2\alpha\beta + 1}. \tag{5.17}$$

Thus the center manifold is known since $y = Ax_1^2$. Ignoring terms of $O(\beta^2, \alpha^2, \alpha\beta)$ (since the product is assumed small in each case), the flow on the center manifold is then described by the equation

$$\dot{x}_1 = x_1^2 + (2\alpha + 2\beta)x_1^3 + (1 - 2\alpha)x_1^4. \tag{5.18}$$

For this example, if we take $\alpha = .0001, \beta = .0001$, we see that the flow on the center manifold becomes

$$\dot{x}_1 = x_1^2 + 0.0004x_1^3 + 0.9998x_1^4. \tag{5.19}$$

Stepping back and comparing (5.19) with the exact flow on the center manifold, equation (5.12), we see that different behavior may occur depending on α, β.

The above error analysis assumed incorrect eigenvectors. If the equilibrium point was also off:

$$x = x_2 + \delta, \quad y = y_2 + \xi, \tag{5.20}$$

equation (5.5) becomes (after ignoring higher order terms in δ, ξ):

$$\begin{aligned} \dot{x}_2 &= x_2^2 + y_2^2 + 2(x_2\delta + y_2\xi) \\ \dot{y}_2 &= -y_2 + x_2^2 + (2x_2\delta - \xi). \end{aligned} \tag{5.21}$$

Again we see that errors in the beginning will propagate throughout. Keeping these examples in mind, we proceed with the analysis of point H.

5.3 Jordan Form

Recall that point H is defined to be the point along the double saddle-node bifurcation curve (in the $\cos\tau - \alpha$ plane) which has two zero eigenvalues; however, numerical roundoff error prevents us from finding point H exactly, no matter how many significant figures are kept. The analysis performed at point H will be, in theory, the same as that performed at point P since both have a two-dimensional center manifold. The standard calculation at point P is to use chain vectors to find the second generalized eigenvector for $\lambda = 0$. But we take a simple example to show our current case will require a more stable algorithm.

5.3.1 Double Zero Eigenvalue

Consider the matrix

$$A = \begin{pmatrix} 1 & -1 \\ 1 & -1 \end{pmatrix} \tag{5.22}$$

which has repeated eigenvalue zero with eigenvector $(1,\ 1)$. If we pick the chain vector $u = \frac{1}{2}(1,\ -1)$, this gives

$$R = \begin{pmatrix} 1 & \frac{1}{2} \\ 1 & -\frac{1}{2} \end{pmatrix}.$$

Since $R^{-1}AR = J$, we find

$$J = \begin{pmatrix} 0 & 1 \\ 0 & 0 \end{pmatrix}.$$

We recall that this was the case at point P. In the present case, we consider a slight change in A:

$$\tilde{A} = A + \epsilon M, \qquad \epsilon << 1. \tag{5.23}$$

It turns out that $\tilde{A}$ has approximate eigenvalues $\lambda, -\lambda$ with eigenvectors $v = (1,\ 1-\lambda), (1,\ 1+\lambda)$ where $\lambda \sim \sqrt{\epsilon}$ (cf. [10]). With point P, we computed a chain vector via $Au = v$ and obtained two linearly independent equations. But $\tilde{A}$ is now invertible (with probability one since the set of singular n-by-n matrices has measure zero [40]) and thus we have $u = \tilde{A}^{-1}v$. But

$$\tilde{A}^{-1} \sim \frac{1}{\lambda^2}\tilde{A} \tag{5.24}$$

so that

$$u \sim \frac{1}{\lambda^2}\tilde{A}v \sim \frac{1}{\lambda}v \tag{5.25}$$

which is parallel to v, whereas for exact A, we know $u \perp v$. Thus an alternative method for computing the chain vector is sought.

Since $Av = 0$ and $Au = v$, we consider $A^2u = 0$ as a more stable method of finding the companion matrix for the Jordan form. Using $\tilde{A}$ from before, we calculate

$$\tilde{A}^2 = A^2 + \epsilon(AM + MA) + O(\epsilon^2). \tag{5.26}$$

Since $\tilde{A}$ has eigenvalues $\lambda, -\lambda$ with eigenvectors $v = (1,\ 1-\lambda), (1,\ 1+\lambda)$, we see that $\tilde{A}^2$ has eigenvalues $\lambda^2, 2+\cdots$ with eigenvectors $v = (1,\ -1+\cdots), (1,\ 1+\cdots)$.

We now consider this type of example in a three-dimensional problem by considering

$$A = \begin{pmatrix} \frac{3}{2} & 0 & -\frac{1}{2} \\ \frac{3}{2} & 0 & -\frac{1}{2} \\ \frac{7}{2} & -2 & -\frac{1}{2} \end{pmatrix},$$

which has eigenvalues $\lambda = 0, 0, 1$ with

$$J = \begin{pmatrix} 0 & 1 & 0 \\ 0 & 0 & 0 \\ 0 & 0 & 1 \end{pmatrix}, \quad R = \begin{pmatrix} 1 & 1 & 1 \\ 1 & 0 & 0 \\ 3 & 1 & 1 \end{pmatrix},$$

where $A = RJR^{-1}$. If we again assume $\tilde{A} = A + \epsilon M$, $\epsilon << 1$, the eigenvalues satisfy $\lambda \sim \sqrt{\epsilon}, -\sqrt{\epsilon}, 1$. Taking $\epsilon \sim O(10^{-4})$, the eigenvector for $\lambda = 1$ is $(1,\ .9994,\ 1.0003)$ whereas it is exactly $(1,\ 1,\ 1)$ for A. One of the eigenvectors for $\lambda = 0$ is calculated to be $(1,\ 1.004,\ 2.9982)$ whereas it is exactly $(1,\ 1,\ 3)$ for A. For the chain vector u, we want $(\tilde{A} - \lambda I)u = v$, i.e., $\tilde{A}u = v$ (since $\lambda = 0$). and so we assume $u = (u_1,\ u_2,\ u_3)$. We need to find 3 equations in our three unknowns u_1, u_2, u_3. From the previous discussion we know that $\tilde{A}^2 u = 0$ gives one equation and $\tilde{A}u = v$ gives one equation (whereas with point P, the latter gave *two* equations). We can always use an orthogonal projection to make u unique:

$$\tilde{u} = u - \left(\frac{u \cdot v}{v \cdot v}\right) v. \tag{5.27}$$

The third equation is thus obtained by subtracting off the v component. In our current example, we find $u = (u_1,\ u_2,\ 2u_2 + u_1)$ from the $\tilde{A}^2 u = 0$ equation. From the $\tilde{A}u = v$ equation, we find $u = (u_1,\ -1 + u_1,\ -2 + 3u_1)$. To make this unique,

we put

$$\tilde{u} = u - \left(\frac{u \cdot v}{v \cdot v}\right) v = \begin{pmatrix} \frac{7}{11} \\ \frac{-4}{11} \\ \frac{-1}{11} \end{pmatrix}. \tag{5.28}$$

Numerically, we find

$$\tilde{u} = \begin{pmatrix} .636 - .0007u_1 \\ -.363 - .0014u_1 \\ -.0911 + .0007u_1 \end{pmatrix}. \tag{5.29}$$

The terms with u_1 will always appear at the significant figure that we have rounded to and in practice, we take care of this by setting $u_1 = 0$ to obtain $\tilde{u} = (.636,\ .363,\ -.0911)$. The important point in these calculations is that the error introduced always appears near the order of the number of decimal places kept. To see this mathematically, we consider the system of equations to be solved as $F(a_e) = 0$, where a_e is the exact answer (and is a row of the matrix A in the present case). For $a \approx a_e$, we have $F(a) = F(a_e) + DF_{a_e}(a - a_e) + \cdots$. Then the error w is given by $w = DF_{a_e}(a - a_e)$, ignoring higher order terms. If DF_{a_e} is invertible, the error will then propagate linearly and the system we are solving is said to be *regular*. In the above calculations and the analogous ones at point H, this is always the case.

In dealing with point H, we know $\lambda = 0, -1$ are the eigenvalues with $\lambda = 0$ being a double zero eigenvalue, by definition. The second eigenvalue is seen to approach $\lambda = -1$ as more significant figures are kept. We calculate the first eigenvector of $\lambda = 0$ by assuming $v = (1,\ v_1,\ v_2)$ (since eigenvectors can always be scaled in magnitude) and solving for v_1, v_2 in the two linearly independent equations generated by $Av = 0$. We then proceed to find the chain vector by the above algorithm.

5.4 Unfolding H

We begin by linearizing about point H by using

$$R_1 = 2.0151 + x, \tag{5.30}$$

$$R_2 = 1.3926 + y, \tag{5.31}$$

$$\phi = 0.56394 + z \tag{5.32}$$

so that the coordinates x, y, z are physical coordinates which are local about point H. Substituting (5.30)-(5.32) into the slow-flow equations (2.24)-(2.26), setting $\mu = \nu = 0$ and ignoring higher order terms, we obtain

$$\begin{pmatrix} x \\ y \\ z \end{pmatrix} = A \begin{pmatrix} x_1 \\ y_1 \\ z_1 \end{pmatrix}, \tag{5.33}$$

where

$$A = \begin{pmatrix} -1.0227 & 0.010972 & 0.28162 \\ -0.17801 & -0.22725 & -0.19462 \\ -0.13871 & 0.20071 & 0.25000 \end{pmatrix}. \tag{5.34}$$

We now impose the eigenvalues (by definition of point H) $\lambda = 0, 0, -1$. Center manifold theory tells us that we can expect a two-dimensional center manifold. As the exact matrix A is not diagonalizable, we follow the above discussion to obtain a generalized set of eigenvectors. We find

$$R = \begin{pmatrix} 1 & 1 & 1.5826 \\ 0.24827 & -4.0279 & 8.8157 \\ 0.071101 & 3.7886 & 8.9548 \end{pmatrix} \tag{5.35}$$

and

$$R^{-1}AR = J = \begin{pmatrix} -1.0000 & 0 & 0 \\ 0 & 0 & 1.0000 \\ 0 & 0 & 0 \end{pmatrix}. \tag{5.36}$$

Now with our full set of generalized eigenvectors, we can rotate to generalized eigencoordinates so that we may apply center manifold theory. The eigencoordinates, x_1, y_1, z_1, are defined by the equation

$$\begin{pmatrix} x \\ y \\ z \end{pmatrix} = R \begin{pmatrix} x_1 \\ y_1 \\ z_1 \end{pmatrix}.$$

We substitute these values of x, y, z into (5.33), which will allow us to obtain the flow on the center manifold in terms of the eigencoordinates.

Since we want to unfold point H, we make the substitution

$$\tau = 4.2026 + \nu \tag{5.37}$$

$$\alpha = 0.40505 + \mu, \tag{5.38}$$

into the previous result. We note here that the analysis at point H was done keeping answers to 50 decimal places in all the variables. (By carefully watching the error propagate, we see that error introduced at each calculation increases linearly since the systems being solve are regular but we do not run into problems similar to those that we encountered in finding the chain vector via an unstable method.) We calculate the expected double saddle-node bifurcation curve

$$\alpha^2 = \frac{1}{8(1 - \cos^2 \tau)}, \quad \cos^2 \tau < \frac{1}{3}$$

to be given, in local coordinates by the equation

$$\mu = -.2264\nu + .3291\nu^2. \tag{5.39}$$

The empirical polynomial expression for the unsymmetrical Hopf bifurcation curve (2.54) is the other curve we expect to see and is given by

$$\mu = 0.000047 - 0.2260\nu \tag{5.40}$$

at point H; however, as with point P, we expect this equation to only roughly approximate the actual curve.

For the unfolding of H, we begin with the three differential equations in terms of the eigencoordinates x_1, y_1, z_1. Proceeding as with point P, we solve for $\dot{x}_1, \dot{y}_1, \dot{z}_1$ and Taylor expand the equations keeping cubic terms in x_1, y_1, z_1 (cf. point P) and quadratic terms in μ, ν. We then have three equations:

$$\dot{x}_1 = G_1(x_1, y_1, z_1, \mu, \nu) \tag{5.41}$$

$$\dot{y}_1 = G_2(x_1, y_1, z_1, \mu, \nu) \tag{5.42}$$

$$\dot{z}_1 = G_3(x_1, y_1, z_1, \mu, \nu). \tag{5.43}$$

We again note that although the notation is the same as that used in the analysis of point Q and P, the values of the variables G_i (and $\tilde{G}_i$ which is used later) are not the same in any of the cases. From center manifold theory, we know the flow on the center manifold is going to be given by a two-dimensional system of equations. In terms of the eigencoordinates, only the x_1 direction has nonzero eigenvalue $\lambda = -1$ and so our center manifold will involve both y_1 and z_1 terms. We thus want to

express x_1 in terms of y_1, z_1. To do this, we need to assume an appropriate form for the center manifold. Trying to stay as general as possible, we assume the form

$$\begin{aligned} x_{1,cm} &= z_1^2(a_1 + a_2\ \mu + a_3\ \nu + a_4\ \mu^2 + a_5\ \mu\ \nu + a_6\ \nu^2) \\ &+ z_1\ y_1(a_7 + a_8\ \mu + a_9\ \nu + a_{10}\ \mu^2 + a_{11}\ \mu\ \nu + a_{12}\ \nu^2) \\ &+ y_1^2(a_{13} + a_{14}\ \mu + a_{15}\ \nu + a_{16}\ \mu^2 + a_{17}\ \mu\ \nu + a_{18}\ \nu^2) \\ &+ z_1(a_{20}\ \mu + a_{21}\ \nu + a_{22}\ \mu^2 + a_{23}\ \mu\ \nu + a_{24}\ \nu^2) \\ &+ y_1(a_{26}\ \mu + a_{27}\ \nu + a_{28}\ \mu^2 + a_{29}\ \mu\ \nu + a_{30}\ \nu^2) \\ &+ (a_{32}\ \mu + a_{33}\ \nu + a_{34}\ \mu^2 + a_{35}\ \mu\ \nu + a_{36}\ \nu^2) \end{aligned} \tag{5.44}$$

where we set $a_{19} = a_{25} = a_{31} = 0$ since we do not want any $O(1)$ translation in the constant or linear terms. Comparing with (3.3), we see that the center manifold at point H will be given by

$$W^c = \{(x_1, y_1, z_1) |\ x_1 = h(y_1, z_1)\} \tag{5.45}$$

with $h(0) = Dh(0) = 0$ and $h(y_1, z_1) = x_{1,cm}$. We substitute this equation into (5.41). This will introduce $\dot{y_1}, \dot{z_1}$ terms after the differentiation is carried out. We then substitute equations (5.42)-(5.43) which reintroduces x_1 into the equations but rids them of any $\dot{x_1}, \dot{y_1}, \dot{z_1}$ terms. One more substitution of equation (5.44) into the new version of equation (5.41) gives an equation which only has y_1, z_1 terms. We move all the terms to one side and Taylor expand the expressions, keeping cubic terms in x_1, y_1, z_1 and quadratic terms in μ, ν. Our resulting equation $\tilde{G}_1(y_1, z_1, \mu, \nu) = 0$ can then be compared to equation (5.44). We thus obtain the

center manifold

$$\begin{aligned} x_{1,cm} &= z_1^2(10.089 - 22.225\mu + 24.131\nu - 227.48\mu^2 + 221.51\mu\nu - 22.448\nu^2) \\ &+ z_1 y_1(6.3626 + 50.924\mu - 34.518\nu + 152.32\mu^2 - 218.23\mu\nu + 26.190\nu^2) \\ &+ y_1^2(-4.7379 - 14.327\mu + 3.8614\nu - 8.1954\mu^2 + 26.445\mu\nu - 4.5501\nu^2) \\ &+ z_1(0.64599\mu + 3.0357\nu - 19.987\mu^2 + 20.377\mu\nu - 2.1065\nu^2) \\ &+ y_1(3.8299\mu - 1.4431\nu + 5.3981\mu^2 - 7.9593\mu\nu + 0.15185\nu^2) \\ &+ 0.34963\nu - 0.40602\mu^2 + 1.4019\mu\nu - 0.10759\nu^2. \end{aligned} \tag{5.46}$$

Note that unlike with point P, we now have linear terms (even though none are $O(1)$ terms). We substitute the above expression for the center manifold into (5.42)-(5.43) and obtain

$$\begin{aligned} \dot{y} &= y^2(0.98661 - 0.60929\mu + 0.39509\nu - 0.13803\nu^2 + 1.6947\nu\mu - 0.044578\mu^2) \\ &+ yz(-5.2574 + 0.57278\mu + 1.7861\nu + 7.5440\mu^2 - 1.0240\nu\mu + 1.5074\nu^2) \\ &+ z^2(1.5616 - 8.1958\mu + 2.1465\nu - 8.3280\mu^2 + 12.295\nu\mu + 1.4497\nu^2) \\ &+ y(0.34740\mu - 0.11105\nu + 0.17847\mu^2 - 0.36642\nu\mu - .0010127\nu^2) \\ &+ z(1 + 1.9284\mu + 0.42867 - 0.13104\mu^2 + 1.5027\mu\nu - 0.41588\nu^2) \\ &+ (0.11416\mu - 0.050703\nu - 0.11102\nu\mu - 0.031126\nu^2) \\ \dot{z} &= y^2(-0.12636 + 1.3503\mu - 0.27086\nu + 1.4980\mu^2 - 1.6311\nu\mu - 0.082164\nu^2) \\ &+ yz(3.1092 + 2.1009\mu + 1.6089\nu - 4.9572\mu^2 + 8.5392\nu\mu - 1.1615\nu^2) \\ &+ z^2(-2.8774 - 2.2378\mu - 0.43067\nu + 2.6039\mu^2 - 2.8088\nu\mu + 0.82512\nu^2) \\ &+ y(-0.16636\mu - 0.13440\nu - 0.18469\mu^2 - 0.18154\nu\mu + 0.000409834\nu^2) \end{aligned}$$

$$+ \quad z(0.19507\mu - 0.29706\nu + 0.015631\mu^2 - 0.91043\nu\mu - 0.031066\nu^2)$$

$$+ \quad (-0.048298\mu - 0.010936\nu - 0.040051\nu\mu + 0.10317\nu^2) \tag{5.47}$$

as the equations describing the flow on the center manifold.

5.5 Normal Form at Point H

Recall that in performing the normal form calculation at point P, we used successive near-identity transformations to convert the $\dot{y}$ equation of our system to the form $\dot{y} = z$ (cf. (4.29)). In our attempt to perfom the same analysis at point H, we unfortunately run into problems due to error propagation. The problems are seen because adding cubic terms to the normal form equations, for instance, changes the bifurcations that we observe while keeping cubic terms in (5.47) doesn't change the bifurcation curves we observe. As we know our entire analysis was approximate, we cannot trust any results which are not stable to small changes such as higher order corrections. But the flow on the center manifold, given by equation (5.47) *does* illustrate the behavior we expect, namely a saddle-node bifurcation and a supercritical Hopf bifurcation both coming in tangent to each other and the Hopf terminating at the intersection point H, as is seen using DsTool. In addition, we observe that the homoclinic bifurcation curve terminates at point H. (See Figure 5.1 and note that the same bifurcation sequence is happening for the partner given by $(R_2, R_1, -\phi)$.) In addition, we graphically estimate the slope of the incoming curves to be given by

$$\mu \approx -0.226\nu \tag{5.48}$$

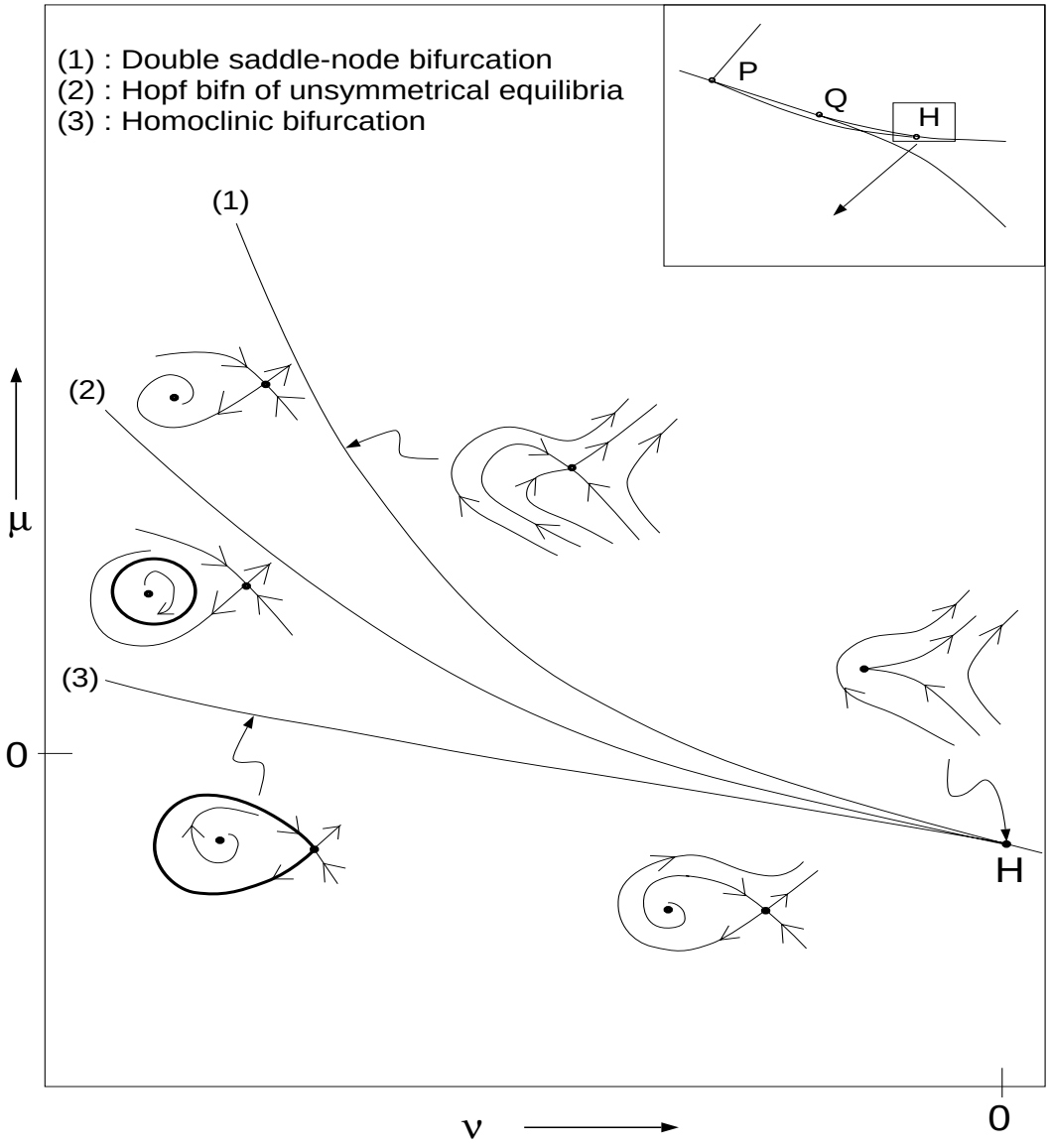

Figure 5.1: Numerical estimates of bifurcation set at point H and corresponding phase portraits. By symmetry, this bifurcation sequence occurs at its mirror image under (2.27) in the $\cos\tau - \alpha$ plane. The bifurcation curves are drawn slightly distorted for better viewing.

which agrees with the linear term of the expected incoming curves; however, these results are only *local* results and thus we must restrict our variables to a small neighborhood around the origin. In this case, we need to keep $-0.0004 < y1, z1 < 0.0004$ and $-0.004 < \mu, \nu < 0.004$ in order to keep extraneous roots from appearing. A closer examination of equation (5.47) and the corresponding bifurcation sequence seen at point H reveals that we actually have an unsymmetric Takens-Bogdanov bifurcation (as opposed to the symmetric Takens-Bogdanov bifurcation which was seen at point P) and numerical simulation using DsTool—both the full equations (2.24)-(2.26) and via center manifold theory—confirms the phase portraits are the ones expected [12].

5.6 Global Results

Recall that we were able to see, through a local analysis, a symmetry-breaking double homoclinic bifurcation at point P (cf. (4.4)) because the two unsymmetrical equilibria were bifurcating off the in-phase mode and the in-phase mode formed the saddle connection for both homoclinic orbits. Now, however, our local behavior is not in the neighborhood of the in-phase mode but is instead local in the neighborhood of one of the unsymmetrical equilibria. This difference turns out to be extremely important because we are not able to infer what happens to the in-phase mode throughout this bifurcation sequence. To be more specific, we observe a stable limit cycle being born as the unsymmetrical Hopf bifurcation curve is crossed from above in the $\nu - \mu$ (or equivalently, the $\cos\tau - \alpha$) parameter plane. This limit

cycle grows and eventually becomes a homoclinic orbit for certain values of μ, ν, see Figure 5.1.

By symmetry arguments, we know this same bifurcation sequence is also occurring at the other unsymmetrical equilibria given by $(R_2, R_1, -\phi)$ in terms of the original slow-flow variables. For slightly lower values of ν with μ fixed, no stable limit cycle exists. Recall that at point P, one large stable limit cycle resulted from the double homoclinic connection. Thus it does not appear that we have anything that can merge with the unstable limit cycle (created from the in-phase mode Hopf bifurcation) which still surrounds all of the equilibria (excluding the out-of-phase mode). We must go back to equations (2.24)-(2.26) to examine the fate of the unstable limit cycle.

Using DsTool, we were able to see that the unstable limit cycle created in the Hopf bifurcation (2.46) and destroyed near point P in the limit cycle coalescence (cf. (2.54),(4.79)) disappears for values of α slightly below the homoclinic bifurcation curve (and thus to the left of point H) which terminates at point H, cf. Figure 5.1. For example, fixing $\tau = 4.15$ and varying α we see that

i) two stable limit cycles exist below $\alpha \approx 0.4172$; unstable limit cycle exists

ii) a homoclinic connection of stable limit cycles occurs at $\alpha \approx 0.4167$; unstable limit cycle exists

iii) no limit cycles exist at or below $\alpha \approx 0.4163$

The last observation was inferred as curves beginning close to the unsymmetrical spiral ended up at the out-of-phase mode, since they are no longer restricted by the unstable limit cycle. We note that the phase portraits for the latter two cases are not

homeomorphic since in one case we have one unstable and two stable limit cycles and in the next case we have no limit cycles. Careful numerical exploration reveals an additional bifurcation curve which creates a stable limit cycle in this region (through a heteroclinic connection) and occurs near $\alpha \approx 0.41636$, see Figure 5.2. (We again note that the pictures in Figures 5.2-5.3 are drawn as if they are two-dimensional because numerical simulation of the slow-flow equations (2.24)-(2.26) indicates that all trajectories are quickly drawn onto a somewhat curved two-dimensional surface on which the dynamics shown in the figure occur.) Independent numerical checks reveal that a limit cycle does indeed exist for certain parameter values, including for instance $\tau = 4.15, \alpha = 0.41635$. As the homoclinic connection curve emanating from point P terminated at point H, we now seek to find the beginning point of this curve of heteroclinic connections which give rise to the large stable limit cycle. Numerical exploration leads us to conjecture that this curve of heteroclinic connections begins at the point where the homoclinic curve passes through the pitchfork bifurcation curve given by equation (2.38) and we label this point S. We also label the intersection of the limit cycle coalescence curve and the in-phase mode pitchfork bifurcation curve as point A. Figure 5.3 shows the bifurcation curves in the neighborhood of point S, while Figure 5.4 shows the bifurcation diagram found by encircling point H. From the discussion above, we know the homoclinic bifurcation curve extends into point H in the $\cos\tau - \alpha$ plane but we now must also consider the fate of the heteroclinic connection curve and the limit cycle fold curve. Although they appear to approach point H they cannot terminate at point H because the stable and unstable manifolds of the unsymmetrical equilibria are needed to sepa-

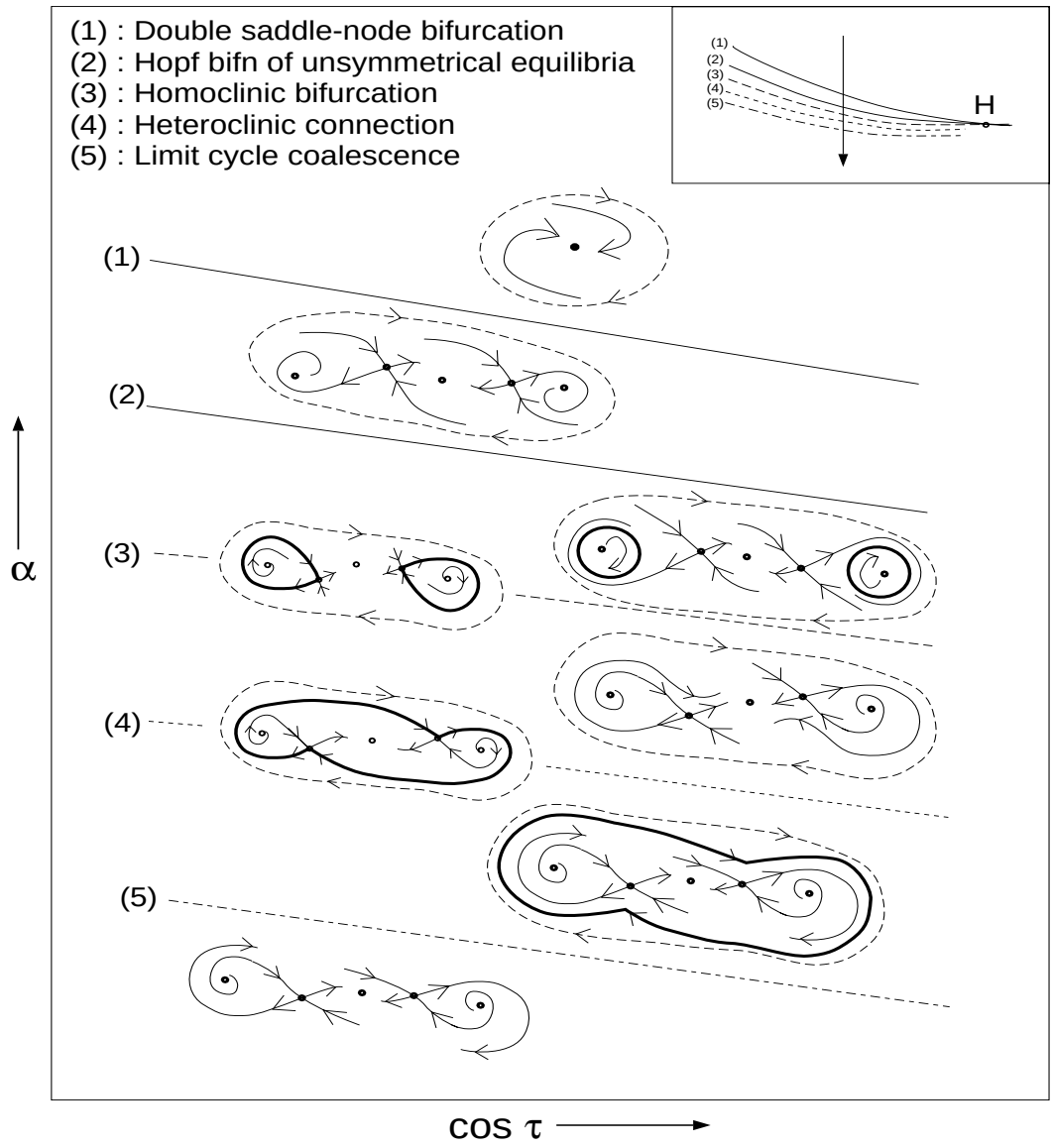

Figure 5.2: Bifurcation sequence to the left of point H. The out-of-phase mode exists (and is stable) throughout. The third eigendirection is contracting and (nearly) normal to the plane of this page.

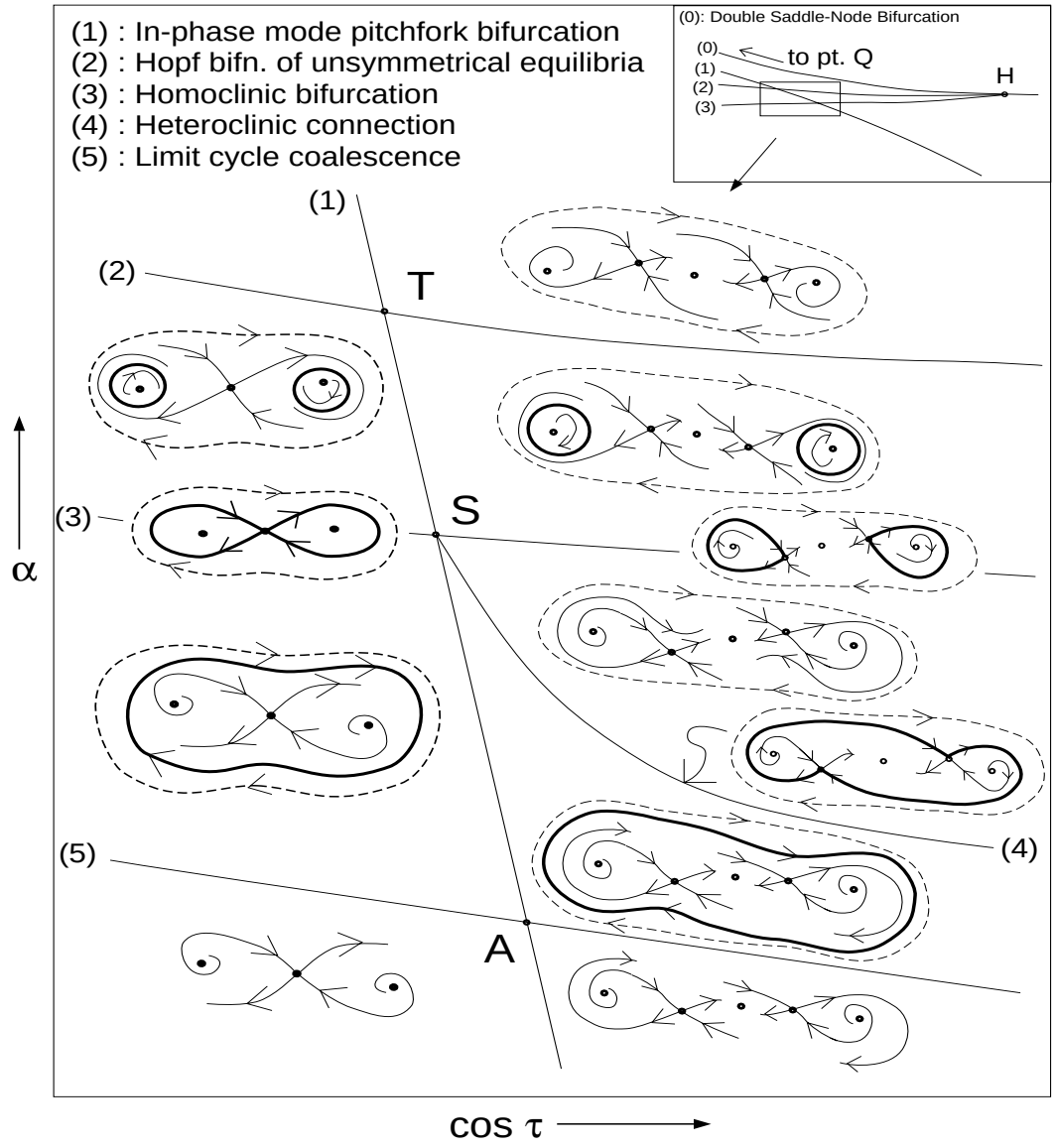

Figure 5.3: Bifurcation set (numerical) near points T, S and A. The out-of-phase mode exists (and is stable) throughout. The third eigendirection is (nearly) normal to the page and has negative eigenvalue. Note that curve (1) is drawn distorted for better viewing.

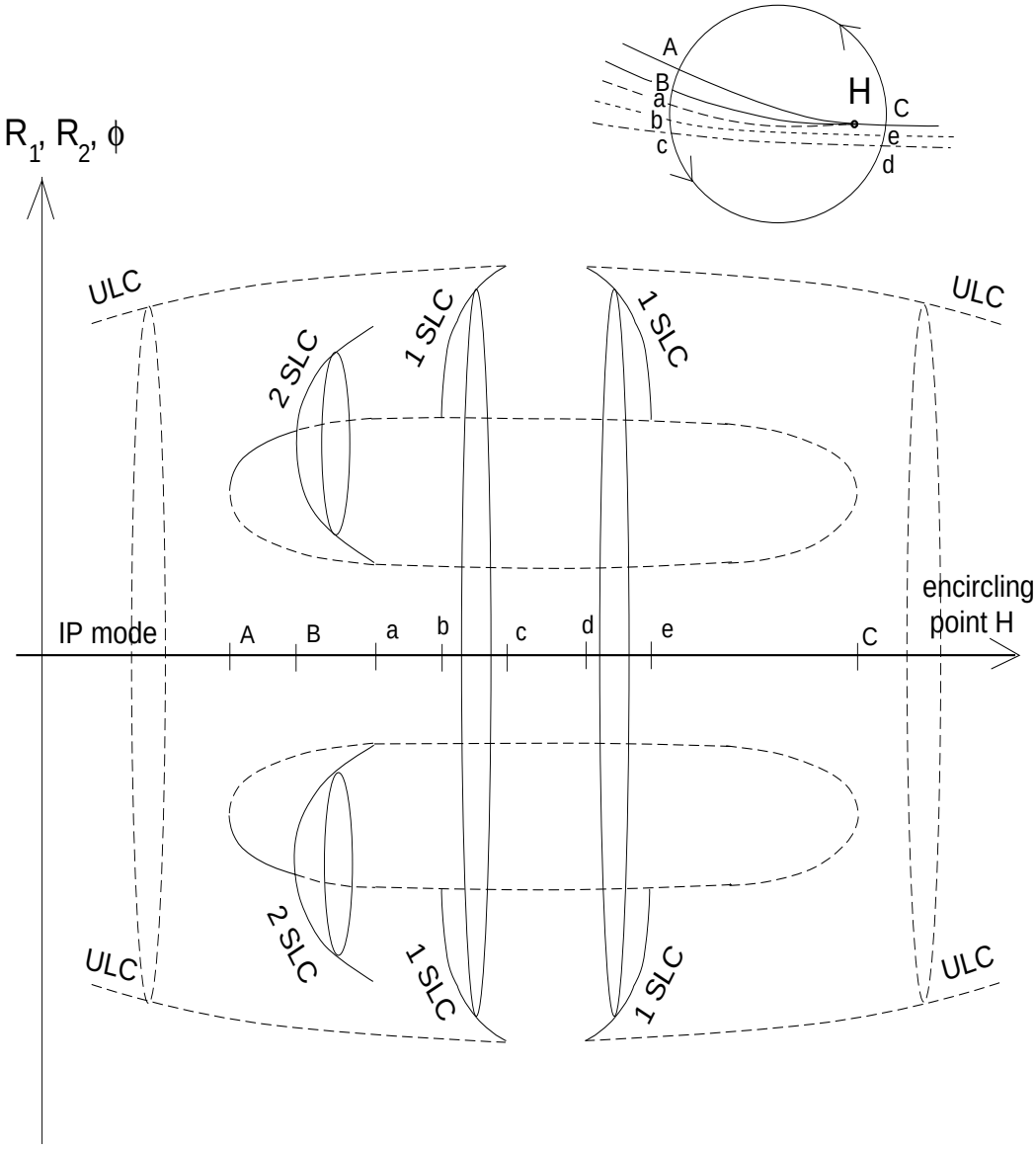

Figure 5.4: Bifurcation diagram encircling point H. Note that stable and unstable limit cycles are shown.

rate the basins of attraction of the stable in-phase mode and the stable limit cycle, see Figures 5.2-5.3. We can also see this by trying to collapse the unsymmetrical equilibria together (which occurs at point H) and then realizing that as a result of the double saddle-node bifurcation, we would have a stable limit cycle surrounding the stable in-phase mode and this clearly cannot happen. The termination point of these two curves will be discussed in the next chapter.

Chapter 6

The Completed Picture

6.1 Introduction

We are now in a position to piece together most of the bifurcation set for the slow-flow equations (2.24)-(2.26). Through unfoldings of the degenerate points Q, P and H, we are able to see the bifurcation sets near these points. Figures 2.4, 3.2, 4.3, 5.1 and 5.3 together with equations (2.37), (2.38), (2.46) and (2.49) give us a nearly complete picture. We will attempt to complete the bifurcation set by considering separately what happens above and below the curve H-H', given by equation (2.49).

6.2 The Unstable Limit Cycle Above H-H'

In determining the termination point of the limit cycle fold and heteroclinic bifurcation curves, we will first examine what happens to the unstable limit cycle created in the Hopf bifurcation across (2.46) by looking along the line $\cos\tau = 0$, where

we will take $\tau = \frac{3\pi}{2}$ for the sake of definiteness. (Choosing $\tau = \frac{\pi}{2}$ simply changes the directions in which the flow rotates.) At this τ value, the slow-flow equations become

$$\dot{R}_1 = \frac{1}{2}\left[R_1 \left(1 - \frac{R_1^2}{4}\right) + \alpha\ R_2\ \sin\phi\right], \tag{6.1}$$

$$\dot{R}_2 = \frac{1}{2}\left[R_2 \left(1 - \frac{R_2^2}{4}\right) - \alpha\ R_1\ \sin\phi\right], \tag{6.2}$$

$$\dot{\phi} = \frac{\alpha}{2}\left[\frac{R_2}{R_1} - \frac{R_1}{R_2}\right]\ \cos\phi. \tag{6.3}$$

Equation (6.3) is zero for $\phi = \frac{\pi}{2}, -\frac{\pi}{2}$ and thus $\phi = \frac{\pi}{2}, -\frac{\pi}{2}$ are invariant planes.

Although we are chasing an unstable limit cycle in a three-dimensional system via numerical integration, we are able to analyze it analytically at $\cos\tau = 0$ because it lies in the invariant planes $\phi = \frac{\pi}{2}, R_2 = 0, \phi = -\frac{\pi}{2}, R_1 = 0$. More specifically, we are able to do this because the unstable limit cycle is actually a *stable* limit cycle in these planes and its only direction of instability is transverse to these invariant planes.

A key step in how this occurs involves what happens as we cross the midpoint of the line segment given by equations (6.1)-(6.3) along which $\cos\tau = 0$. Recall that $R_1, R_2 \geq 0$ and ϕ is 2π periodic. At $\cos\tau = 0$ the unstable limit cycle touches the singular planes $R_1 = 0, R_2 = 0$. By blowing up the singularity at $R_2 = 0$ via the transformation $d\eta = \frac{dt}{R_2}$ we see that $R_2 = 0$ is an invariant manifold with non-isolated equilibria occurring at $\phi = \frac{\pi}{2}, -\frac{\pi}{2}$ [5]. A similar situation occurs in the $R_1 = 0$ plane. Thus the flow along the unstable limit cycle involves two jumps along the singular planes $R_1 = 0$ and $R_2 = 0$, see Figure 6.1. Just to the left of the midpoint, i.e., when $\cos\tau < 0$, the jump occurs from $\phi = \frac{\pi}{2}$ to $\phi = -\frac{\pi}{2}$, and then

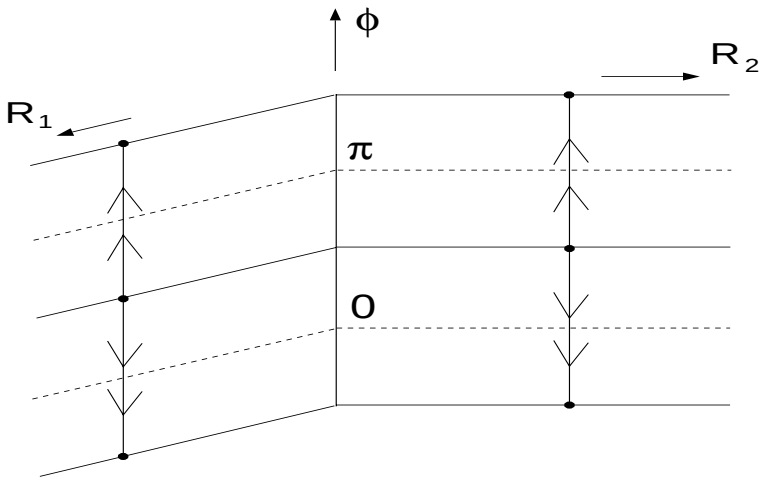

Figure 6.1: Flow in the $R_1 = 0$ and $R_2 = 0$ planes. The solid lines represent non-isolated equilibria. The lines with arrows in the $R_1 = 0$ and $R_2 = 0$ planes represent flow along constant R_2 and R_1, respectively.

back up, from $\phi = -\frac{\pi}{2}$ to $\phi = \frac{\pi}{2}$. The unstable limit cycle has grown from its initial little circle shape surrounding the in-phase mode to a large closed orbit, which still may be said to surround the in-phase mode, in the sense that the jumps go past $\phi = 0$; however, when we cross the midpoint of the line segment in parameter space (so that now $\cos\tau > 0$), the jump occurs from $\phi = \frac{\pi}{2}$ to $\phi = \frac{3\pi}{2}$ ($\equiv -\frac{\pi}{2}$ since ϕ is 2π periodic) and then back from $\phi = \frac{3\pi}{2}$ to $\phi = \frac{\pi}{2}$. The unstable limit cycle has grown from its initial little circle shape surrounding the out-of-phase mode to a large closed orbit, which still may be said to surround the out-of-phase mode, in the sense that the jumps go past $\phi = \pi$.

We now show the unstable limit cycle exists for all coupling values satisfying $\alpha > \frac{1}{\sqrt{8}}$ along the line $\tau = \frac{3\pi}{2}$. We note that when the flow requires that trajectories leave the first quadrant, we interpret them as having a phase change of 180 degrees,

i.e. $x_i = R_i \cos(t + \phi_i) = -R_i \cos(t + \phi_i + \pi), i = 1, 2$. This corresponds to a jump in $R_1 - R_2 - \phi$ space from $\phi = \frac{\pi}{2}$ to $\phi = -\frac{\pi}{2}$ or vice-versa, as will be shown in the ensuing discussion. (When τ isn't quite equal to $\frac{3\pi}{2}, \phi = \frac{\pi}{2}$ is no longer an invariant plane, and the orbit in $R_1 - R_2 - \phi$ space gets close to the jump, but forms a smooth curve.) The equations in the $\phi = \frac{\pi}{2}$ invariant plane become

$$\dot{R}_1 = \frac{1}{2}\left[R_1 \left(1 - \frac{R_1^2}{4}\right) + \alpha\, R_2\right], \tag{6.4}$$

$$\dot{R}_2 = \frac{1}{2}\left[R_2 \left(1 - \frac{R_2^2}{4}\right) - \alpha\, R_1\right]. \tag{6.5}$$

We construct a trapping region D in the first quadrant of the $\phi = \frac{\pi}{2}$ plane as follows (see Figure 6.2):

i) cut out a circle of radius $\epsilon << 1$ from the origin (since $R_1 = R_2 = 0$ is an unstable equilibrium point of (6.4)-(6.5).

ii) choose the box $0 \leq R_1, R_2 \leq \alpha_b$ where

$$\alpha_b = \begin{cases} 7 & \text{if} \quad \alpha \leq 2(1 + \sqrt{2}) \\ \alpha & \text{if} \quad \alpha > 2(1 + \sqrt{2}). \end{cases}$$

A simple calculation shows all trajectories are drawn into this region except along $R_2 = 0$ where $\dot{R}_2 < 0$ for all $\alpha > 0$. But any trajectory touching this line, say at $R_1 = k \leq \alpha_b$ is immediately taken to the $\phi = -\frac{\pi}{2}$ plane and is thus at $R_1 = k, R_2 = 0, \phi = -\frac{\pi}{2}$. By the invariance (2.27) which states $(R_1,\ R_2,\ \phi) \mapsto (R_2,\ R_1, -\phi)$, we can map the current position to the line $R_1 = 0, R_2 = k, \phi = \frac{\pi}{2}$ and we are again in the situation shown in Figure 6.2. The conclusion is that there exists a stable limit cycle in region D and hence an unstable limit cycle in the full $R_1 - R_2 - \phi$ space and that it exists for all $\alpha > \frac{1}{\sqrt{8}}$.

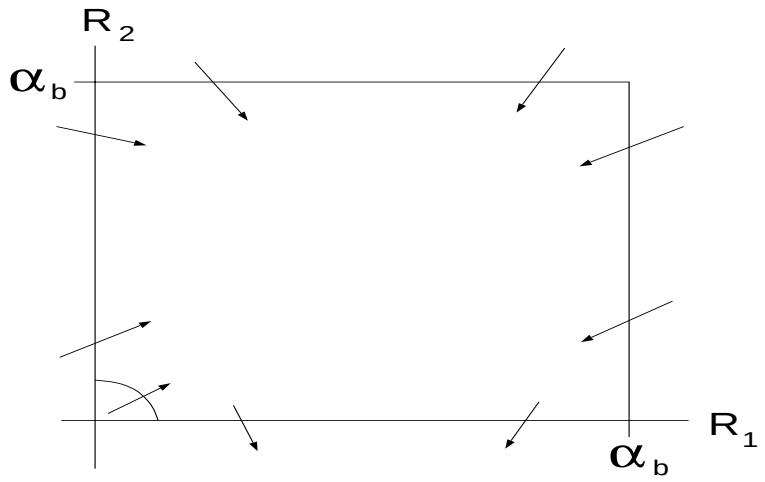

Figure 6.2: Trapping region D in $\phi = \frac{\pi}{2}$ plane for $\tau = \frac{3\pi}{2}, \alpha > \frac{1}{\sqrt{8}}$. Note that $R_2 = 0$ maps to $R_1 = 0$.

Now that we have shown an unstable limit cycle exists for all $\alpha > \frac{1}{\sqrt{8}}$, consider what happens as we move along a horizontal straight line in the parameter plane, above point P, say for $\alpha = 1$ (see Figure 6.3). When we cross the in-phase Hopf curve, given by (2.46), an unstable limit cycle is born which surrounds the in-phase mode, i.e., it is a little circle enclosing $R_1 = R_2 = 4, \phi = 0$, from equation (2.32). Similarly, when we cross the Hopf curve through point P' an unstable limit cycle is born which surrounds the out-of-phase mode, i.e., it is a little circle enclosing $R_1 = R_2 = 4, \phi = \pi$, from equation (2.47). As we move along this straight line, the unstable limit cycle thus transforms from a little circle around $\phi = 0$ to a little circle around $\phi = \pi$ for $R_1 = R_2 = 4$. Thus we now understand the unstable limit cycle for all parameter values in which only the in-phase and out-of-phase modes exist.

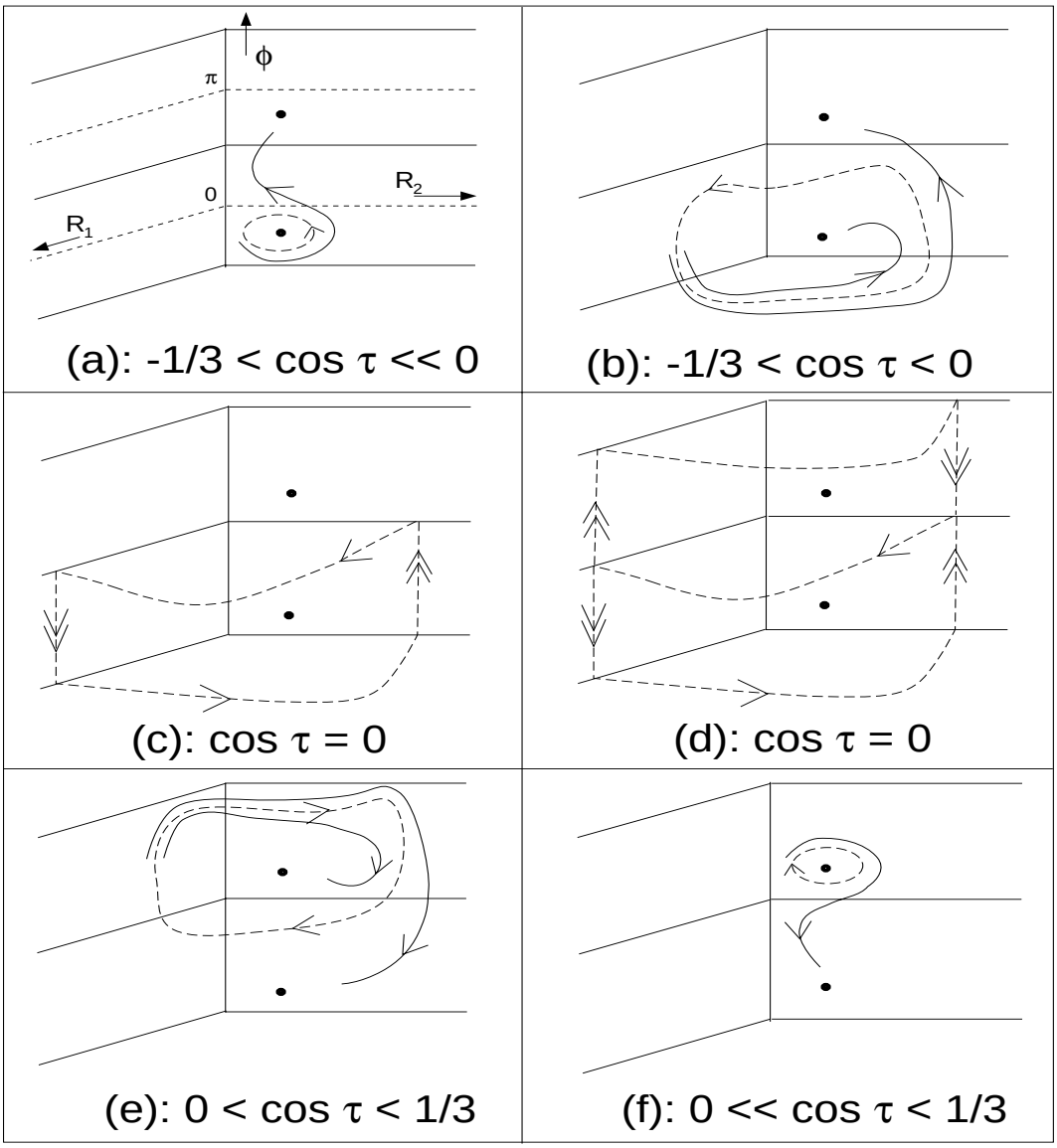

Figure 6.3: Unstable limit cycle for increasing values of $\cos\tau$ (with $\pi < \tau < 2\pi$) for $\alpha = 1$. Note that (c) and (d) are the same picture since ϕ is 2π periodic. See (a) for labeling of axes.

6.3 The Unstable Limit Cycle Below H-H'

We begin by defining point V, which lies on H-H' in the $\cos\tau - \alpha$ parameter plane, by $\cos\tau = 0, \alpha = \frac{1}{\sqrt{8}}$. Examining the phase portrait for $\alpha > \frac{1}{\sqrt{8}}$ (with $\cos\tau = 0$) allowed us to complete the picture for large coupling and we will see that this also happens for $\alpha < \frac{1}{\sqrt{8}}$. At point V, the double saddle-node bifurcation given by (2.49) occurs and the two pair of unsymmetrical equilibria are born at

$$R_1 = \frac{\sqrt{3}+1}{\sqrt{2}}\left(3-\sqrt{3}\right), R_2 = \left(3-\sqrt{3}\right), \phi = \frac{\pi}{2} \tag{6.6}$$

and its partner under (2.27). The eigenvalues at that point are $0, \frac{1}{4}, -\frac{5}{4}$ with corresponding eigenvectors

$$\begin{pmatrix} \frac{-5\sqrt{2}+3\sqrt{6}}{2} \\ 1 \\ 0 \end{pmatrix}, \quad \begin{pmatrix} 0 \\ 0 \\ 1 \end{pmatrix}, \quad \begin{pmatrix} \frac{5\sqrt{2}+3\sqrt{6}}{2} \\ 1 \\ 0 \end{pmatrix} \tag{6.7}$$

which have approximate values $(.1387,\ 1,\ 0), (0,\ 0,\ 1), (7.210,\ 1,\ 0)$. If we again consider the first quadrant of the $\phi = \frac{\pi}{2}$ plane, we see a saddle-node bifurcation occurring in the trapping region D defined above.

We now piece together the remainder of the bifurcation set by process of elimination. Recall that we are considering the termination point of the heteroclinic and limit cycle fold curves, cf. Figures (2.4), (4.3) and (5.4). Numerical simulation in the reduced system (6.4)-(6.5) at and below point V shows that the saddle-node bifurcation appears to occur on the limit cycle in an infinite period bifurcation, thereby destroying the limit cycle. Thus the limit cycle does not exist along $\cos\tau = 0$ when $\alpha \leq \frac{1}{\sqrt{8}}$. In considering what happens to the heteroclinic and limit

cycle fold curves, we can discount the case of the curves extending, uninterrupted from P to P' (i.e., never touching the double saddle-node curve (2.49)), the reason being that the pictures at the line $\cos\tau = 0$ would then be inconsistent. We can also discount the case where the curves join point O, defined by $\cos\tau = \alpha = 0$ because the pictures would again be inconsistent. Thus we conclude the curves must terminate along the double saddle-node (2.49) and to the right of point H in the $\cos\tau - \alpha$ plane.

We now consider the scenario shown in Figure 6.4. We note that due to the type of Takens-Bogdanov bifurcation that occurred at point H, there exists a curve extending to the right of point H satisfying $\Sigma\lambda_i = 0$ where λ_i are the two principal eigenvalues. Since this is just the trace of the matrix corresponding to these eigenvalues, we will refer to the curve as the $\mathbf{tr} = 0$ curve. This curve may be thought of as an extension of the unsymmetrical Hopf bifurcation curve and indeed, we used this extension to calculate the empirical equation for the Hopf, given by (2.54). This extension goes from H to H' and enters tangent to (2.49) at the respective points. The significance of this curve is that the heteroclinic and limit cycle fold curves must intersect it. For values of α below the $\mathbf{tr} = 0$ extension, the limit cycle born in the heteroclinic bifurcation must be stable; however, for values of α above the $\mathbf{tr} = 0$ extension, the limit cycle born in the heteroclinic bifurcation must be *unstable*. Thus the limit cycle fold curve and the heteroclinic bifurcation curves must join together at the $\mathbf{tr} = 0$ extension curve with only the heteroclinic bifurcation curve continuing on the other side, see Figure 6.5. We label this point along the $\mathbf{tr} = 0$ curve at which the two curves join as point B.

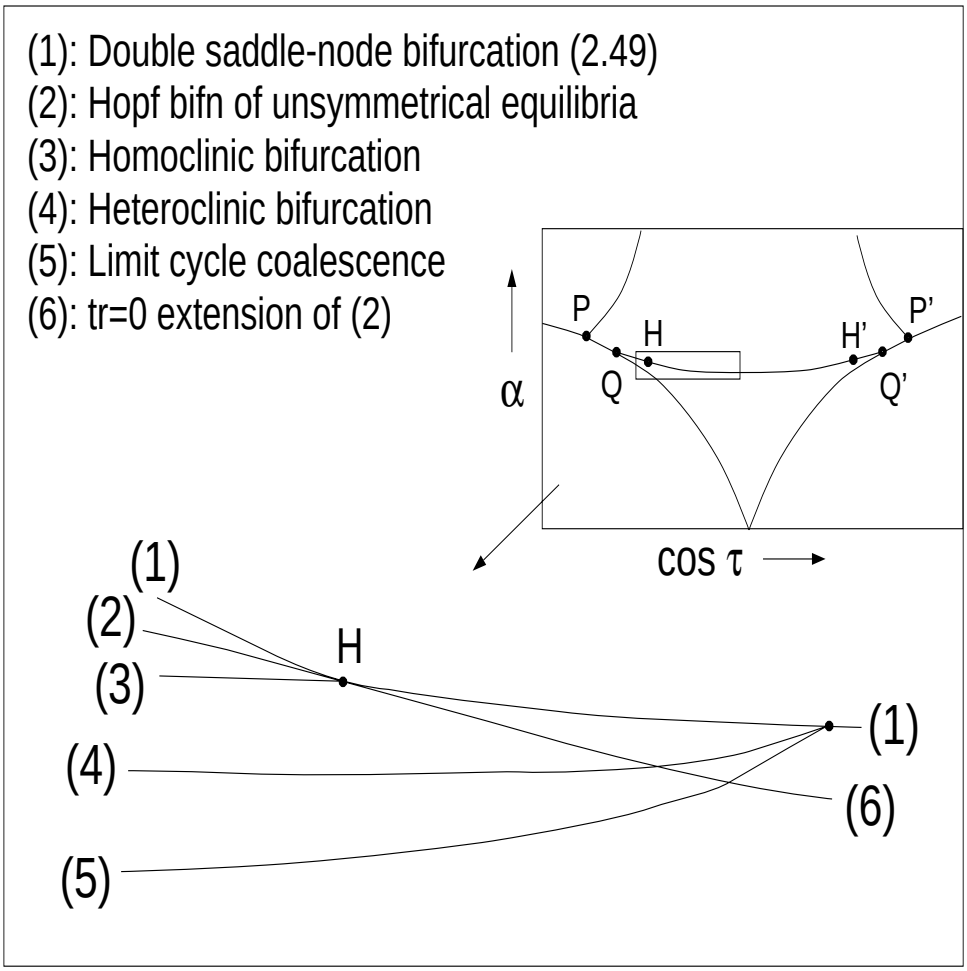

Figure 6.4: Scenario under consideration for termination point of heteroclinic bifurcation and limit cycle coalescence curves.

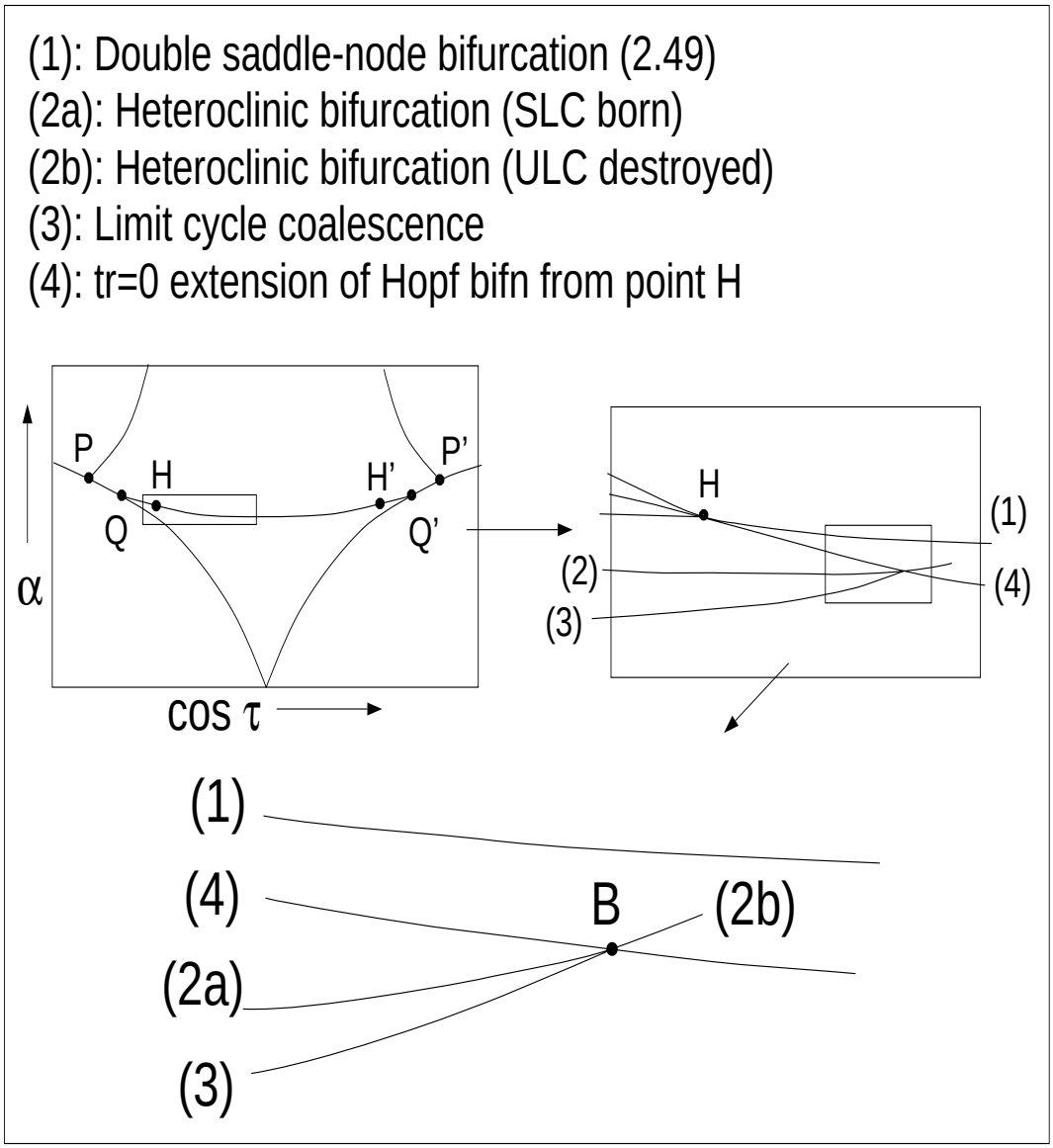

Figure 6.5: Intersection of heteroclinic bifurcation and limit cycle coalescence curves at the **tr**=0 extension of the Hopf bifurcation. Note only the heteroclinic bifurcation survives above this **tr**=0 curve.

Note that when the portion of the heteroclinic bifurcation curve lying above the $\mathbf{tr} = 0$ extension is crossed from above, the unstable limit cycle created in the Hopf bifurcation across (2.46) is destroyed.

We are thus left with two possible scenarios which can be consistent with Figure 6.5 and these are shown in Figure 6.6. In the case of (a), we have the heteroclinic bifurcation curve joining to some point N which lies along H-H' (equation (2.49)) and to the left of point V. In the case of (b), we have the heteroclinic bifurcation curve joining with point V. We now argue that the latter scenario gives an inconsistent picture.

From Figures 5.2-5.3, we see that the heteroclinic connection, shown there as a two-dimensional projection, has the structure of that shown in Figure 6.7. But at point V, we know the saddle-node bifurcations occur in the $\phi = \pm\frac{\pi}{2}$ planes and this situation is shown in Figure 6.8, where we have used the eigenvalues and eigenvectors from equation (6.7) to draw the picture. Recall that $\phi = \pm\frac{\pi}{2}$ are invariant planes. If scenario (b) of Figure 6.6 is to occur, at point V the heteroclinic orbit must be able to leave the invariant plane and then cross back through it which clearly cannot happen. In other words, it is the nature of this particular heteroclinic connection to have an unstable manifold leaving in a direction different from that along which the saddle-node bifurcation occurs, even though it joins to the stable manifold of the other saddle-node along the same direction that the saddle-node occurs, see Figure 6.7. Thus we conjecture that scenario (a) of Figure 6.6 must occur and that there exists a point N on H-H', lying neither close to H nor to V at which point the heteroclinic bifurcation curve terminates (see Figure 6.9 for the phase portraits).

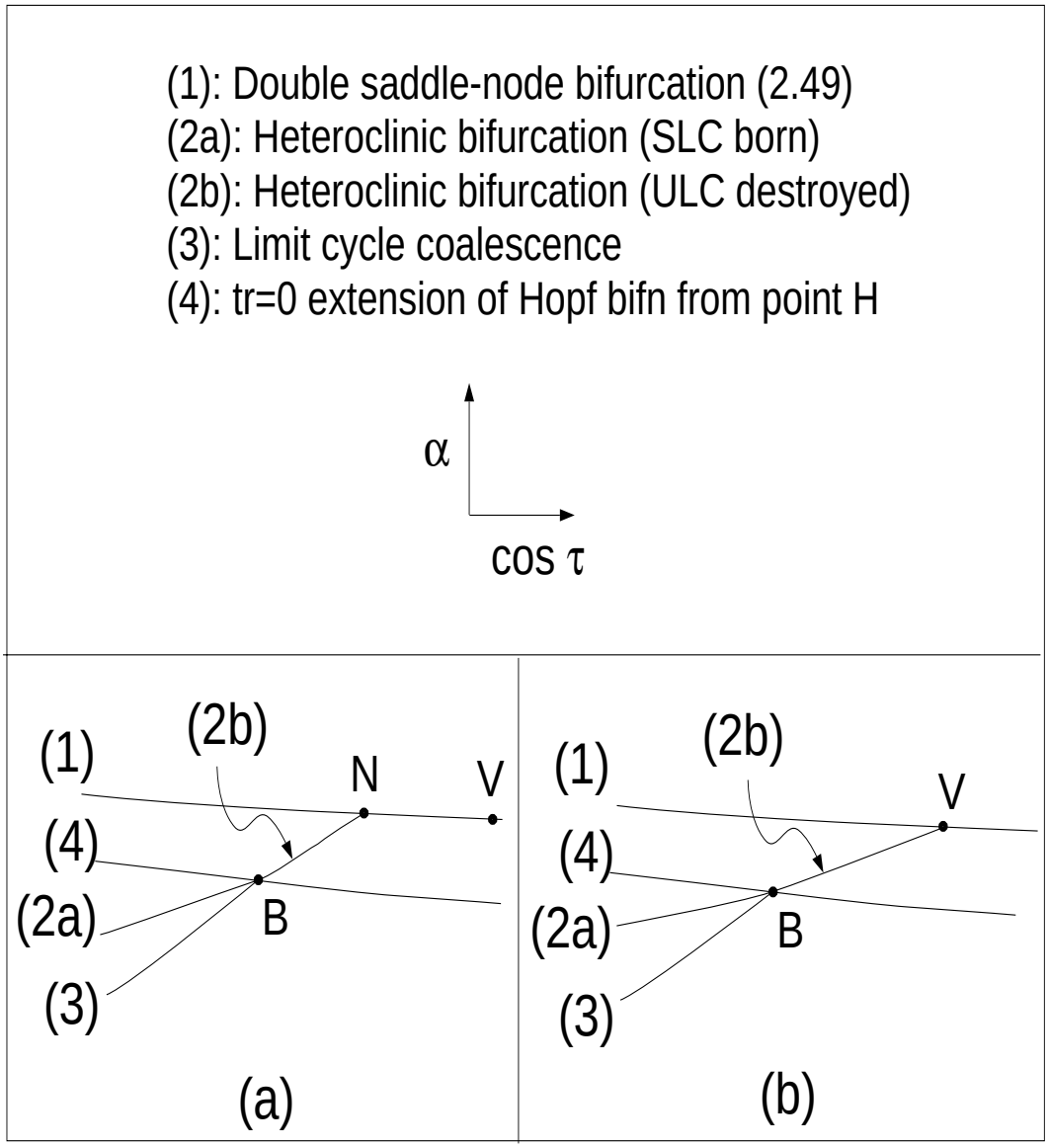

Figure 6.6: Two possible scenarios for the termination point of the heteroclinic bifurcation curve.

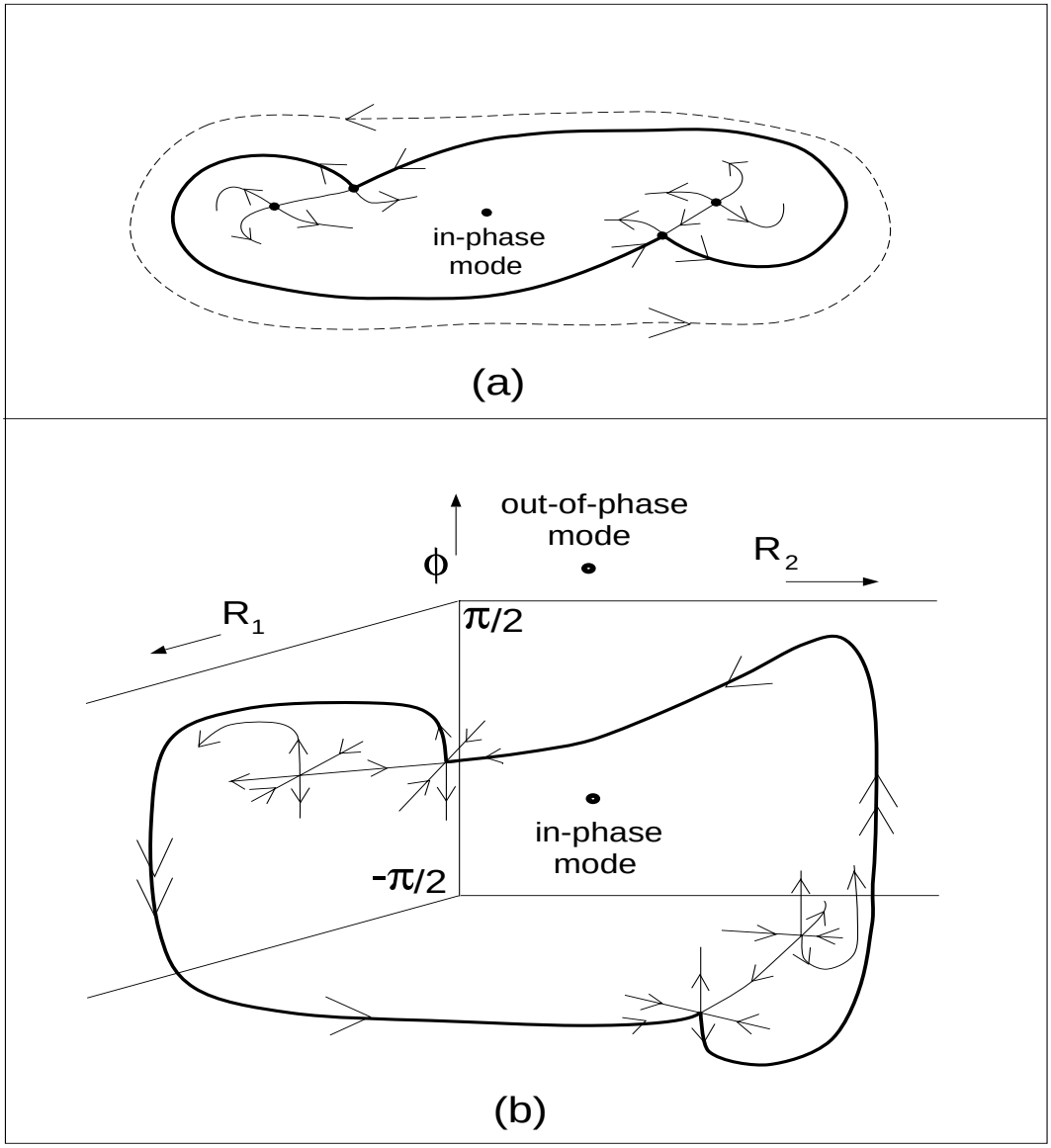

Figure 6.7: Heteroclinic connection close to H-H'. (a) shows the two-dimensional projection of this connection observed in Figures 5.2, 5.3 while (b) shows the full three-dimensional connection.

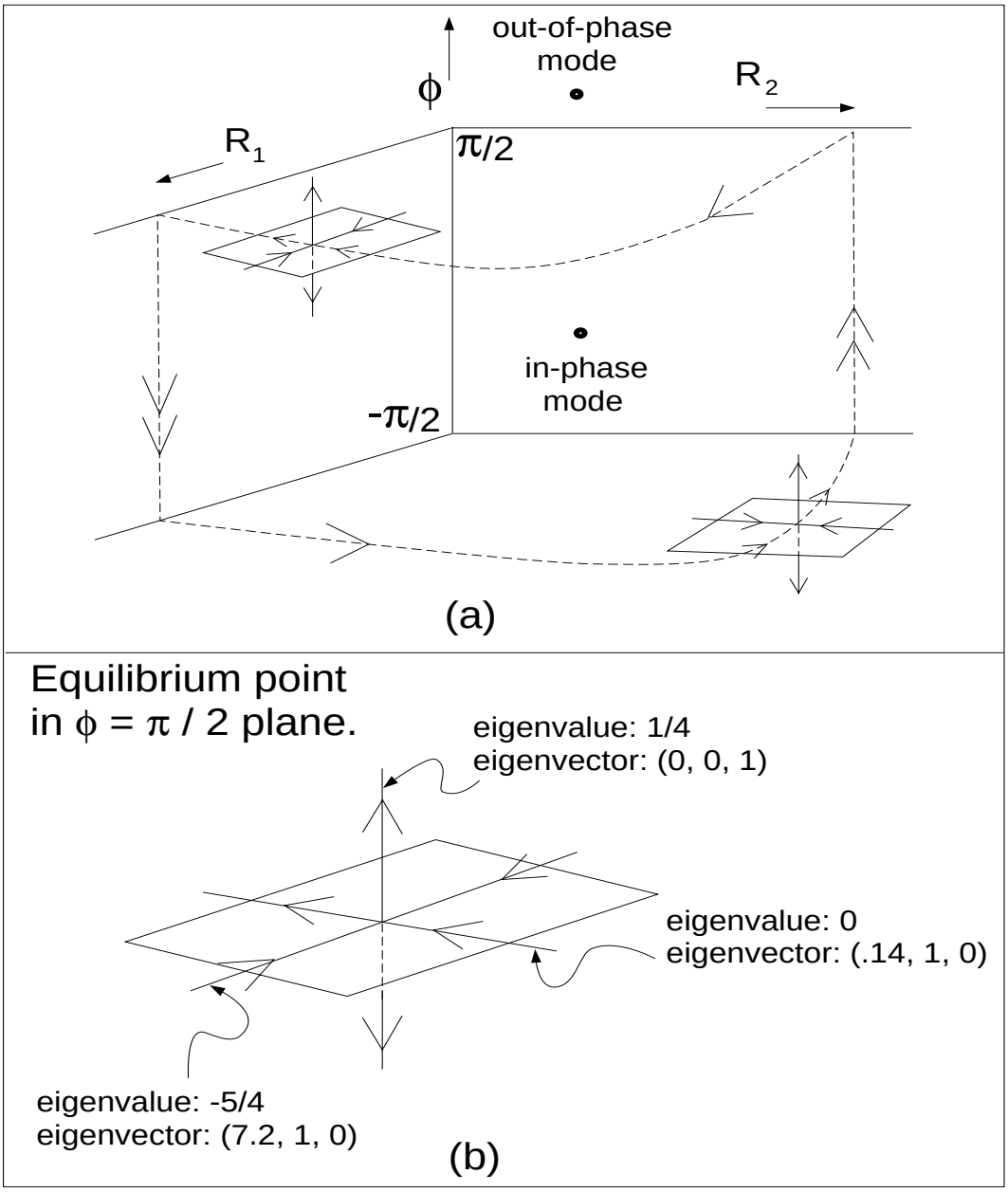

Figure 6.8: Double saddle-node bifurcation on unstable limit cycle at point V.

This then implies that along N-V-N', the saddle-node bifurcation occurs *on* the unstable limit cycle, thus destroying it. Although this occurrence may seem highly unusual, it has been observed in similar systems [12],[18].

The complete bifurcation sets for the slow-flow equations (2.24)-(2.26) are shown in Figure 6.10. See the previous chapters for the corresponding phase portraits.

6.4 Physical Implications

We now are able to discuss the behavior of the slow-flow equations (2.24)-(2.26) for all pairs of parameters. The first important point to note is the existence of a stable mode for all parameter values. Thus we never will have the case of phase drift (i.e., $\phi(t)$ growing unbounded). We also note that as the coupling continues to increase, the range of delay values for which the in-phase and out-of-phase mode exist and are stable approaches zero. Recall that the respective modes gain their stability in a Hopf bifurcation (cf. Figures 2.2-2.3) and the limit cycle created is unstable. It is thus of no practical importance except to note whether the in-phase mode or out-of-phase mode has the larger basin of attraction of initial values. In the region in which only the in-phase and/or out-of-phase modes exist, we expect the characteristic hysteresis to occur as we vary the delay [41]. We also expect this hysteresis to occur as we vary the delay for sufficiently low coupling, where all the unsymmetrical equilibria are unstable and no periodic motions exist in (2.24)-(2.26).

For moderate coupling strengths, varying the delay and coupling slightly can lead to drastically different behavior in the system. In the region where it exists,

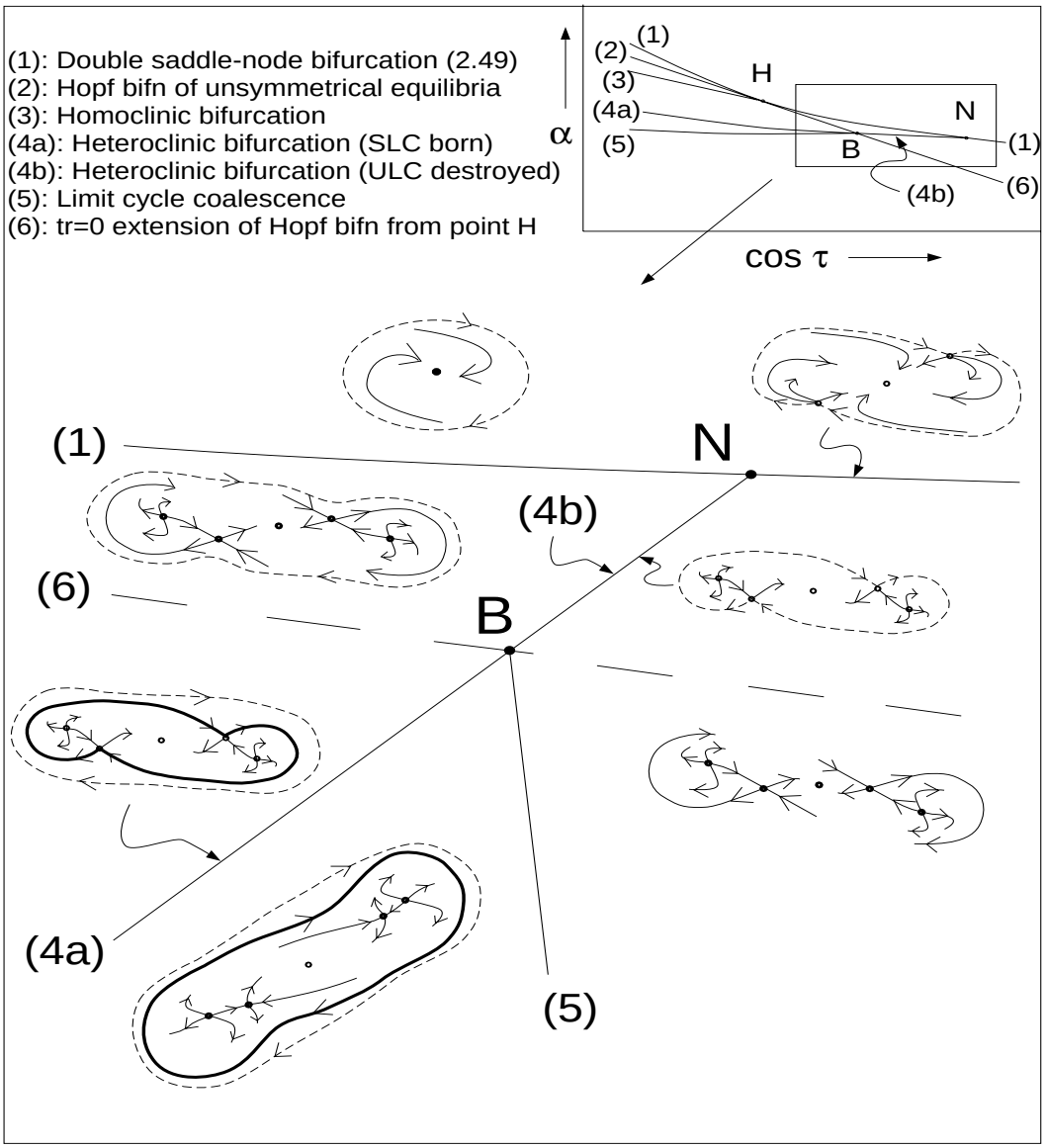

Figure 6.9: Bifurcation set and phase portraits near point N with curves drawn distorted for better viewing. Note that the phase portraits above and below (6) are identical and are thus only drawn once. Also, the third eigendirection is contracting and in a direction (nearly normal) to the plane of the page.

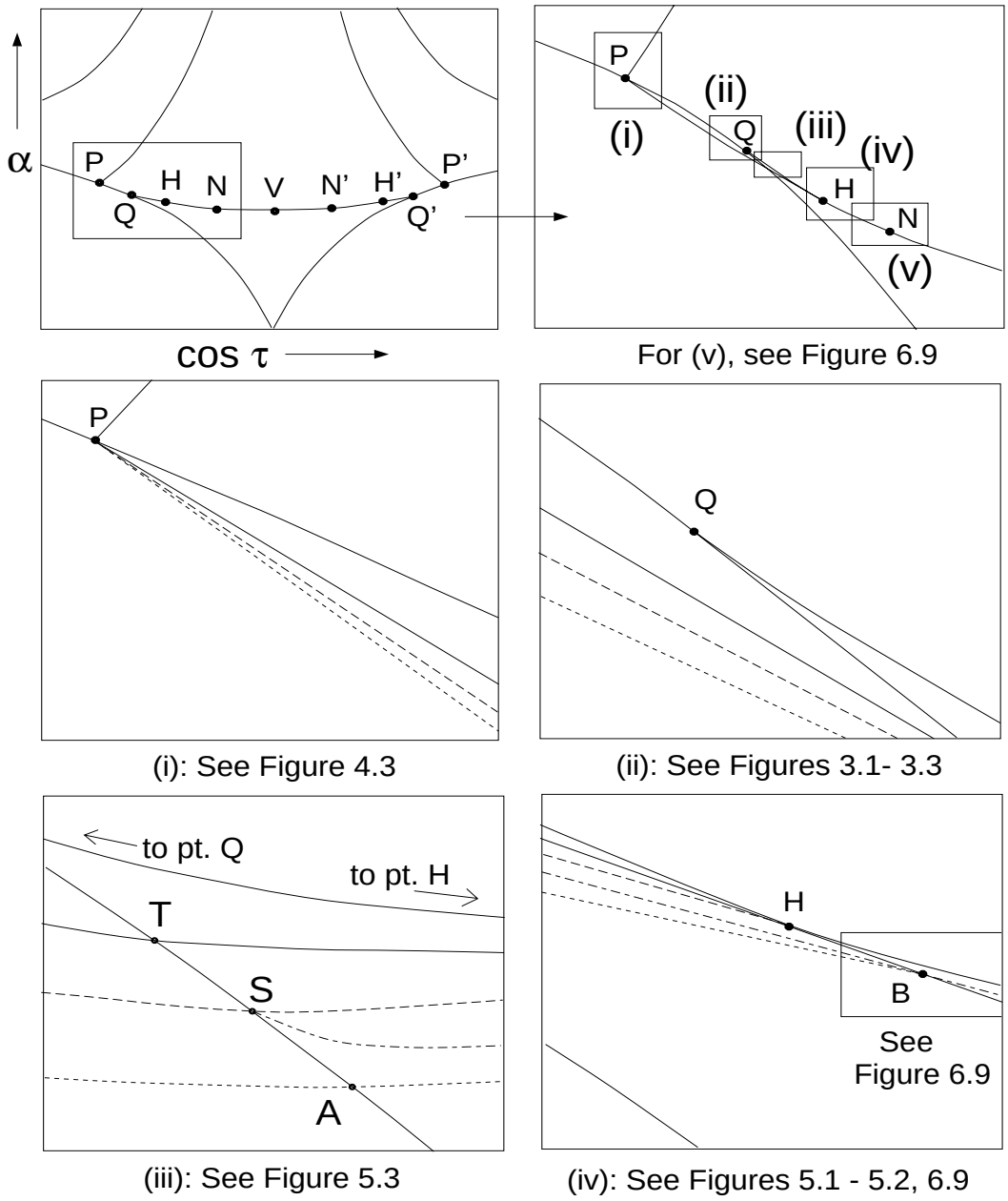

Figure 6.10: Complete bifurcation set of equations (2.24)-(2.26). For the top left frame, cf. Figure 2.3 and for the top right frame, cf. Figure 2.4. Note also that the same bifurcation curves exist under $\cos\tau \mapsto -\cos\tau$.

the stable limit cycle is an attractor for the system. For certain parameter values the stable limit cycle exists along with one or two other attractors. As the stable limit cycle itself is attracting, it does have physical importance. As we cross PB (the curve of limit cycle coalescence, see Figure 6.10) from right to left, the stable limit cycle is destroyed. Oscillations in the neighborhood of this stable limit cycle (and hence near 1:1 phase entrainment) must then jump to the nearest attractor, thereby approaching a phase locked state. Along PA the only attractor is the out-of-phase mode, while along AB both in-phase and out-of-phase modes are stable. This annhilation of an attractor is known as a strong bifurcation and has physical importance in control applications as the system exhibits a sudden jump in behavior. In contrast, weak bifurcations involve the continuous evolution of attractors and hysteresis, both of which were observed in the case of large and small coupling discussed above [18].

We also see strong bifurcations along SB and SH as limit cycles are born in heteroclinic and destroyed in homoclinic bifurcations, respectively. Along SB and SH, both in-phase and out-of-phase modes are attractors to which trajectories are now drawn. The limit cycles created in weak bifurcations along PH (the Hopf bifurcation of the unsymmetrical equilibria) are stable and it is interesting that the homoclinic bifurcation along PS is *not* a strong bifurcation (as it was along SH) since it is a symmetry breaking bifurcation in which the two limit cycles gives rise to a single large limit cycle in the neighborhood of the two smaller stable limit cycles.

Chapter 7

Numerical Integration

7.1 Introduction

Since our analysis is approximate, it is desirable to compare our analytical results with direct numerical integration of equations (2.1)-(2.2):

$$\begin{aligned} \ddot{x}_1 + x_1 - \epsilon\,(1 - x_1^2)\,\dot{x}_1 &= \epsilon\,\alpha\,\dot{x}_2\,(t-\tau), \\ \ddot{x}_2 + x_2 - \epsilon\,(1 - x_2^2)\,\dot{x}_2 &= \epsilon\,\alpha\,\dot{x}_1\,(t-\tau), \end{aligned}$$

where α is a coupling parameter, τ is the delay time, and where $\epsilon << 1$. We approximated this system twice—first with the method of averaging and then with a Taylor expansion of the delay terms. Thus our entire analysis can be considered two steps removed from the original motivating problem, equations (2.1)-(2.2). The first approximation has well-known results for non-delay cases [5],[32],[37],[38],[43]. In the second approximation, however, we profoundly changed the nature of the system in question. Even assuming small expansion parameters, i.e., $\epsilon\tau << 1$,

we might suspect problems to arise. Fortunately, this is not the case. For small values of ϵ, and $O(1)$ values of τ, we find excellent agreement between numerical integration of equations (2.1),(2.2) and stable periodicity predicted by the analytic results obtained in this work. We now address the question of the methods used in the numerical integration of our original equations.

7.2 Modified Runge-Kutta

Our original system is of the form

$$\dot{\mathbf{x}}(t) = \mathbf{f}(\mathbf{x}(t), \mathbf{x}(t-\tau)) \tag{7.1}$$

where we will consider only the case of strictly positive delays, $\tau > 0$. Although we will usually restrict ourselves to discussing our particular system, the results hold for more general systems of differential delay equations (cf. [14]). If we can find a solution of the form

$$\mathbf{x}(t) = \mathbf{\Phi}(t), \quad t_0 - \tau \leq t \leq t_0 \tag{7.2}$$

then $\mathbf{x}$(t) will be a known function of t for all t satisfying $t_0 \leq t \leq t_0 + \tau$ and (7.1) becomes an ordinary differential equation. Known existence theories for ordinary differential equations thus assure us that we know $\mathbf{x}$(t) for $t_0 \leq t \leq t_0 + \tau$ (e.g. [40]). We can then use these values to calculate the solution of $\mathbf{x}$(t) for $t_0 + \tau \leq t \leq t_0 + 2\tau$. Continuing in a similar manner with this "method of steps" thus gives us existence and uniqueness of the solution for all time.

Our numerical integration scheme starts the oscillators out as uncoupled at time $t = 0$ and lets them run backward in time until $t = -\tau$. This allows us to obtain

an *interval* of initial conditions $\mathbf{x}(t) = \mathbf{\Phi}(t), t_0 - \tau \leq t \leq t_0$. We then reset the time to $t = 0$, and begin numerically integrating the *coupled* delay equations, taking into account what happened τ units ago. Here we use a fourth order Runge-Kutta scheme with fixed step size, appropriately modified to account for delay [14]. Recall the numerical integration of the (non-delayed) system $\dot{x} = f(t, x(t))$ involves the evaluation of

$$k_1 = hf(t_n, x_n),\ k_2 = hf(t_n + \frac{h}{2}, x_n + \frac{k_1}{2}), \tag{7.3}$$

$$k_3 = hf(t_n + \frac{h}{2}, x_n + \frac{k_2}{2}), k_4 = hf(t_n + h, x_n + k_3) \tag{7.4}$$

in order to calculate the next value, given by $x_{n+1} = x_n + \frac{k_1}{6} + \frac{k_2}{3} + \frac{k_3}{3} + \frac{k_4}{6} + O(h^5)$, where h is the fixed step size [28]. For the case of delay, our system is of the form $\dot{x} = f(t, x(t), x(t-\tau))$ and we use the notation $\Phi_{n-\frac{\tau}{h}} \equiv x(t_n - \tau)$ to denote the value of the system τ time units ago (and we assume for convenience that $hm = \tau$, for some integer m). We now must evaluate

$$k_1 = hf(t_n, x_n, \Phi_{n-\frac{\tau}{h}}), \tag{7.5}$$

$$k_2 = hf(t_n + \frac{h}{2}, x_n + \frac{k_1}{2}, \frac{\Phi_{n-\frac{\tau}{h}} + \Phi_{n+1-\frac{\tau}{h}}}{2}), \tag{7.6}$$

$$k_3 = hf(t_n + \frac{h}{2}, x_n + \frac{k_2}{2}, \frac{\Phi_{n-\frac{\tau}{h}} + \Phi_{n+1-\frac{\tau}{h}}}{2}), \tag{7.7}$$

$$k_4 = hf(t_n + h, x_n + k_3, \Phi_{n+1-\frac{\tau}{h}}) \tag{7.8}$$

where $\Phi_{n+1-\frac{\tau}{h}}$ is the system τ time units before x_{n+1}. Note that since the evaluation of k_2, k_3 requires an evaluation of $x(t)$ at the midpoint between t_n and $t_{n+1} \equiv t_n + h$ in the non-delay case, here the corresponding evaluation is at the average of the known delayed values $\Phi_{n-\frac{\tau}{h}}, \Phi_{n+1-\frac{\tau}{h}}$, which is the function value between $t_{n-\frac{\tau}{h}}$ and $t_{n+1-\frac{\tau}{h}}$.

Thus at every step of the integration, we see that we must carry the behavior of the system for the previous τ time units with us. The only other modification needed is to update the entries of the delay interval at each step by 1) shifting the entries to overwrite the value of the system at $x(t-\tau)$ and 2) inserting the newly calculated value of the system in the appropriate position. For example, if $\phi[j], j = 1, \cdots, m$ (where $m = \frac{\tau}{h}$ is an integer) contains the values of the system for $t_c - \tau \leq t < t_c$ where t_c is the current time, $\phi[1] = x(t_c - \tau)$ and $x_{new} = x(t_c)$, the update line would be

for $j = 1$ to m

$\phi[j] = \phi[j+1]$

end

$\phi[m] = x_{new}$

7.3 Results

So as to avoid unnecessarily long runs, we begin "close" to the equilibrium point whose stability we are checking. For example, in the case of the in-phase mode we will have $x_1 \approx x_2$, $\dot{x}_1 \approx \dot{x}_2$. To check stability, we see if the trajectory in four-dimensional space is continuing to spiral into the in-phase mode, defined by $x_1 \equiv x_2, \dot{x}_1 \equiv \dot{x}_2$. In this way we were able to confirm that the stability of the in-phase and out-of-phase modes agreed with the predictions of the analytical method made in Figure 2.2. (see Figures 7.1-7.2).

In addition, by carefully choosing initial conditions based on the bifurcation sequence in Figure 3.3, we were able to observe periodic motions other than the in-

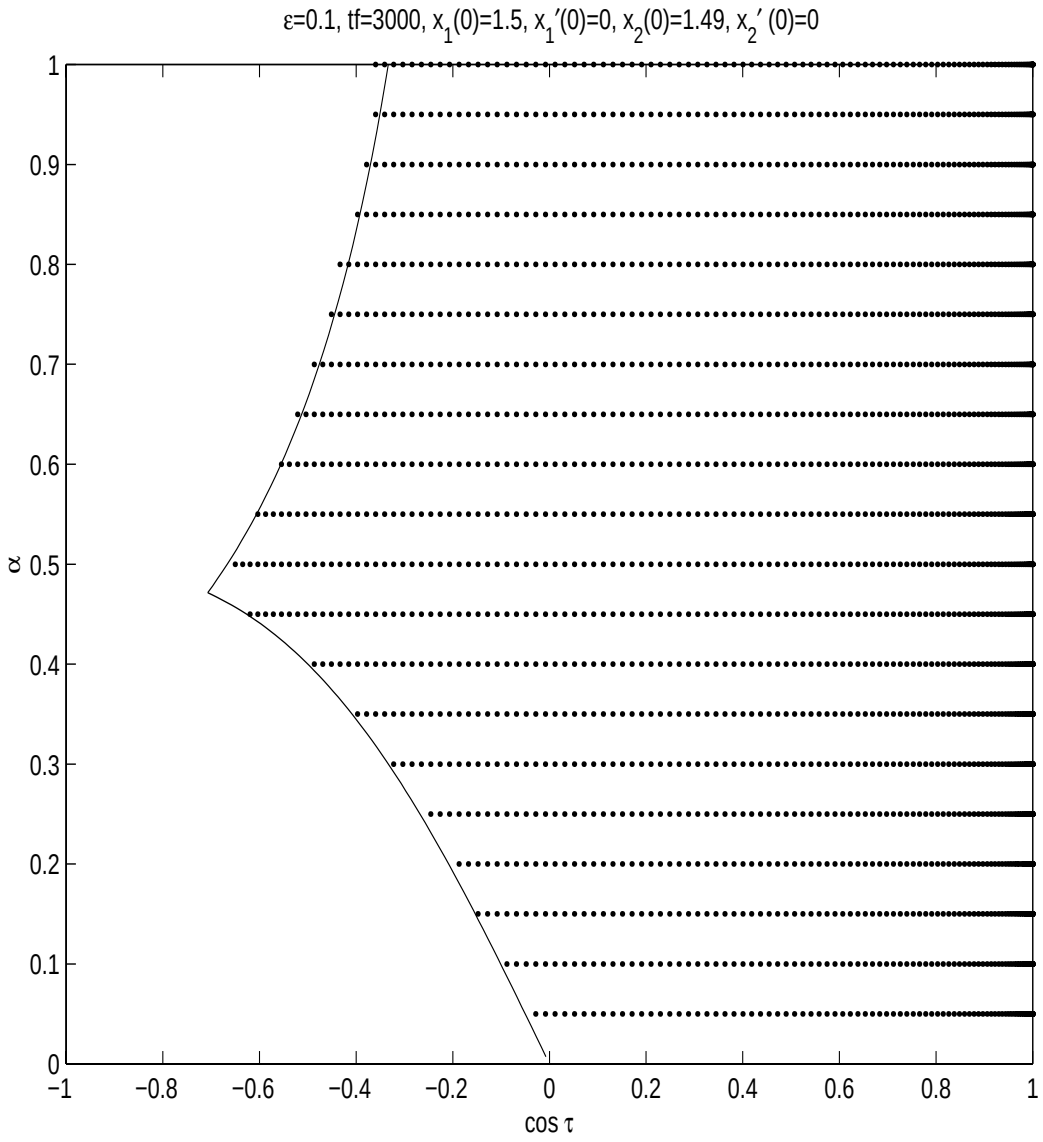

Figure 7.1: In-phase mode stability: solid line is analytic prediction of stability given by (2.38),(2.46); dots represent stability via numerical integration of (2.1)-(2.2).

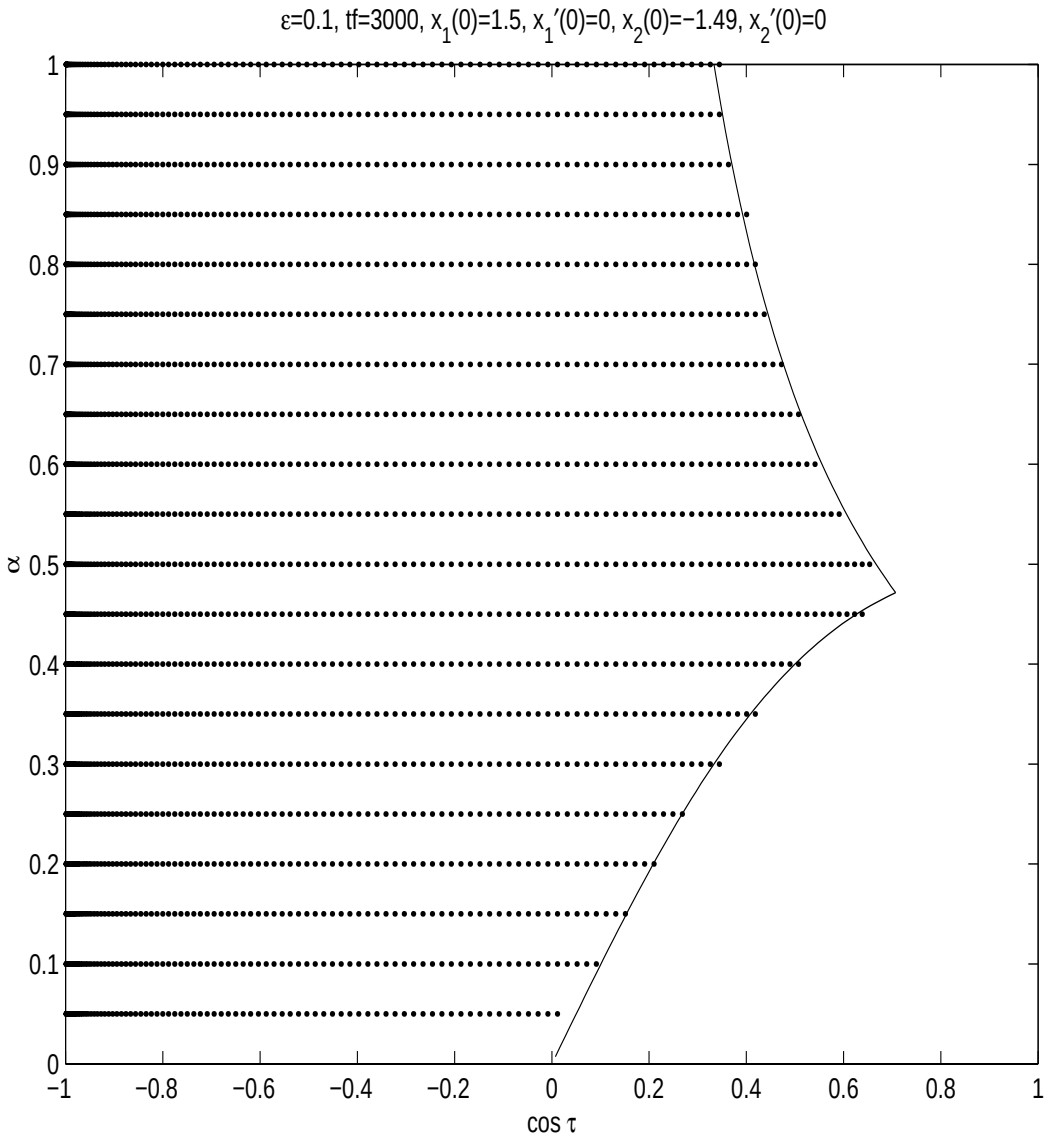

Figure 7.2: Out-of-phase mode stability: solid line is analytic prediction of stability given by (2.38),(2.46); dots represent stability via numerical integration of (2.1)-(2.2).

phase and out-of-phase modes in the original delay equations (2.1)-(2.2). It might be expected that the existence of stable periodic motions in such a small region of parameter space as seen in Figure 3.3 is simply a construct of our numerous approximations. The fact that we actually *do* see these periodic motions predicted by the slow-flow equations is important because it demonstrates that the approximations made still allow us to capture the behavior of the original equations under certain assumptions. In the case of Figure 7.3, we chose $\tau = 2.26, \alpha = .45, \epsilon = 0.01$ which corresponds to a slow-flow equilibrium at $R_1 = 1.5253234, R2 = 1.8161932, \phi = 0.20669649$. Using (2.3)-(2.4), we calculate the initial conditions:

$$x_1 = R_1 \cos\phi, \qquad \dot{x}_1 = -R_1 \sin\phi, \tag{7.9}$$

$$x_2 = R_2, \qquad \dot{x}_2 = 0.0 \tag{7.10}$$

where the value for $\dot{x}_2$ is found by choosing $\theta_1 = \phi, \theta_2 = 0.0$. As stated previously, we run the uncoupled system backward for τ time units to generate the necessary interval of initial conditions. We then couple the system together and integrate forward in time, beginning at $t = 0$, for $30,000$ time units and plot the last $2,000$ points.

We obtain a similar figure for the unsymmetrical equilibrium's stable partner obtained from $(R_1, R_2, \phi) \mapsto (R_2, R_1, -\phi)$. To be more precise, the unsymmetrical periodic motion in (2.1)-(2.2) which corresponds to the slow-flow equilibria $R1 = 1.8161932, R_2 = 1.5253234, \phi = -0.20669649$ is obtained from Figure 7.3 by letting $(x_1, x_2) \mapsto (x_2, x_1)$.

In terms of the slow-flow equilibria, the periodic motion displayed in Figure 7.3

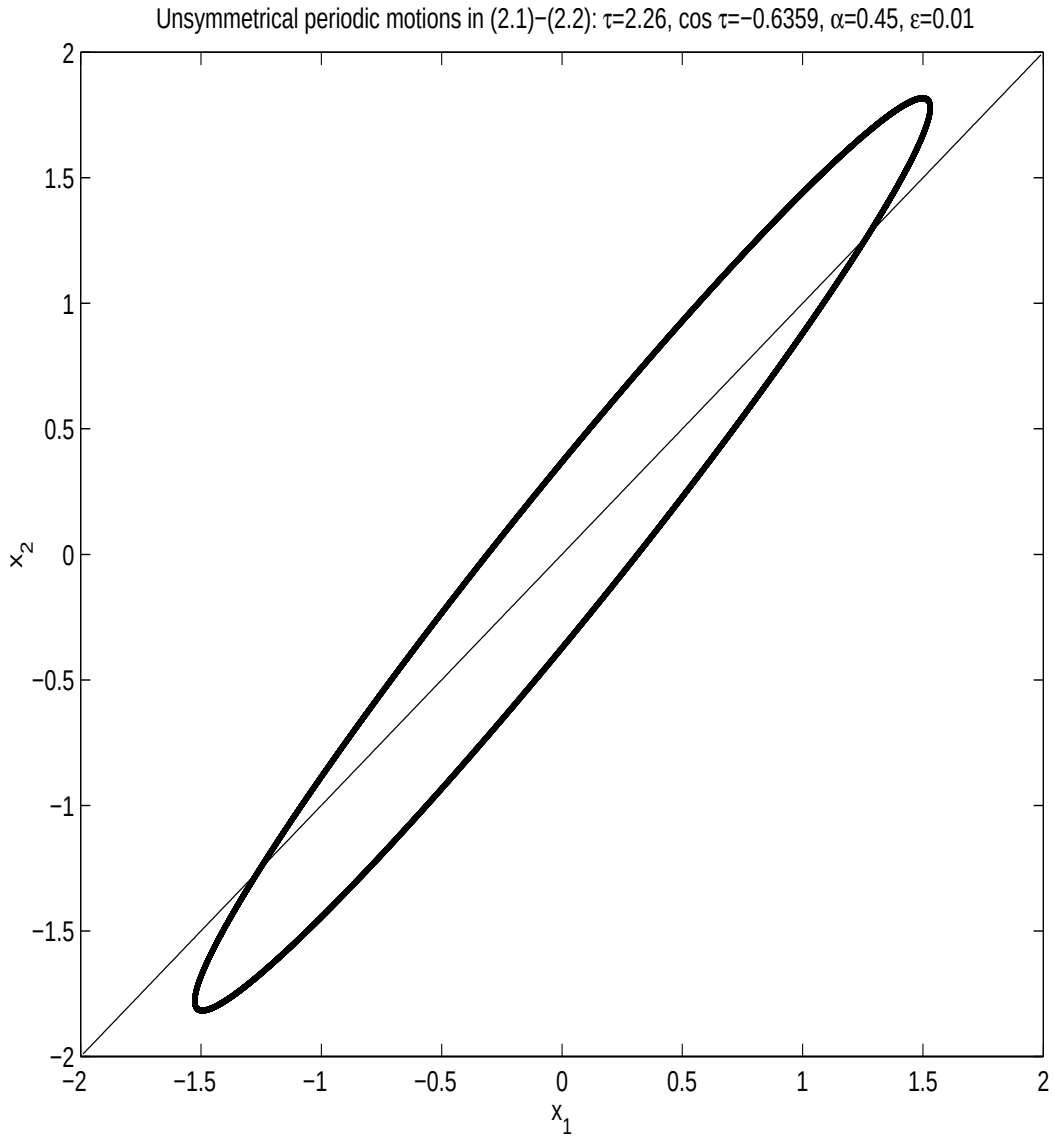

Figure 7.3: Unsymmetrical periodic motions in (2.1)-(2.2) which correspond to unsymmetrical equilibria in (2.24)-(2.26). The initial condition used to generate the interval of delay values is $R_1 = 1.5253234, R2 = 1.8161932, \phi = 0.20669649$. Equations (2.3)-(2.4) are also plotted.

and its partner periodic motion under $(x_1, x_2) \mapsto (x_2, x_1)$ represent the two stable unsymmetrical equilibria which occur below the unsymmetrical Hopf bifurcation curve (cf.(2.54)) and the in-phase pitchfork bifurcation curve (2.38). Since ϵ is small, we would expect equations (2.3)-(2.4) to give a good approximation to these unsymmetrical equilibria for the same R_1, R_2, ϕ values. This is indeed the case and Figure 7.3 actually has equations (2.3)-(2.4) superimposed, only the respective curves cannot be distinguished from those of the integrated differential delay equations.

The numerical integration thus confirms that our analysis of the approximate system (2.24)-(2.26) is an excellent approximation of the differential delay equations (2.1)-(2.2) under the assumption that $\epsilon\tau$ is small. In terms of the physical implications, perhaps the most important conclusion of this work is the prediction that both the in-phase and out-of-phase modes are stable for values of $\cos\tau$ close to zero, i.e., for delays of about $\frac{1}{4}$ of the uncoupled period of the oscillators, see Figure 2.1, 7.1, 7.2. In addition, with a knowledge of the bifurcations that occur in the slow-flow equations, we are better able to understand the transition between periodic motions in the original delay equations.

Chapter 8

Concluding Remarks

In this work we studied the dynamics of two van der Pol oscillators with delay coupling in the limit in which (i) the oscillators behave sinusoidally, (ii) the coupling is weak, and (iii) the delay is not too large. We found that the in-phase and out-of-phase modes coexisted and were both stable in the parameter range for which the delay is about $\frac{1}{4}$ of the unperturbed limit cycle period. We also found that the in-phase mode ceased to exist if the delay was about $\frac{1}{2}$ of the unperturbed period and the coupling was strong enough. Similarly the out-of-phase mode ceased to exist if the delay was approximately the same as that of the unperturbed period. We also found that if the coupling was sufficiently small, various other motions were predicted to exist besides the in-phase and out-of-phase modes. These additional motions were predicted to change their form through a series of elaborate bifurcations. Nevertheless all these motions were predicted to be periodic, and we did not observe chaos for any parameter values.

Our analysis was approximate, based on a perturbation theory called averaging. The original differential delay equations were replaced by the "slow-flow" of ordinary differential equations given in (2.24)-(2.26), a step expected to be valid for small values of a parameter ϵ. Our analysis of the slow-flow equations then utilized a variety of theorems about center manifolds, normal forms, Hopf bifurcations, etc. Although these theorems are exact, the conclusions drawn from them apply *exactly* only to the slow-flow equations and not to the original differential delay equations (2.1)-(2.2). Although such theorems exist for differential delay equations, we have not applied them here due to the approximate nature of our analysis [9],[16],[15].

Our treatment of this problem involves three time scales:

1) the period of the unforced oscillator, 2π

2) the delay time, τ

3) the slow time scale, $\frac{1}{\epsilon}$.

(We note that the slow time scale arises due to the nature of the perturbation method we used.) In this work, we have restricted attention to cases where $\epsilon << 1$ and where $\tau = O(1)$, that is, we have assumed that time scales 1) and 2) are of the same order, while time scale 3) is much longer than both 1) and 2). Specifically, we have assumed $\epsilon\tau << 1$.

The research in this thesis may be extended in a number of directions:

1) In checking the stability results from the numerical integration of the original equations (2.1)-(2.2) against the slow-flow predictions as the limits of these time scales are reached, we restricted ourself to the case $\epsilon << 1$. We could also do comparisons for larger values of ϵ.

2) The delay appears in our system as $\cos\tau$ and our numerical integration only considered the case $\tau = O(1)$. Thus our results predict that the bifurcation set is periodic with respect to τ. We expect, however, that for fixed ϵ, taking $\tau = O(\frac{1}{\epsilon})$ would give non-periodic dependence on τ [19],[45].

3) In obtaining the first time scale above, we assumed a sinusoidal solution since ϵ was small. We could also consider the case where ϵ was not small, i.e. where the oscillators function in the relaxation range instead of the sinusoidal range. This would be an extension of previous work which did not include delay [35],[36].

4) After obtaining, (2.15)-(2.18), we immediately approximated the delay terms without first attempting a stability analysis with the delay terms $\tilde{R}_i, \tilde{\theta}_i$ still present. Performing a stability check of this kind would help in confirming the validity of our subsequent approximations.

5) We could also consider some generalizations of the model:

a) We began by assuming in (2.1)-(2.2) that our nonlinear coupling was symmetrical. One possible extension would involve considering the effects of two different coupling parameters. The equations that we would analyze would then be

$$\ddot{x}_1 + x_1 - \epsilon\,(1 - x_1^2)\,\dot{x}_1 \;=\; \alpha_1\,\dot{x}_2\,(t-\tau), \tag{8.1}$$

$$\ddot{x}_2 + x_2 - \epsilon\,(1 - x_2^2)\,\dot{x}_2 \;=\; \alpha_2\,\dot{x}_1\,(t-\tau). \tag{8.2}$$

Now there would be two different coupling parameters in our system and the results could be compared with the symmetrical version.

b) Another possibility of extending this work would be to consider different

forms of coupling. One could generalize equations (2.1)-(2.2) in the form

$$\ddot{x}_1 + x_1 - \epsilon\ (1 - x_1^2)\ \dot{x}_1 \ = \ \epsilon\ \alpha\ \dot{x}_2(t-\tau) + \epsilon\ \beta\ x_2(t-\tau), \tag{8.3}$$

$$\ddot{x}_2 + x_2 - \epsilon\ (1 - x_2^2)\ \dot{x}_2 \ = \ \epsilon\ \alpha\ \dot{x}_1(t-\tau) + \epsilon\ \beta\ x_1(t-\tau) \tag{8.4}$$

where α, β are coupling parameters, τ is the delay time, and where $\epsilon << 1$. Similar equations without delay have been considered by others [39]. We have considered only the case $\beta = 0$ thus far. One could also consider the case with $\alpha = 0$ (with $\beta \neq 0$) and then the general case in which both α and β are nonzero. Since the stability of the in-phase and out-of-phase modes is expected to depend on both parameters, we foresee the possibility of using displacement coupling to stabilize the system, i.e., to increase the region in parameter space where the in-phase mode is the only stable attractor. Comparing the analytical work with numerical integration of the original system would also be of interest.

c) Either of the forms of coupling (displacement or velocity) could be used in considering a system of N oscillators. Thus one could consider an array of oscillators (assuming nearest neighbor velocity coupling, for example):

$$\ddot{x}_1 + \omega_1^2\ x_1 - \epsilon\ (1 - x_1^2)\ \dot{x}_1 \ = \ \epsilon\ \alpha\ \dot{x}_2\ (t-\tau), \tag{8.5}$$

$$\vdots$$

$$\ddot{x}_i + \omega_i^2\ x_i - \epsilon\ (1 - x_i^2)\ \dot{x}_i \ = \ \epsilon\ \alpha\ (\dot{x}_{i-1}\ (t-\tau) + \dot{x}_{i+1}\ (t-\tau)), \tag{8.6}$$

$$\vdots$$

$$\ddot{x}_N + \omega_N^2\ x_N - \epsilon\ (1 - x_N^2)\ \dot{x}_N \ = \ \epsilon\ \alpha\ \dot{x}_{N-1}\ (t-\tau), \tag{8.7}$$

where $\omega_i = 1 + \delta_i$ represents a slight detuning of the oscillators from its own uncou-

pled frequency. Then set $x_i = R_i \cos(t + \theta_i)$ and after averaging obtain

$$\dot{R}_i = \frac{\epsilon}{2}\left[R_i\ (1 - \frac{R_i^2}{4}) + \alpha \sum_j R_j \sin(\theta_j - \theta_i - \tau)\right] \tag{8.8}$$

$$\dot{\theta}_i = \epsilon\ \delta_i + \frac{\epsilon\ \alpha}{2} \sum_j \frac{R_j}{R_i} \sin(\theta_j - \theta_i - \tau), \tag{8.9}$$

where the sum is taken over the nearest neighbors.

d) Although equations (8.5)-(8.7) represent the full generalization of our original equations, a natural step to simplify the system is to consider phase only oscillators. Such simplifications in the non-delayed cases have been useful in understanding the dynamics of large numbers of coupled oscillators [7],[31]. To be more specific, one could study the dynamics of larger systems of delay-coupled limit cycle oscillators by simplifying the model equations in a manner similar to that used in previous studies of non-delayed systems (e.g., [20],[41]). Non-delayed systems similar to equations (8.3)-(8.4) have been modeled by considering phase-only, a step which has been accomplished by assuming that $R_1 = R_2 = 2$ (the uncoupled, small ϵ limit cycle amplitude). While sacrificing some of the dynamics, this assumption hopefully still captures some basic features of the original system. The phase-only simplification comes from ignoring the R_i equations and setting $R_1 = R_2 = \cdots = R_N$ in the phase-only equations (cf. [45]):

$$\dot{\theta}_i = \epsilon\ \delta_i + \frac{\epsilon\ \alpha}{2} \sum_j \sin(\theta_j - \theta_i - \tau). \tag{8.10}$$

These equations may be reduced in number by one by setting

$$\phi_1 = \theta_1 - \theta_2, \phi_2 = \theta_2 - \theta_3, \cdots, \phi_{N-1} = \theta_{N-1} - \theta_N, \tag{8.11}$$

$$\Omega_1 = (\delta_1 - \delta_2)\ \frac{2}{\alpha}, \Omega_2 = (\delta_2 - \delta_3)\ \frac{2}{\alpha}, \cdots, \Omega_{N-1} = (\delta_{N-1} - \delta_N)\ \frac{2}{\alpha}, \tag{8.12}$$

where the appearance of $\frac{2}{\alpha}$ is due to the choice of the independent variable as $T = \frac{\epsilon\ \alpha\ t}{2}$. In the case of three oscillators, the system becomes

$$\phi_1' = \Omega_1 - \sin(\phi_1 + \tau) - \sin(\phi_1 - \tau) + \sin(\phi_2 + \tau), \tag{8.13}$$

$$\phi_2' = \Omega_2 + \sin(\phi_1 - \tau) - \sin(\phi_2 + \tau) - \sin(\phi_2 - \tau). \tag{8.14}$$

Any number of oscillators could then be studied, with the goal being to understand the dynamics in the general case of N oscillators.

Bibliography

[1] M. Abramowitz and I. Stegun. *Handbook of mathematical functions with formulas, graphs, and mathematical tables*. U.S. Govt. Print. Off., 1970.

[2] D. Armbruster, J. Guckenheimer, and P. Holmes. Heteroclinic cycles and modulated travelling waves in systems with O(2) symmetry. *Physica D*, 29:257–282, 1988.

[3] P. F. Byrd and M. D. Friedman. *Handbook of Elliptic Integrals for Engineers and Scientists*. Springer-Verlag, 1971.

[4] J. Carr. *Application of Centre Manifold Theory*. Springer-Verlag, 1981.

[5] T. Chakraborty and R. H. Rand. The transition from phase locking to drift in a system of two weakly coupled van der Pol oscillators. *Int. J. Nonlinear Mechanics*, 23:369–376, 1988.

[6] B. W. Char et al. *Maple V (Symbolic Computation System)*. Waterloo Maple Publishing, Waterloo, 1991.

[7] A. H. Cohen, P. J. Holmes, and R. H. Rand. The nature of the coupling between segmental oscillators of the lamprey spinal generator for locomotion: a mathematical model. *J. Math. Biology*, 13:345–369, 1982.

[8] V. T. Coppola and R. H. Rand. Averaging using elliptic functions: approximation of limit cycles. *Acta Mechanica*, 81:125–142, 1990.

[9] O. Diekmann, S. A. van Gils, S. M. Verduyn Lunel, and H. O. Walther. *Delay Equations: Functional-, Complex-, and Nonlinear Analysis*. Springer-Verlag, 1995.

[10] G. H. Golub and C. F. Van Loan. *Matrix Computations*. John Hopkins, Baltimore, 1996.

[11] J. Grasman. *Asymptotic Methods for Relaxation Oscillations and Applications*. Springer-Verlag, 1987.

[12] J. Guckenheimer and P. Holmes. *Nonlinear Oscillations, Dynamical Systems, and Bifurcations of Vector Fields*. Springer-Verlag, New York, 1983.

[13] J. Guckenheimer, M. Myers, F. Wicklin, and P. Worfolk. *DsTool: A Dynamical System Toolkit with an Interactive Graphical Interface*. Deparment of Applied Mathematics, Cornell University, Ithaca, 1991.

[14] E. Hairer, S. P. Nørsett, and G. Wanner. *Solving Ordinary Differential Equations I: Nonstiff Problems*. Springer-Verlag, Berlin, 1987.

[15] J. Hale. *Theory of Functional Differential Equations*. Springer-Verlag, 1977.

[16] J. Hale. Nonlinear oscillations in equations with delays. In F. Hoppensteadt, editor, *Nonlinear oscillations in biology*, volume 17 of *Lectures in Applied Mathematics*. American Mathematical Society, 1979.

[17] M. Hirsch and S. Smale. *Differential Equations, Dynamical Systems, and Linear Algebra*. Academic Press, 1974.

[18] P. Holmes and D. Rand. Bifurcations of the forced van der Pol oscillator. *Quart. Appl. Math.*, 35:495–509, 1978.

[19] T. Kalmar-Nagy, G. Stepan, and F. C. Moon. Regenerative machine tool oscillations. To appear in *Dynamics of Continuous, Discrete, and Impulsive Systems*.

[20] W. L. Keith and R. H. Rand. Dynamics of a system exhibiting the global bifurcation of a limit cycle at infinity. *Int. J. Nonlinear Mechanics*, 20:325–338, 1985.

[21] D. A. Linkens and R. I. Kitney. Mode analysis of physiological oscillators intercoupled via pure time delays. *Bull. Math. Biol.*, 44:57–74, 1982.

[22] J. J. Lynch. *Analysis and design of systems of coupled microwave oscillators*. PhD thesis, Department of Electrical and Computer Engineering, University of California at Santa Barbara, 1995.

[23] J. J. Lynch and R. A. York. Stability of mode locked states of coupled oscillator arrays. *IEEE Trans. on Circuits and Systems*, 42:413–417, 1995.

[24] S. A. Maas. *Nonlinear Microwave Ciruits*. Artech House, 1988.

[25] MACSYMA Reference Manual. Prepared by the MACSYMA group of SYMBOLICS, Inc., 11 Cambridge Center, MA 02142, 1988.

[26] F. C. Moon and M. A. Johnson. Nonlinear dynamics and chaos in manufacturing processes. In F. C. Moon, editor, *Dynamics and Chaos in Manufacturing Processes*. Wiley, 1998.

[27] L. Perko. *Differential Equations and Dynamical Systems*. Springer-Verlag, 1996.

[28] W. Press, S. Teukolsky, W. Vetterling, and B. Flannery. *Numerical Recipes in C: The art of scientific computing*. Cambridge, 1995.

[29] R. Rand. *Computer Algebra in Applied Mathematics: An Introduction to MACSYMA*. Pitman Advanced Publishing Program, 1984.

[30] R. H. Rand. *Topics in Nonlinear Dynamics with Computer Algebra*. Gordon and Breach Science Publishers, Langhorne, 1994.

[31] R. H. Rand, A. H. Cohen, and P. J. Holmes. Systems of coupled oscillators as models of central pattern generators. In A. H. Cohen, editor, *Neural Control of Rhythmic Movements in Vertebrates*. John Wiley, 1988.

[32] R. H. Rand and P. J. Holmes. Bifurcation of periodic motions in two weakly coupled van der Pol oscillators. *Int. J. Nonlinear Mechanics*, 15:387–399, 1980.

[33] D. V. R. Reddy, A. Sen, and G. L. Johnston. Time delay induced death in coupled limit cycle oscillators. *Physical Review Letters*, 80:23:5109–5112, 1998.

[34] M. Sargent III, M. O. Scully, and W. E. Lamb, Jr. *Laser Physics*. Addison-Wesley, Reading, 1974.

[35] D. Storti and R. Rand. A simplified model of coupled relaxation oscillators. *Int. J. Non-Linear Mechanics*, 22(4):283–289, 1987.

[36] D. Storti and R. Rand. Subharmonic entrainment of a forced relaxation oscillator. *Int. J. Non-Linear Mechanics*, 23(3):231–239, 1988.

[37] D. W. Storti and R. H. Rand. Dynamics of two strongly coupled van der Pol oscillators. *Int. J. Nonlinear Mechanics*, 17:143–152, 1982.

[38] D. W. Storti and R. H. Rand. Dynamics of two strongly coupled relaxation oscillators. *SIAM J. Applied Math.*, 46:56–67, 1986.

[39] D. W. Storti and P. G. Reinhall. Stability of in-phase and out-of-phase modes for a pair of linearly coupled van der Pol oscillators. In A. Guran, editor, *Nonlinear Dynamics: The Richard Rand 50th Anniversary Volume*, Series on Stability, Vibration and Control Systems Series B: Vol. 2. World Scientific Publishing Company, 1997.

[40] R. Strichartz. *The Way of Analysis.* Jones and Bartlett Publishers, 1995.

[41] S. H. Strogatz. *Nonlinear Dynamics and Chaos.* Addison-Wesley, Reading, 1994.

[42] S. H. Strogatz. Death by delay. *Nature*, 394:317–318, 1998.

[43] F. Verhulst. *Nonlinear Differential Equations and Dynamical Systems.* Springer-Verlag, Berlin, 1990.

[44] S. A. Wirkus and R. H. Rand. Dynamics of two coupled van der Pol oscillators with delay coupling. In *Proceedings of ASME Design Engineering Technical Conference*, New York, 1997. Am.Soc.Mech.Eng.

[45] M. K. S. Yeung and S. H. Strogatz. Time delay in the Kuramoto model of coupled oscillators. *Physical Review Letters*, 82:3:648–651, 1999.

[46] R. A. York. Nonlinear analysis of phase relationships in quasi-optical oscillator arrays. *IEEE Trans. on Microwave Theory and Tech.*, 41:1799–1809, 1993.

[47] R. A. York and R. C. Compton. Quasi-optical power combining using mutually synchronized oscillator arrays. *IEEE Trans. on Microwave Theory and Tech.*, 39:1000–1009, 1991.

[48] R. A. York and R. C. Compton. Experimental observation and simulation of mode-locking phenomena in coupled-oscillator arrays. *J. Appl. Phys.*, 71:2959–2965, 1992.